

EUROPEAN ORGANISATION FOR NUCLEAR RESEARCH (CERN)



Submitted to: JHEP



CERN-PH-2015-181
24th September 2018

arXiv:1509.07335v2 [hep-ex] 14 Jan 2016

Measurement of four-jet differential cross sections in $\sqrt{s} = 8$ TeV proton–proton collisions using the ATLAS detector

The ATLAS Collaboration

Abstract

Differential cross sections for the production of at least four jets have been measured in proton–proton collisions at $\sqrt{s} = 8$ TeV at the Large Hadron Collider using the ATLAS detector. Events are selected if the four anti- k_t $R = 0.4$ jets with the largest transverse momentum (p_T) within the rapidity range $|y| < 2.8$ are well separated ($\Delta R_{4j}^{\min} > 0.65$), all have $p_T > 64$ GeV, and include at least one jet with $p_T > 100$ GeV. The dataset corresponds to an integrated luminosity of 20.3 fb^{-1} . The cross sections, corrected for detector effects, are compared to leading-order and next-to-leading-order calculations as a function of the jet momenta, invariant masses, minimum and maximum opening angles and other kinematic variables.

© 2018 CERN for the benefit of the ATLAS Collaboration.

Reproduction of this article or parts of it is allowed as specified in the CC-BY-3.0 license.

Contents

| | | |
|-----------|--|-----------|
| 1 | Introduction | 2 |
| 2 | The ATLAS detector | 3 |
| 3 | Cross-section definition | 4 |
| 4 | Monte Carlo samples | 6 |
| 5 | Theoretical predictions | 7 |
| 5.1 | Normalisation | 8 |
| 5.2 | Theoretical uncertainties | 8 |
| 6 | Data selection and calibration | 8 |
| 6.1 | Trigger | 9 |
| 6.2 | Jet reconstruction and calibration | 9 |
| 6.3 | Data quality criteria | 10 |
| 7 | Data unfolding | 10 |
| 8 | Experimental uncertainties | 12 |
| 9 | Results | 13 |
| 10 | Conclusion | 34 |
| A | Tables of the measured cross sections | 36 |
| | References | 56 |

1. Introduction

The production of particle jets at hadron colliders such as the Large Hadron Collider (LHC) [1] provides a fertile testing ground for the theory describing strong interactions, Quantum Chromodynamics (QCD). In QCD, jet production is interpreted as the fragmentation of quarks and gluons produced in the scattering process followed by their subsequent hadronisation. At high transverse momenta (p_T) the scattering of partons can be calculated using perturbative QCD (p QCD) and experimental jet measurements are directly related to the scattering of quarks and gluons. The large cross sections for such processes allow for differential measurements in a wide kinematic range and stringent testing of the underlying theory.

This analysis studies events where at least four jets are produced in a hard-scatter process. These events are of particular interest as the corresponding Feynman diagrams require several vertices even at leading-order (LO) in the strong coupling constant α_S . The current state-of-the-art theoretical predictions for such processes are at next-to-leading-order in α_S (next-to-leading-order perturbative QCD, NLO p QCD) [2, 3], and they have recently been combined with parton shower (PS) simulations [4]. An alternative approach is taken by generators which provide a matrix element (ME) for the hardest $2 \rightarrow 2$ process while the

rest of the jets are provided by a PS model, which implements a resummation of the leading-logarithmic terms (e.g. PYTHIA 8 [5] and HERWIG++ [6]). It is also interesting to test multi-leg (i.e., $2 \rightarrow n$) LO p QCD generators (e.g. SHERPA [7] or MADGRAPH [8]), since they may provide adequate descriptions of the data in specific kinematic regions and have the advantage of being less computationally expensive than NLO calculations.

It is interesting to note that the previous ATLAS measurement of multi-jet production at $\sqrt{s} = 7$ TeV [9] indicates that predictions may differ from data by $\sim 30\%$ even at NLO [10]. This work explores a variety of kinematic regimes and topological distributions to test the validity of QCD calculations, including the PS approximation and the necessity of higher-order ME in Monte Carlo (MC) generators.

Additionally, four-jet events represent a background to many other processes at hadron colliders. Hence, the predictive power of the QCD calculations, in particular their ability to reproduce the shapes of the distributions studied in this analysis, is of general interest. While searches for new phenomena in multi-jet events use data-driven techniques to estimate the contribution from QCD events, as was done for example in ref. [11], these methods are tested in MC simulations. The accuracy of the theoretical predictions remains therefore important.

Three-jet events have been measured differentially by many experiments. Indeed it was observations of such events that heralded the discovery of the gluon [12–15]. More recently, at the LHC, ATLAS has measured the three-jet cross section differentially [16] and CMS has used the ratio of three to two jet events to measure α_s [17]. Event shape variables have also been measured, showing sensitivity to higher-order p QCD effects [18, 19]. Multi-jet cross sections have been measured previously at CMS [20], ATLAS [9], CDF [21, 22] and D0 [23, 24], although with smaller datasets and/or lower energy, and generally focussed on different observables.

This paper presents the differential cross sections for events with at least four jets, studied as a function of a variety of kinematic and topological variables which include momenta, masses and angles. Events are selected if the four anti- k_t $R = 0.4$ jets with the largest transverse momentum within the rapidity range $|y| < 2.8$ are well separated, all have $p_T > 64$ GeV, and include at least one jet with $p_T > 100$ GeV. The measurements are corrected for detector effects. The variables are binned in the leading jet p_T and the total invariant mass, such that different regimes and configurations can be tested. The measurements are sensitive to the various mass scales in an event, the presence of forward jets, or the azimuthal configuration of the jets – that is, one jet recoiling against three, or two recoiling against two.

The structure of the paper is as follows. Section 2 introduces the ATLAS detector. The observables and phase space of interest are defined in section 3. The MC simulation samples studied in this work are summarised in section 4, while the theory predictions and their uncertainties are described in section 5. The trigger, jet calibration and data cleaning are presented in section 6. The unfolding of detector effects is detailed in section 7. Section 8 provides the experimental uncertainties included in the final distributions. Finally, the results are shown in section 9 and the conclusions are drawn in section 10.

2. The ATLAS detector

The ATLAS experiment [25] is a multi-purpose particle physics detector with a forward-backward symmetric cylindrical geometry and nearly 4π coverage in solid angle, with instrumentation up to $|\eta| = 4.9$.¹

¹ ATLAS uses a right-handed Cartesian coordinate system with its origin at the nominal interaction point (IP) in the centre of the detector. The z -axis is taken along the beam pipe, and the x -axis points from the IP to the centre of the LHC ring. Cylindrical coordinates (r, ϕ) are used in

The layout of the detector is based on four superconducting magnet systems, which comprise a thin solenoid surrounding the inner tracking detectors (ID) and a barrel and two end-cap toroids generating the magnetic field for a large muon spectrometer. The calorimeters are located between the ID and the muon system. The lead/liquid-argon (LAr) electromagnetic (EM) calorimeter is split into two regions: the barrel ($|\eta| < 1.475$) and the end-cap ($1.375 < |\eta| < 3.2$). The hadronic calorimeter is divided into four regions: the barrel ($|\eta| < 0.8$) and the extended barrel ($0.8 < |\eta| < 1.7$) made of scintillator/steel, the end-cap ($1.5 < |\eta| < 3.2$) with LAr/copper modules, and the forward calorimeter ($3.1 < |\eta| < 4.9$) composed of LAr/copper and LAr/tungsten modules.

A three-level trigger system [26] is used to select events for further analysis. The first level (L1) of the trigger reduces the event rate to less than 75 kHz using hardware-based trigger algorithms acting on a subset of detector information. The second level (L2) uses fast online algorithms, while the final trigger stage, called the Event Filter (EF), uses reconstruction software with algorithms similar to the offline versions. The last two software-based trigger levels, referred to collectively as the High-Level Trigger (HLT), further reduce the event rate to about 400 Hz.

3. Cross-section definition

This measurement uses jets reconstructed with the anti- k_t algorithm [27] with four-momentum recombination as implemented in the FastJet package [28]. The radius parameter is $R = 0.4$.

Cross sections are calculated for events with at least four jets within the rapidity range $|y| < 2.8$. Out of those four jets, the leading one must have $p_T > 100$ GeV, while the next three must have $p_T > 64$ GeV. In addition, these four jets must be well separated from one another by $\Delta R_{4j}^{\min} > 0.65$, where $\Delta R_{4j}^{\min} = \min_{i,j \in [1,4], i \neq j} (\Delta R_{ij})$, and $\Delta R_{ij} = (|y_i - y_j|^2 + |\phi_i - \phi_j|^2)^{1/2}$. This set of criteria is also referred to as the ‘inclusive analysis cuts’ to differentiate them from the cases where additional requirements are made, for example on the invariant mass of the four leading jets. The inclusive analysis cuts are mainly motivated by the triggers used to select events, described in section 6.1.

Cross sections are measured differentially as a function of the kinematic variables defined in table 1; the list includes momentum variables, mass variables and angular variables. The only jets used in all cases are the four leading ones in p_T . The observables were selected for their sensitivity to differences between different Monte Carlo models of QCD processes and their ability to describe the dynamics of the events. For example, the H_T variable is often used to set the scale of multi-jet processes. The four-jet invariant mass m_{4j} is representative of the largest energy scale in the event whereas m_{2j}^{\min} , the minimum dijet invariant mass, probes the smallest jet-splitting scale. The ratio m_{2j}^{\min}/m_{4j} therefore provides information about the range of energy scales relevant to the QCD calculation. The $\Delta\phi_{2j}^{\min}$ and Δy_{2j}^{\min} variables quantify the minimum angular separation between any two jets. The azimuthal variable $\Delta\phi_{3j}^{\min}$ distinguishes events with pairs of nearby jets (which have large $\Delta\phi_{3j}^{\min}$) from the recoil of three jets against one (leading to small $\Delta\phi_{3j}^{\min}$ values). The rapidity variable Δy_{3j}^{\min} works in a similar way. The Δy_{2j}^{\max} and $\Sigma p_T^{\text{central}}$ variables are designed to be sensitive to events with forward jets. In order to build $\Sigma p_T^{\text{central}}$, first the two jets with the largest rapidity interval in the event are identified, and then the scalar sum of the p_T of the remaining two jets is calculated.

the transverse plane, ϕ being the azimuthal angle around the beam pipe. The rapidity y is defined by $\frac{1}{2} \ln \frac{E+p_z}{E-p_z}$, the pseudorapidity in terms of the polar angle θ as $\eta = -\ln \tan(\theta/2)$.

| Name | Definition | Comment |
|--|--|--|
| $p_{\text{T}}^{(i)}$ | Transverse momentum of the i th jet | Sorted descending in p_{T} |
| H_{T} | $\sum_{i=1}^4 p_{\text{T}}^{(i)}$ | Scalar sum of the p_{T} of the four jets |
| $m_{4\text{j}}$ | $\left(\left(\sum_{i=1}^4 E_i \right)^2 - \left(\sum_{i=1}^4 \mathbf{p}_i \right)^2 \right)^{1/2}$ | Invariant mass of the four jets |
| $m_{2\text{j}}^{\text{min}}/m_{4\text{j}}$ | $\min_{\substack{i,j \in [1,4] \\ i \neq j}} \left((E_i + E_j)^2 - (\mathbf{p}_i + \mathbf{p}_j)^2 \right)^{1/2} / m_{4\text{j}}$ | Minimum invariant mass of two jets relative to invariant mass of four jets |
| $\Delta\phi_{2\text{j}}^{\text{min}}$ | $\min_{\substack{i,j \in [1,4] \\ i \neq j}} (\phi_i - \phi_j)$ | Minimum azimuthal separation of two jets |
| $\Delta y_{2\text{j}}^{\text{min}}$ | $\min_{\substack{i,j \in [1,4] \\ i \neq j}} (y_i - y_j)$ | Minimum rapidity separation of two jets |
| $\Delta\phi_{3\text{j}}^{\text{min}}$ | $\min_{\substack{i,j,k \in [1,4] \\ i \neq j \neq k}} (\phi_i - \phi_j + \phi_j - \phi_k)$ | Minimum azimuthal separation between any three jets |
| $\Delta y_{3\text{j}}^{\text{min}}$ | $\min_{\substack{i,j,k \in [1,4] \\ i \neq j \neq k}} (y_i - y_j + y_j - y_k)$ | Minimum rapidity separation between any three jets |
| $\Delta y_{2\text{j}}^{\text{max}}$ | $\Delta y_{ij}^{\text{max}} = \max_{i,j \in [1,4]} (y_i - y_j)$ | Maximum rapidity difference between two jets |
| $\Sigma p_{\text{T}}^{\text{central}}$ | $ p_{\text{T}}^c + p_{\text{T}}^d $ | If $\Delta y_{2\text{j}}^{\text{max}}$ is defined by jets a and b , this is the scalar sum of the p_{T} of the other two jets, c and d ('central' jets) |

Table 1: Definitions of the various kinematic variables measured. Only the four jets with the largest p_{T} are considered in all cases.

Different phase-space regions are probed by binning the variables in regions defined by a lower bound on $p_{\text{T}}^{(1)}$ and $m_{4\text{j}}$. This allows one to distinguish between the two types of topologies characterised by $\Delta\phi_{3\text{j}}^{\text{min}}$, or to track the position of the leading jet with respect to the forward–backward pair in the $\Sigma p_{\text{T}}^{\text{central}}$ variables. Table 2 summarises all the phase-space regions considered in the analysis for each of the variables.

The resulting differential cross-section distributions are corrected for detector effects (*unfolding*) and taken to the so-called particle-jet level, or simply ‘particle level’. In the MC simulations used in the unfolding procedure, particle jets are built from particles with a proper lifetime τ satisfying $c\tau > 10$ mm, including muons and neutrinos from hadron decays. The event selection described above is applied to particle jets to define the phase space of the unfolded results.

Double parton interactions have not been investigated independently, so the measurement is inclusive in this respect. They are expected to contribute 1% or less to the results.

| Observable | $\Delta R_{4j}^{\min} > \dots$ | $p_T^{(4)} > \dots$ [GeV] | $p_T^{(1)} > \dots$ [GeV] | $m_{4j} > \dots$ [GeV] | $\Delta y_{2j}^{\max} > \dots$ |
|-------------------------------|--------------------------------|---------------------------|---------------------------|------------------------|--------------------------------|
| $p_T^{(i)}$ | | | 100 | - | - |
| H_T | | | 100 | - | - |
| m_{4j} | | | 100 | - | - |
| m_{2j}^{\min}/m_{4j} | | | 100 | 500, 1000, 1500, 2000 | - |
| $\Delta\phi_{2j}^{\min}$ | 0.65 | 64 | 100, 400, 700, 1000 | - | - |
| Δy_{2j}^{\min} | | | 100, 400, 700, 1000 | - | - |
| $\Delta\phi_{3j}^{\min}$ | | | 100, 400, 700, 1000 | - | - |
| Δy_{3j}^{\min} | | | 100, 400, 700, 1000 | - | - |
| Δy_{2j}^{\max} | | | 100, 250, 400, 550 | - | - |
| $\Sigma p_T^{\text{central}}$ | | | 100, 250, 400, 550 | - | 1, 2, 3, 4 |

Table 2: Summary of the analysed phase-space regions, including the $p_T^{(1)}$, m_{4j} and Δy_{2j}^{\max} bins into which each of the differential cross-section measurements is split (a dash indicates when the cut is not applied on a variable). The ΔR_{4j}^{\min} and $p_T^{(4)}$ requirements, specified in the second and third columns respectively, apply to all variables. The observables are defined in table 1.

| Name | Hard scattering | LO/NLO | PDF | PS/UE | Tune | Factor |
|-----------------|-----------------|-------------|---------|----------|-----------------|--------|
| Pythia | PYTHIA 8 | LO (2 → 2) | CT10 | PYTHIA 8 | AU2-CT10 | 0.6 |
| Herwig++ | HERWIG++ | LO (2 → 2) | CTEQ6L1 | HERWIG++ | UE-EE-3-CTEQ6L1 | 1.4 |
| MadGraph+Pythia | MADGRAPH | LO (2 → 4) | CTEQ6L1 | PYTHIA 6 | AUET2B-CTEQ6L1 | 1.1 |
| HEJ | HEJ | All † | CT10 | — | — | 0.9 |
| BlackHat/Sherpa | BLACKHAT/SHERPA | NLO (2 → 4) | CT10 | — | — | — |
| NJet/Sherpa | NJET/SHERPA | NLO (2 → 4) | CT10 | — | — | — |

Table 3: The generators used for comparison against the data are listed, together with the parton distribution functions (PDFs), PS algorithms, underlying event (UE) and parameter tunes. Each MC prediction is multiplied by a normalisation factor (last column) as described in section 5.1, except BLACKHAT/SHERPA and NJET/SHERPA. (†) The HEJ sample is based on an approximation to all orders in α_S .

4. Monte Carlo samples

Monte Carlo samples are used to estimate experimental systematic uncertainties, deconvolve detector effects, and provide predictions to be compared with the data. Leading-order Monte Carlo samples are used for all three purposes. A set of theoretical calculations at higher orders, described in section 5, are also compared to the data. The full list of generators is shown in table 3.

The samples used in the experimental studies comprise two LO 2 → 2 generators, PYTHIA 8.160 [5] and HERWIG++ 2.5.2 [6], and the LO multi-leg generator MADGRAPH5 v1.5.12 [8]. As described in the introduction, LO generators are still widely used in searches for new physics, which motivates the comparison of their predictions to the data.

Both PYTHIA and HERWIG++ employ leading-logarithmic PS models matched to LO ME calculations. PYTHIA uses a PS algorithm based on p_T ordering, while the PS model implemented in HERWIG++ follows an angular ordering. The ME calculation provided by MADGRAPH contains up to four outgoing partons in the ME. It is matched to a PS generated with PYTHIA 6.427 [29] using the shower k_T -jet MLM matching [30], where the jet-parton matching scale is set to 20 GeV. Hadronisation effects are included via the string model in the case of the PYTHIA and MADGRAPH samples [29], or the cluster model [31] in events simulated with HERWIG++. The parton distribution functions (PDFs) used are the NLO CT10 [32] or the LO distributions of CTEQ6L1 [33] as shown in table 3.

Simulations of the underlying event, including multiple parton interactions, are included in all three LO samples. The parameter tunes employed are the ATLAS tunes AU2 [34] and AUET2B [35] for PYTHIA and MADGRAPH respectively, and the HERWIG++ tune UE-EE-3 [36].

The multiple pp collisions within the same and neighbouring bunch crossings (pile-up) are simulated as additional inelastic pp collisions using PYTHIA 8. Finally, the interaction of particles with the ATLAS detector is simulated using a GEANT4-based program [37, 38].

5. Theoretical predictions

The results of the measurement are compared to NLO predictions, in addition to the LO samples described in section 4. These are calculated using BLACKHAT/SHERPA [2, 3] and NJET/SHERPA [39, 40], and have been provided by their authors. They are both fixed-order calculations with no PS and no hadronisation. Therefore, the results are presented at the parton-jet level, that is, using jets built from partons instead of hadrons. For the high- p_T phase space covered in this analysis, non-perturbative corrections are expected to be small [41, 42]. BLACKHAT performs one-loop virtual corrections using the unitarity method and on-shell recursion. The remaining terms of the full NLO computation are obtained with AMEGIC++ [43, 44], part of SHERPA. NJET makes a numerical evaluation of the one-loop virtual corrections to multi-jet production in massless QCD. The Born matrix elements are evaluated with the COMIX generator [45, 46] within SHERPA. SHERPA also performs the phase-space integration and infra-red subtraction via the Catani-Seymour dipole formalism. Both the BLACKHAT/SHERPA and NJET/SHERPA predictions use the CT10 PDFs.

The results are also compared to predictions provided by HEJ [47–49]. HEJ is a fully exclusive Monte Carlo event generator based on a perturbative cross-section calculation which approximates the hard-scattering ME to all orders in the strong coupling constant α_S for jet multiplicities of two or greater. The approximation is exact in the limit of large separation in rapidity between partons. The calculation uses the CT10 PDFs. As in the case of the NLO predictions, no PS or hadronisation are included.

The different predictions tested are expected to display various levels of agreement in different kinematic configurations. The generators which combine $2 \rightarrow 2$ parton matrix elements (MEs) with parton showers (PSs) are in principle not expected to provide a good description of the data, particularly in regions where the additional jets are neither soft nor collinear. A previous measurement of multi-jet cross sections at 7 TeV by the ATLAS Collaboration [9] found that the cross section predicted by MC models typically disagreed with the data by $\mathcal{O}(40\%)$. It also found disagreements of up to 50% in the shape of the differential cross section measured as a function of $p_T^{(1)}$ or H_T . Nevertheless, there are also examples of exceptional cases where these calculations perform well, which adds interest to the measurement; for example, the same 7 TeV ATLAS paper observed that the shape of the $p_T^{(4)}$ distribution was described by PYTHIA within just 10%. It is also interesting to test whether PSs based on an angular ordering perform

better in angular variables such as $\Delta\phi_{2j}^{\min}$ or $\Delta\phi_{3j}^{\min}$ than those using momentum ordering. In contrast to PS predictions, multi-leg matrix element calculations matched to parton showers (ME+PS) were seen at 7 TeV to significantly improve the accuracy of the cross-section calculation and the shapes of the momentum observables. In the present analysis, such calculations are expected to perform better in events with additional high- p_T jets and/or large combined invariant masses of jets. This is also the type of scenario where HEJ is expected to perform well, since it provides an all-order description of processes with more than two hard jets, and it is designed to capture the hard, wide-angle emissions which a standalone PS approach would miss. Variables such as Δy_{2j}^{\max} , Δy_{3j}^{\min} or $\Sigma p_T^{\text{central}}$ were included in the analysis with this purpose in mind. Finally, the fixed-order, four-jet NLO predictions are expected to provide a better estimation of the cross sections than the LO calculations. Interestingly, studies at 7 TeV found that the NLO cross section for four-jet events was $\sim 30\%$ higher than the data [10].

5.1. Normalisation

To facilitate comparison with the data, the cross sections predicted by the LO generators as well as HEJ are multiplied by a scale factor. The factor is such that the integrated number of events in the region $500 \text{ GeV} < p_T^{(1)} < 1.5 \text{ TeV}$ which satisfy the inclusive analysis cuts in section 3 is equal to the corresponding number in data. The full set of normalisation factors is shown in table 3. No scale factor is ascribed to BLACKHAT/SHERPA and NJET/SHERPA such that the level of agreement with data can be assessed in light of the theoretical uncertainties, as discussed in section section 5.2.

5.2. Theoretical uncertainties

Theoretical uncertainties have been computed for HEJ and the NLO predictions. The sensitivity of the HEJ calculation to higher-order corrections was determined by the authors of the calculation by varying independently the renormalisation and factorisation scales by factors of $\sqrt{2}$, 2, $1/\sqrt{2}$ and $1/2$ around the central value of $H_T/2$. The total uncertainty is the result of taking the envelope of all the variations. The typical size of the uncertainty is $^{+50\%}_{-30\%}$, and it is not drawn on the figures for clarity.

The central value of the renormalisation and factorisation scales used in the NJET/SHERPA and BLACKHAT/SHERPA samples is also $H_T/2$. Scale uncertainties are evaluated for NJET/SHERPA by simultaneously varying both scales by factors of $1/2$ and 2. PDF uncertainties are obtained by reweighting the distributions for all the PDF error sets using LHAPDF [50], following the recommendations from ref. [51]. The additional PDF sets include variations in the value of α_S . The sum in quadrature of the resulting scale and PDF variations defines the NLO theoretical uncertainty included in the result figures in section 9. The uncertainty is dominated by the scale component due to the rapid drop of the cross section with decreasing values of the renormalisation and factorisation scales. As a result, the uncertainty is significantly asymmetric.

6. Data selection and calibration

The data sample used was taken during the period from March to December 2012 with the LHC operating at a pp centre-of-mass energy of $\sqrt{s} = 8 \text{ TeV}$. The application of data-quality requirements results in an integrated luminosity of 20.3 fb^{-1} .

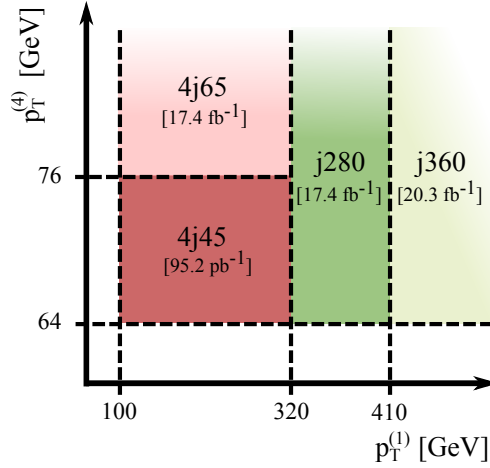


Figure 1: Schematic of the kinematic regions in which the four different jet triggers are used, including the total luminosity that each of them recorded. The term 4j45 (4j65) refers to a trigger requiring at least four jets with $p_T > 45$ GeV (65 GeV), where the p_T is measured at the EF level of the triggering system. The term j280 (j360) refers to a trigger requiring at least one jet with $p_T > 280$ GeV (360 GeV) at the EF level. The horizontal and vertical axes correspond to $p_T^{(1)}$ and $p_T^{(4)}$ respectively, both calculated at the offline level (i.e., including the full object calibration).

6.1. Trigger

The events used in this analysis are selected by a combination of four jet triggers, consisting of the three usual levels and defined in terms of the jets produced in the event. The hardware-based L1 trigger provides a fast decision based on the energy measured by the calorimeter. The L2 trigger performs a simple jet reconstruction procedure in the geometric regions identified by the L1 trigger. The final decision taken by the EF trigger is made using jets from the region of $|\eta| < 3.2$, and reconstructed from topological clusters [52] using the anti- k_t algorithm with $R = 0.4$.

The four different triggers used in this paper are shown in figure 1. Two of the triggers select events with at least four jets, while the remaining two select events with at least one jet at a higher p_T threshold. Events are split into the four non-overlapping kinematic regions shown in figure 1, requiring at least four well-separated jets with varying p_T thresholds in order to apply the corresponding trigger. This ensures trigger efficiencies greater than 99% for any event passing the inclusive analysis cuts. The small residual loss of data due to trigger inefficiency is corrected as a function of jet p_T using the techniques described in section 7.

As noted in figure 1, three out of the four triggers only recorded a fraction of the total dataset. The contributions from the events selected by those three triggers are scaled by the inverse of the corresponding fraction.

6.2. Jet reconstruction and calibration

Jets are reconstructed using the anti- k_t jet algorithm [27] with four-momentum recombination and radius parameter $R = 0.4$. The inputs to the jet algorithm are locally-calibrated topological clusters of calori-

meter cells [52], which reconstruct the three-dimensional shower topology of each particle entering the calorimeter.

ATLAS has developed several jet calibration schemes [53] with different levels of complexity and different sensitivities to systematic effects. In this analysis the local cluster weighting (LCW) calibration [52] method is used, which classifies topological clusters as either being of electromagnetic or hadronic origin. Based on this classification, specific energy corrections are applied, improving the jet energy resolution. The final jet energy calibration, generally referred to as the jet energy scale, corrects the average calorimeter response to reproduce the energy of the true particle jet.

The jet energy scale and resolution have been measured in pp collision data using techniques described in references [54–56]. The effects of pile-up on jet energies are accounted for by a jet-area-based correction [57] prior to the final calibration, where the area of the jet is defined in η - ϕ space. Jets are then calibrated to the hadronic energy scale using p_T - and η -dependent calibration factors based on MC simulations, and their response is corrected based on several observables that are sensitive to fragmentation effects. A residual calibration is applied to take into account differences between data and MC simulation based on a combination of several in-situ techniques [54].

6.3. Data quality criteria

Before applying the selection that defines the kinematic region of interest, events are required to pass the trigger, as described in section 6.1, and to contain a primary vertex with at least two tracks. Events which contain energy deposits in the calorimeter consistent with noise, or with incomplete event data, are rejected. In addition, events containing jets pointing to problematic calorimeter regions, or originating from non-collision background, cosmic rays or detector effects, are vetoed. These cleaning procedures are emulated in the MC simulation used to correct for experimental effects, as is discussed in detail in section 7.

No attempt is made to exclude jets that result from photons or leptons impacting the calorimeter, nor are the contributions from such signatures corrected for. Events containing photons or τ leptons are expected to contribute less than 0.1% to the cross sections under study.

Distributions of two example variables ($p_T^{(1)}$ and $p_T^{(4)}$) can be seen at the detector level (i.e. prior to unfolding detector effects) in figure 2. Different sets of points correspond to the data and the different MC generators, which are normalised to data with the scale factors indicated in table 3. These are constant factors used to facilitate the comparison with data, as described in section 5.1. Given that the generators have only LO or even only leading-logarithmic accuracy, the observed agreement is reasonable.

7. Data unfolding

Cross sections are measured differentially in several variables, each of which is binned in $p_T^{(1)}$ or m_{4j} . Each of the corresponding distributions is individually unfolded to deconvolve detector effects such as inefficiencies and resolutions. The unfolding is performed using the Bayesian Iterative method [58, 59], as implemented in the RooUnfold package [60]. The algorithm builds an unfolding matrix starting with an initial prior probability distribution taken from MC simulation, and improves it iteratively. The method takes into account migrations between bins. It also corrects the results for the presence of events which

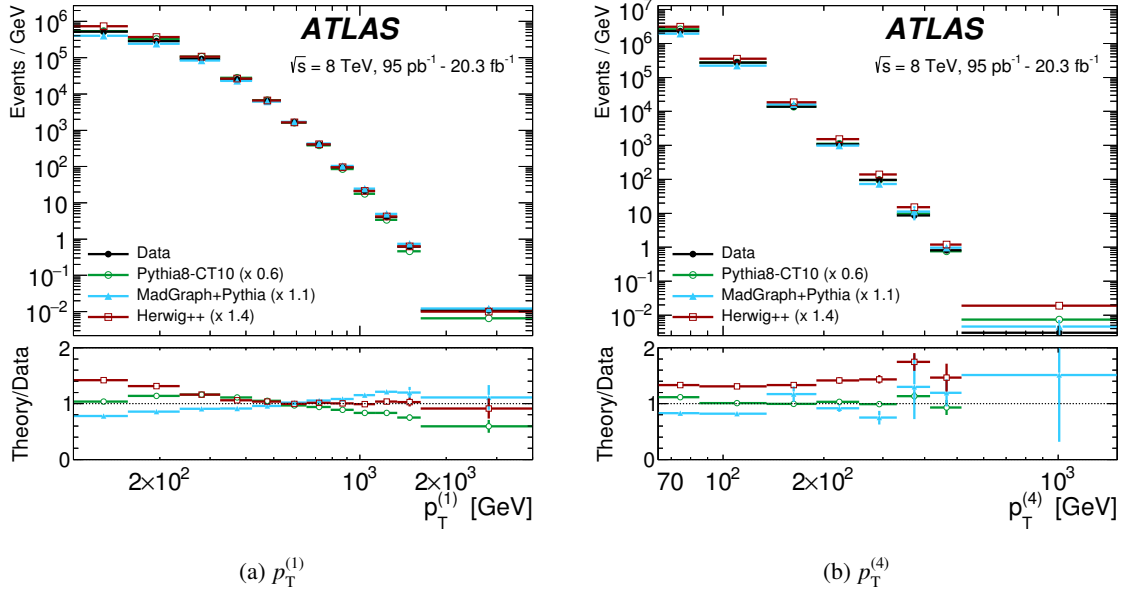


Figure 2: Detector-level distributions of (a) $p_T^{(1)}$ and (b) $p_T^{(4)}$ for data and for example MC predictions. The MC predictions have passed through detector simulation. The lower panel in each plot shows the ratios of the MC predictions to data. For better comparison, the predictions are multiplied by the factors indicated in the legend.

pass the selection at reconstructed-level but not at the particle level; and for detector inefficiencies, which have the opposite effect. The number of iterations is optimised in order to minimise the size of the statistical and systematic uncertainties. A lower number of iterations results in a higher dependence on the MC simulation, whereas higher values give larger statistical uncertainties. For the analysis presented in this paper, two iterations are used.

The data are unfolded to the particle-jet level using the PYTHIA MC simulation to build the unfolding matrix. In order to construct the matrix, events are required to pass the inclusive analysis cuts at both the reconstructed and particle levels. The cuts require that events have at least four jets within $|y| < 2.8$, with $p_T^{(1)} > 100$ GeV and $p_T^{(2)}, p_T^{(3)}, p_T^{(4)} > 64$ GeV. The four leading jets must in addition be separated by $\Delta R_{4j}^{\min} > 0.65$. For observables requiring additional kinematic cuts, these are also applied both at the reconstructed and particle levels. No spatial matching is performed between reconstructed-level and particle-level jets.

The correlation between the observables before and after the incorporation of experimental effects tends to be higher for p_T -based variables, such as H_T . In the case of angular variables, such as $\Delta\phi_{2j}^{\min}$, the correlation is weakened due to cases where energy resolution effects lead to re-ordering of the jet p_T . Nevertheless, even in the case of such angular variables the entries far from the diagonal of the correlation matrix are significantly smaller than the diagonal elements. The binning is derived from an optimisation procedure such that the purity of the bins is between 70% and 90%, and the statistical uncertainty of the measurement is $\lesssim 10\%$. The purity is defined as the fractional number of events per bin which do not migrate to other bins after the detector simulation, calculated with respect to the number of events which pass the particle-level cuts.

The possible presence of biases in the unfolded spectra due to MC mismodelling of the reconstructed-level spectrum is evaluated using a data-driven closure test. In this study, the MC distributions are reweighted

to match the shape of those obtained from the data, and then unfolded using the same unfolding matrix as for the data. A data-driven systematic uncertainty is computed by comparing the result obtained from this procedure and the original reweighted particle-level MC distributions. With two iterations of the unfolding algorithm, this systematic uncertainty is found to be negligible.

A second unfolding uncertainty is evaluated to account for the model dependence of the efficiency with which both the reconstructed- and particle-level cuts are satisfied in each MC event. The systematic uncertainty is derived from the differences between the efficiencies calculated with HERWIG++ and those calculated using PYTHIA. The resulting uncertainty is found to be subdominant in most cases, with typical sizes of 2–10%. The uncertainty is rebinned and smoothed, such that its statistical uncertainty is smaller than 40%.

The statistical uncertainties are calculated with pseudo-experiments. For each pseudo-experiment, the data and MC distributions are reweighted event by event following a Poisson distribution centred at one. Each resulting Poisson replica of the data is unfolded using the corresponding fluctuated unfolding matrix. The random numbers for the pseudo-experiments are generated using unique seeds, following the same scheme used by the inclusive jet [42], dijet [61] and three-jet [16] measurements at $\sqrt{s} = 7$ TeV, to allow for possible future combination of results with the same dataset used for this analysis.

The integral of the unfolded distributions, corresponding to the cross section in the fiducial range determined by the inclusive analysis cuts, was compared for all the variables defined in the same region of phase space and found to agree with each other within 0.5%.

8. Experimental uncertainties

Several sources of experimental uncertainty are considered in this analysis. Those arising from the unfolding procedure are described in section 7. This section presents the uncertainties which arise from the jet energy scale (JES), jet energy resolution (JER), jet angular resolution and integrated luminosity. The dominant source of uncertainty in this measurement is the JES.

The uncertainty in the JES calibration is determined in the central detector region by exploiting the transverse momentum balance in Z +jet, γ +jet or multi-jet events, which are measured in situ. The uncertainties in the energy of the reference object are propagated to the jet whose energy scale is being probed. The uncertainty in the central region is propagated to the forward region using dijet systems balanced in transverse momentum. The procedure is described in detail in ref. [54].

The total JES uncertainty is decomposed into eighteen components, which account for the uncertainty in the jet energy scale calibration itself, as well as uncertainties due to the pile-up subtraction procedure, parton flavour differences between samples, b -jet energy scale and punch-through. Each of these uncertainties is incorporated as a coherent shift of the scale of the jets in the MC simulation. The energies and transverse momenta of all jets with $p_T > 20$ GeV and $|y| < 2.8$ are varied up and down by one standard deviation of each uncertainty component; these components are asymmetric, i.e. the values of the upwards and downwards variations are different. The shifts are then propagated through the unfolding. The unfolded distributions corresponding to the systematically varied spectra are compared one by one to the nominal ones, and the difference taken as the unfolded-level uncertainty due to that JES uncertainty component. The total JES uncertainty is obtained by summing all such contributions quadratically, respecting the sign of the variations in the event yields; that is, positive and negative event yield variations are added independently.

Statistical uncertainties on each of the JES uncertainty components are obtained by creating Poisson replicas of the systematically varied spectra, obtained as explained in section 7. Such statistical uncertainties are used to evaluate the significance of the uncertainty for each component and for each bin of all the differential distributions. As in the case of the unfolding uncertainty, the unfolded-level uncertainty due to each JES component is then rebinned and smoothed using a Gaussian kernel regression in order to get statistical uncertainties smaller than 40% in all bins. The typical size of the JES uncertainty is 4–15%.

Jets may be affected by additional energy originating from pile-up interactions. This effect is corrected for as part of the jet energy calibration. The distributions were binned in different ranges of the average number of interactions per bunch crossing in order to test the possible presence of residual effects. No significant deviations were observed, therefore no uncertainty associated with pile-up mismodelling was considered beyond the pile-up uncertainty already included in the jet calibration procedure.

The JER has been measured in data using dijet events [62], and an uncertainty was derived from the differences seen between data and MC prediction. In general, the energy resolution observed in data is somewhat worse than that in MC simulations. The uncertainty on the observables can therefore be evaluated by smearing the energy of the reconstructed jets in the MC simulation. After applying this smearing to the jets, an alternative unfolding matrix is derived and used to unfold the nominal MC prediction. Then the MC distribution is unfolded using both the nominal and the smeared matrices, and the difference between the two is symmetrised and taken as the JER systematic uncertainty. The typical size of this uncertainty is 1–10% of the cross section.

The jet angular resolution was estimated in MC simulation for the pseudorapidity and ϕ by matching spatially jets at the reconstructed and particle level, and found to be $\lesssim 2\%$. This is in agreement with in-situ measurements, so no systematic uncertainty is assigned.

Finally, the uncertainty on the integrated luminosity is $\pm 2.8\%$. It is derived following the same methodology as that detailed in ref. [63].

Two examples of the values of the total experimental systematic uncertainty are shown in figure 3 for two representative variables, namely H_T and $\Delta\phi_{2j}^{\min}$. The jet energy scale and resolution uncertainties dominate in the majority of bins, being larger at the high and low ends of the H_T spectrum. The unfolding uncertainty is nearly as large at low values of the jet momenta, and it is therefore an important contribution in most of the $\Delta\phi_{2j}^{\min}$ bins.

9. Results

The various differential cross sections measured in events with at least four jets are shown in figures 4 to 19 for jets reconstructed with the anti- k_t algorithm with $R = 0.4$. The observables used for the measurements are defined in table 1. The measurements are performed for a wide range of jet transverse momenta from 64 GeV to several TeV, spanning two orders of magnitude in p_T and over seven orders of magnitude in cross section. The measured cross sections are corrected for all detector effects using the unfolding procedure described in section 7. The theoretical predictions described in sections 4 and 5 are compared to the unfolded results.

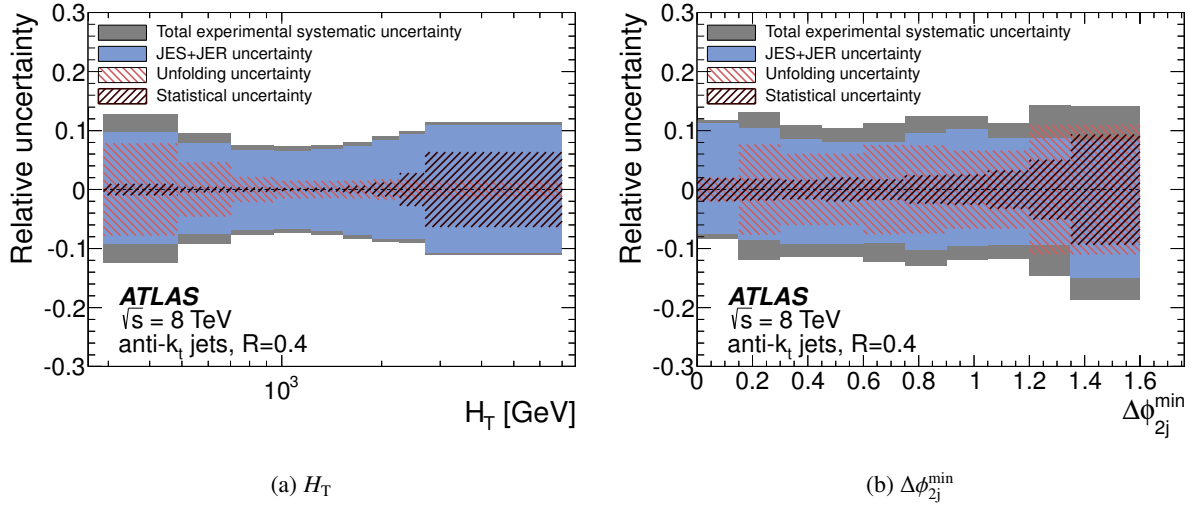


Figure 3: Total systematic uncertainty in the four-jet cross section measurement for anti- k_t $R = 0.4$ jets as a function of (a) H_T and (b) $\Delta\phi_{2j}^{\min}$. In both cases the event selection corresponds to the inclusive analysis cuts, namely $p_T^{(4)} > 64$ GeV, $p_T^{(1)} > 100$ GeV and $\Delta R_{4j}^{\min} > 0.65$. Separate bands show the jet energy scale (JES) and resolution (JER), and the unfolding uncertainty, as well as the combined total systematic uncertainty resulting from adding in quadrature all the components. The total statistical uncertainty of the unfolded data spectrum is also shown. The luminosity uncertainty is not shown separately but is included in the total uncertainty band.

Summary of the results The scale factors applied to LO generators (see section 5.1) are found to vary between 0.6 and 1.4, as shown previously in table 3. Not all generators describe the shape of $p_T^{(1)}$ correctly, so these scale factors should not be seen as a measure of the level of agreement between MC simulation and data, which may vary as a function of the cuts in $p_T^{(1)}$ and m_{4j} . The cross section predicted by BLACKHAT/SHERPA and NJET/SHERPA is larger than that measured in data, but overall the difference is covered by the scale and PDF uncertainties evaluated using NJET/SHERPA, with only a few exceptions. BLACKHAT/SHERPA and NJET/SHERPA give identical results within statistical uncertainties; therefore only one of the two (NJET/SHERPA) is discussed in the following, for simplicity. It is nevertheless interesting to compare experimental results with two different implementations of the same NLO p QCD calculations as an additional cross-check.

In general, an excellent description of both the shape and the normalisation of the variables is given by NJET/SHERPA. The small differences found are covered by theoretical and statistical uncertainties in almost all cases; only the tails of $p_T^{(4)}$ and Δy_{2j}^{\max} hint at deviations from the measured distribution. MADGRAPH+PYTHIA describes the data very well in most regions of phase space, the most significant discrepancy being in the slopes of $p_T^{(1)}$ and $p_T^{(2)}$ and derived variables. HEJ also provides a good description of most variables; the most significant discrepancy occurs for the angular variables Δy_{2j}^{\min} and Δy_{2j}^{\max} when $p_T^{(1)}$ is small. However when $p_T^{(1)}$ is large, HEJ describes Δy_{2j}^{\max} better than NJET/SHERPA, which highlights one of the strengths of this calculation. The $2 \rightarrow 2$ ME calculations matched to parton showers provide different levels of agreement depending on the variable studied; the only variable whose shape is reasonably well described by both PYTHIA and HERWIG++ is H_T .

The following discussion is based on the results obtained after applying the particular choice of normalisation of the theoretical predictions as explained at the beginning of this section. NJET/SHERPA, which

generally gives very good agreement with the data, is only discussed for those cases where some deviations are present.

Momentum variables The momentum variables comprise the p_T of the four leading jets and H_T . Part of the importance of these variables lies in their wide use in analyses, alone or as inputs to more complex observables. They are also interesting in themselves: it has been shown that the ratio of the NLO to the LO predictions is relatively flat across the $p_T^{(1)}$ spectrum with a maximum variation of approximately 25% [10]. Perhaps surprisingly, the PS description of $p_T^{(4)}$ was found to be better than that of $p_T^{(1)}$ in the 7 TeV multi-jet measurement published by ATLAS [9].

Figures 4 to 7 show the p_T distributions of the leading four jets. All the LO generators show a slope with respect to the data in the leading jet p_T (figure 4). The ratios of HERWIG++ and HEJ to data are remarkably flat above ~ 500 GeV and ~ 300 GeV respectively. MADGRAPH+PYTHIA is within the experimental uncertainties above ~ 300 GeV, and it is the only one with a positive slope in the ratio to data.

The subleading jet p_T (figure 5) is well described by HEJ, while the LO generators show similar trends to those in $p_T^{(1)}$. MADGRAPH+PYTHIA describes both $p_T^{(3)}$ and $p_T^{(4)}$ well, as shown in figures 6 and 7. As the 7 TeV results suggested, PYTHIA gives a good description of the distribution of $p_T^{(4)}$. HEJ and HERWIG++ overestimate the number of events with high $p_T^{(4)}$. NJET/SHERPA shows a similar trend at high $p_T^{(4)}$, but the discrepancy is mostly covered by the theoretical uncertainties. H_T , shown in figure 8, exhibits features similar to those in $p_T^{(1)}$.

In summary, PYTHIA and HERWIG++ tend to describe the p_T spectrum of the leading jets with similar levels of agreement, whereas PYTHIA is better at describing $p_T^{(4)}$. MADGRAPH+PYTHIA does a reasonable job for all of them, while HEJ and NJET/SHERPA are very good for the leading jets and less so for $p_T^{(4)}$. This could perhaps be improved by matching the calculations to PSs.

Mass variables Mass variables are widely used in physics searches, and they are also sensitive to events with large separations between jets, which puts the HEJ and MADGRAPH+PYTHIA predictions to the test, as they are expected to be especially accurate in this regime.

The distribution of the total invariant mass m_{4j} is studied in figure 9. PYTHIA and MADGRAPH+PYTHIA describe the data very well. HERWIG++ describes the shape of the data between 1 TeV and 3–6 TeV. HEJ is mostly compatible with the measurement, but the ratio to data has a bump structure in the region of approximately 1 to 2 TeV. This feature is also shared by NJET/SHERPA, but the differences with respect to the data are covered by the NLO uncertainties.

The description of different splitting scales is tested in figure 10 through the variable m_{2j}^{\min}/m_{4j} . This distribution is well described by PYTHIA, whereas HERWIG++ gets worse with increasing m_{4j} , consistently overestimating the two ends of the m_{2j}^{\min}/m_{4j} spectrum. MADGRAPH+PYTHIA provides a very good description, with a flat ratio for all the m_{4j} cuts. The HEJ prediction shows trends similar to those of HERWIG++ at higher values of m_{4j} . These differences are covered in all cases by the large associated scale uncertainty. NJET/SHERPA overestimates the number of events in the very first bin, possibly due to the lack of a PS, but otherwise agrees with the data within the theoretical uncertainties.

Overall, MADGRAPH+PYTHIA provides the best description of mass variables.

Angular variables Similarly to mass variables, angular variables are able to test the description of events with small- and wide-angle radiation. In addition, they can also provide information on the global spatial distribution of the jets. High- p_T , large-angle radiation should be well captured by the ME+PS description of MADGRAPH+PYTHIA, or the all-orders approximation of HEJ – particularly the rapidity variables Δy_{2j}^{\min} , Δy_{2j}^{\max} and Δy_{3j}^{\min} . PS generators are expected to perform poorly at large angles, given that they only contain two hard jets, and the rest is left to the soft- and collinear-enhanced PS. The fixed-order NLO prediction of NJET/SHERPA should provide a very good description of these variables too, as long as they are far from the infrared limit. This is indeed the case, and therefore no detailed comments about its performance are given here.

Figure 11 compares the distributions of $\Delta\phi_{2j}^{\min}$ for different cuts in $p_T^{(1)}$. PYTHIA has a small downwards slope with respect to the data in all the $p_T^{(1)}$ ranges. MADGRAPH+PYTHIA also shows a small slope. The other generators, both LO and NLO, reproduce the data very well. HERWIG++, in particular, provides a very good description of the data.

The $\Delta\phi_{3j}^{\min}$ spectrum is shown in figure 12. The different $p_T^{(1)}$ cuts change the spatial distribution of the events, such that at low $p_T^{(1)}$ most events contain two jets recoiling against two, while at high $p_T^{(1)}$ the events where one jet recoils against three dominate. In general, the description of the data improves as $p_T^{(1)}$ increases. For PYTHIA, the number of events where one jet recoils against three (low $\Delta\phi_{3j}^{\min}$) is significantly overestimated when $p_T^{(1)}$ is low; as $p_T^{(1)}$ increases, the agreement improves such that the $p_T^{(1)} > 1000$ GeV region is very well described. MADGRAPH+PYTHIA, HERWIG++ and HEJ are mostly in good agreement with data.

Figure 13 compares the distributions of Δy_{2j}^{\min} with data. This variable is remarkably well described by PYTHIA, showing no significant trend. MADGRAPH+PYTHIA mostly underestimates high Δy_{2j}^{\min} values, while HERWIG++ has a tendency to underestimate the low values. HEJ overestimates the number of events with high Δy_{2j}^{\min} values at low $p_T^{(1)}$, but describes the data very well at larger values of $p_T^{(1)}$.

For the variable Δy_{3j}^{\min} , presented in figure 14, the predictions provided by PYTHIA and HERWIG++ show in general a positive slope with respect to the data. MADGRAPH+PYTHIA reproduces the shape of the data well, as does HEJ for $p_T^{(1)} > 400$ GeV. However, for smaller values of $p_T^{(1)}$ HEJ overestimates the number of events at the end of the spectrum, as was the case for Δy_{2j}^{\min} .

The variable Δy_{2j}^{\max} , shown in figure 15, is very well described by HEJ in events with $p_T^{(1)} > 400$ GeV. The ratios to data in both PYTHIA and HERWIG++ have upwards slopes in all $p_T^{(1)}$ bins. MADGRAPH+PYTHIA provides mostly a good description of the data, with a tendency to underestimate the extremes of the distribution. Interestingly, NJET/SHERPA seems to overestimate the number of events in the tail, although it is a statistically limited region and the comparison with BLACKHAT/SHERPA is not conclusive.

In summary: NJET/SHERPA mostly agrees with the data within the uncertainties, but its ratio to data has an upwards trend in the tail of Δy_{2j}^{\max} . HEJ provides a very good description of all angular variables for the region $p_T^{(1)} > 400$ GeV, as expected, but shows significant discrepancies with respect to the data in all the rapidity variables for lower $p_T^{(1)}$ values. It is important to keep in mind, though, that the associated scale uncertainties are large. MADGRAPH+PYTHIA describes all the data well, apart from the tail of Δy_{2j}^{\min} and the extreme values of Δy_{2j}^{\max} , which it underestimates. HERWIG++ gives good descriptions of the ϕ

variables, but fails at describing the rapidity variables. PYTHIA has some problems describing both three-jet variables, as well as Δy_{2j}^{\max} . These variables highlight the need to combine four-jet ME calculations with parton showers.

$\Sigma p_T^{\text{central}}$ variables The variables setting a minimum forward–backward rapidity interval and measuring the total p_T of the central jets ($\Sigma p_T^{\text{central}}$) were defined to test the framework of HEJ. HEJ has been designed to describe events with two jets significantly separated in rapidity with additional, central, high- p_T radiation. These variables are also useful to describe the spatial configuration of the events, as they represent the forward–backward rapidity span of the jets, and whether the leading jet is among the two central ones or not. The NLO predictions and MADGRAPH+PYTHIA are also expected to be successful in this regime, whereas the $2 \rightarrow 2$ generators with PSs are expected to be less suitable.

The variable $\Sigma p_T^{\text{central}}$ is studied for values of Δy_{2j}^{\max} larger than 1, 2, 3 or 4, and for different cuts in $p_T^{(1)}$. In most cases, the description of the observable worsens significantly with increasing Δy_{2j}^{\max} and $p_T^{(1)}$. Figures 16 to 19 correspond to the results for $\Delta y_{2j}^{\max} > 1, 2, 3, 4$.

The generators with $2 \rightarrow 2$ MEs have problems describing the data around the threshold values where the contribution from different jets changes, which results in kinks in the ratio distributions. One such transition occurs at the $\Sigma p_T^{\text{central}}$ value for which the leading jet is first allowed to be central. For $p_T^{(1)} > 400$ GeV, this happens at $\Sigma p_T^{\text{central}} > 464$ GeV, at which point there is a major jump in PYTHIA in the second ratio plot of figure 16. PYTHIA gives in general the most discrepant prediction, with kinks in the ratio to data at the transition points that reach differences of 70% at high $p_T^{(1)}$, as well as global slopes. HERWIG++ describes the data very well at lower Δy_{2j}^{\max} values, but as Δy_{2j}^{\max} grows its normalisation worsens, as well as the shape – particularly at high $p_T^{(1)}$.

MADGRAPH+PYTHIA provides an excellent description of the $\Sigma p_T^{\text{central}}$ variables, especially at low $p_T^{(1)}$. The agreement deteriorates at high $p_T^{(1)}$, but it is not very much affected by the changes between different jet configurations, providing overall a very good description of the shapes. Most distributions are well described by HEJ, especially the high $\Sigma p_T^{\text{central}}$ region; the low $\Sigma p_T^{\text{central}}$ region shows more shape differences, which get worse at large Δy_{2j}^{\max} . This is compatible with similar observations made in previous ATLAS measurements performed with 7 TeV data [64], where it was also shown that the agreement was significantly improved after interfacing HEJ with a PS generator. NJET/SHERPA has a tendency to overestimate the number of events with very low $\Sigma p_T^{\text{central}}$, which may be correlated with the $p_T^{(4)}$ discrepancy discussed earlier. It provides a very good description of the data otherwise.

Tables 4 to 49 in appendix A contain the numerical values of the measured differential cross sections and their corresponding uncertainties. The quoted values correspond to the average differential cross sections over the bin ranges given.

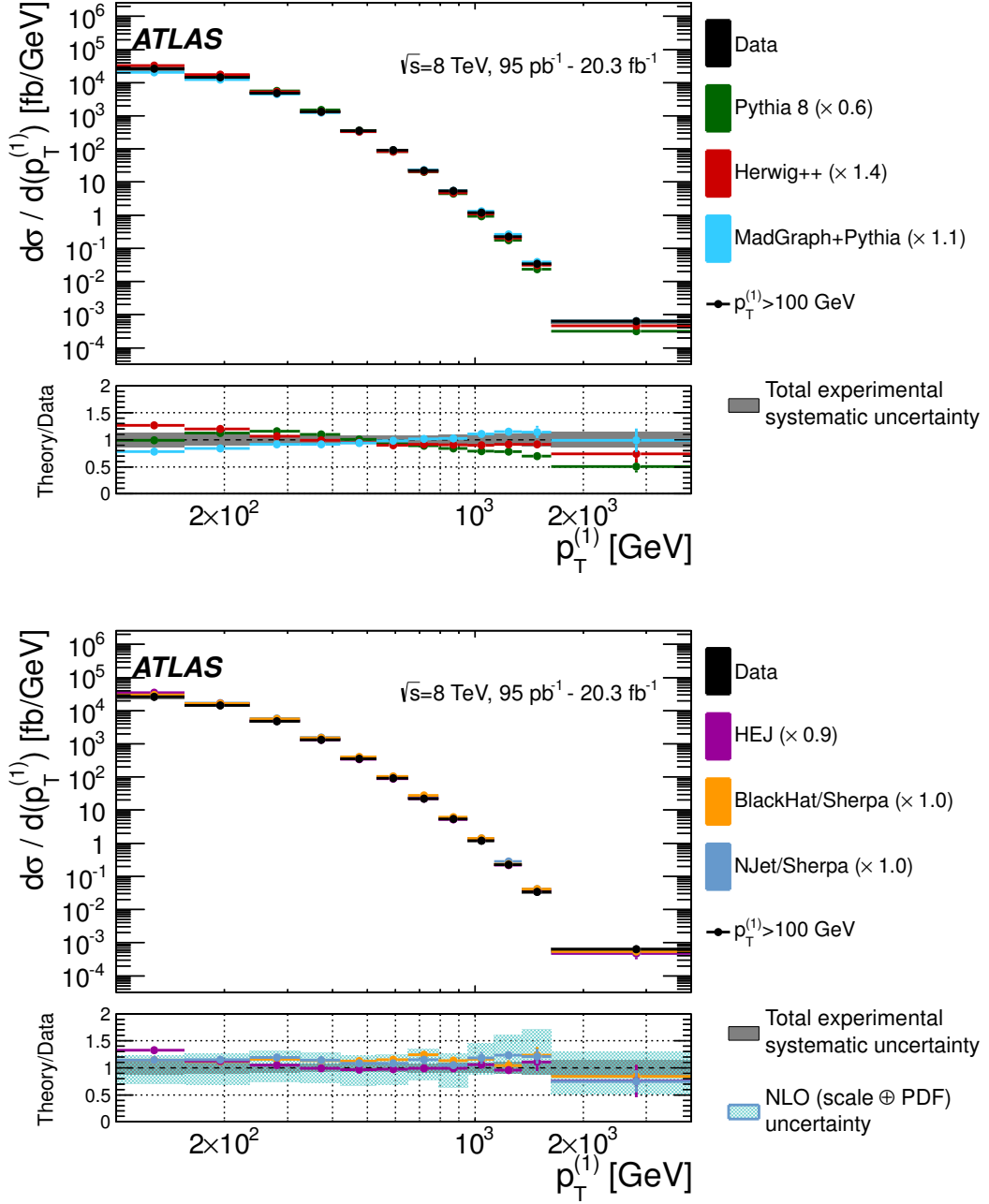


Figure 4: The four-jet differential cross section as a function of leading jet p_T ($p_T^{(1)}$), compared to different theoretical predictions: PYTHIA, HERWIG++ and MADGRAPH+PYTHIA (top), and HEJ, NJET/SHERPA and BLACKHAT/SHERPA (bottom). For better comparison, the predictions are multiplied by the factors indicated in the legend. In each figure, the top panel shows the full spectra and the bottom panel the ratios of the different predictions to the data. The solid band represents the total experimental systematic uncertainty centred at one. The patterned band represents the NLO scale and PDF uncertainties calculated from NJET/SHERPA centred at the nominal NJET/SHERPA values. The scale uncertainties for HEJ (not drawn) are typically $^{+50\%}_{-30\%}$. The ratio curves are formed by the central values with vertical uncertainty lines resulting from the propagation of the statistical uncertainties of the predictions and those of the unfolded data spectrum.

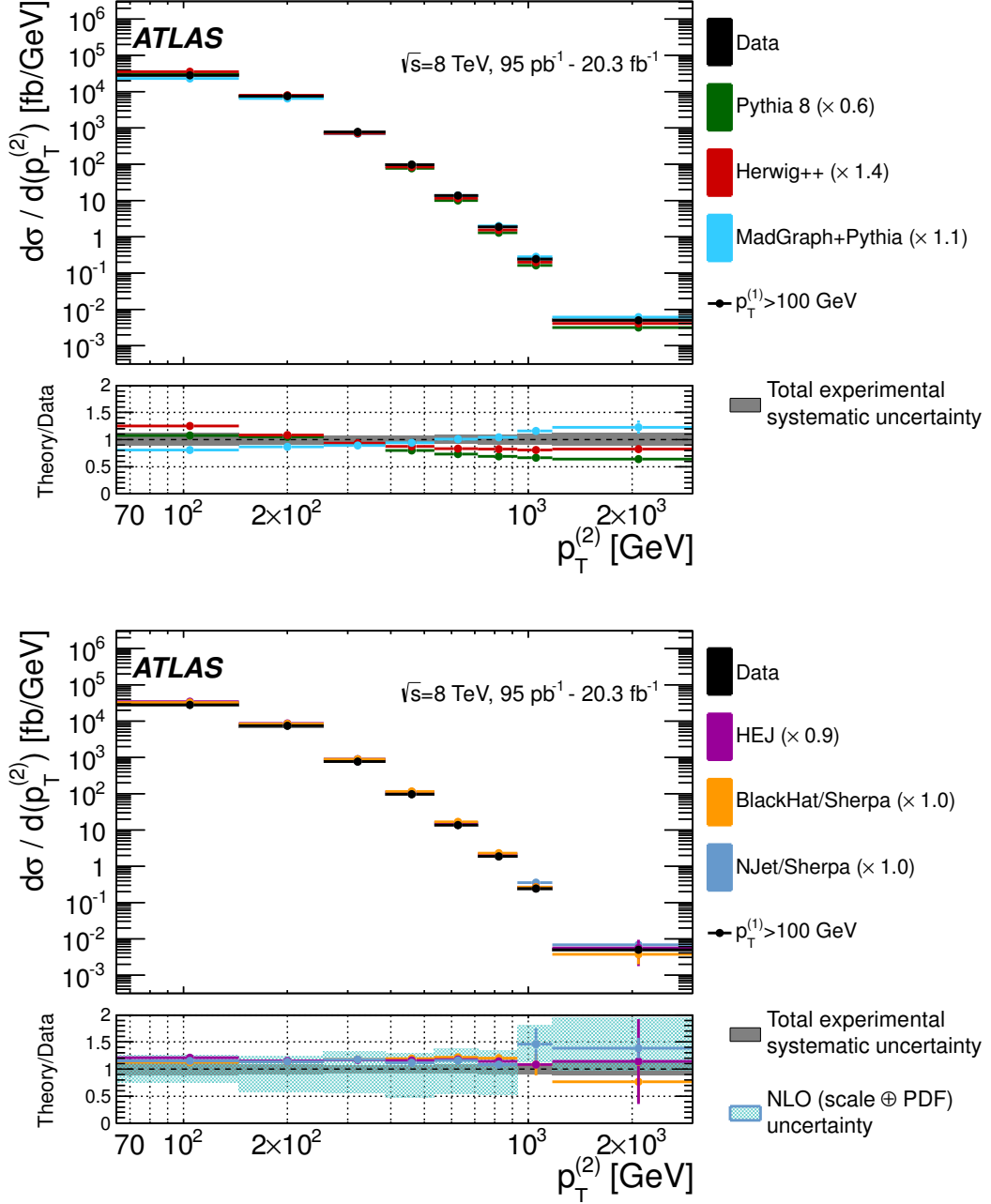


Figure 5: Unfolded four-jet differential cross section as a function of $p_T^{(2)}$, compared to different theoretical predictions. The other details are as for figure 4.

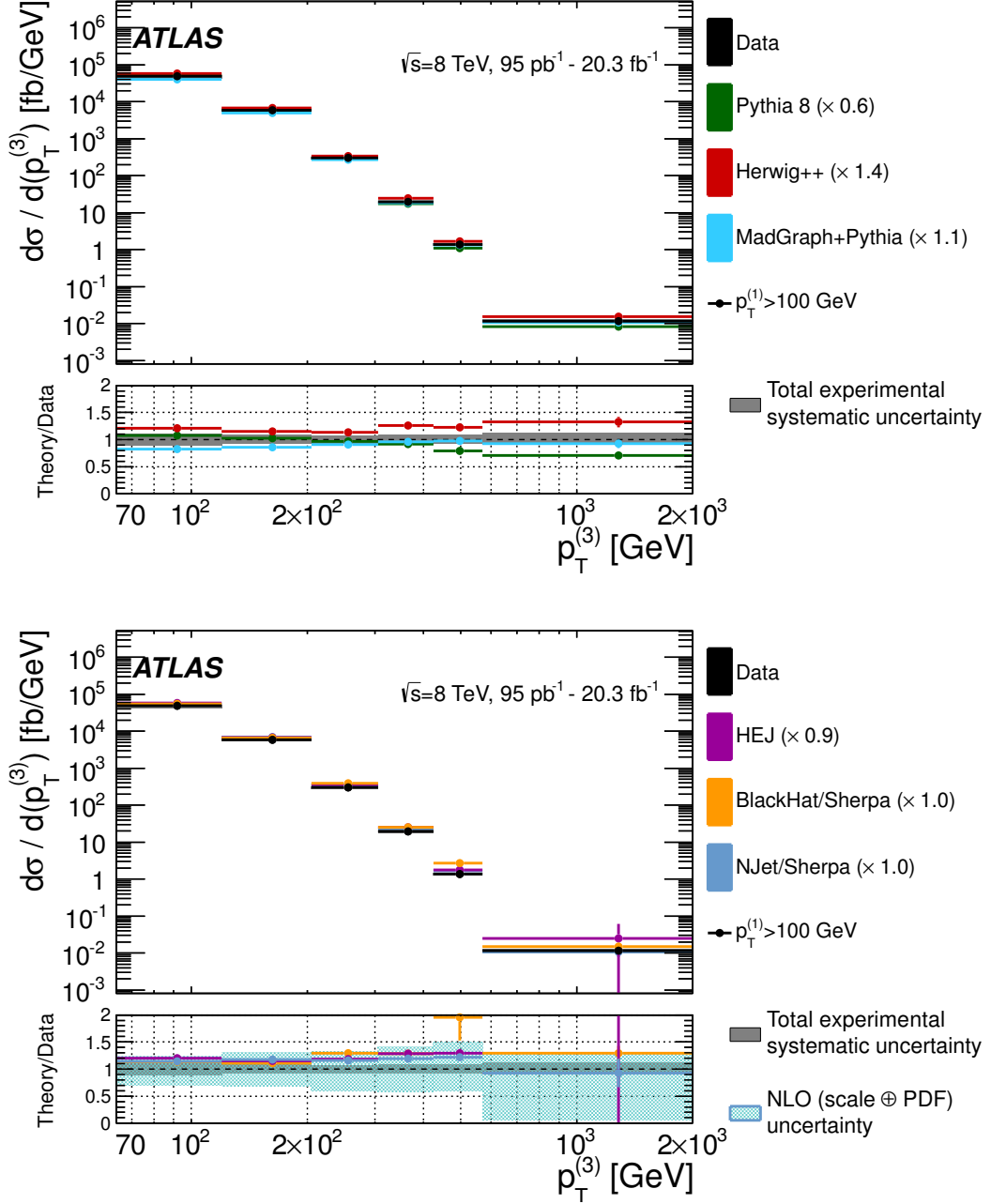


Figure 6: Unfolded four-jet differential cross section as a function of $p_T^{(3)}$, compared to different theoretical predictions. The other details are as for figure 4.

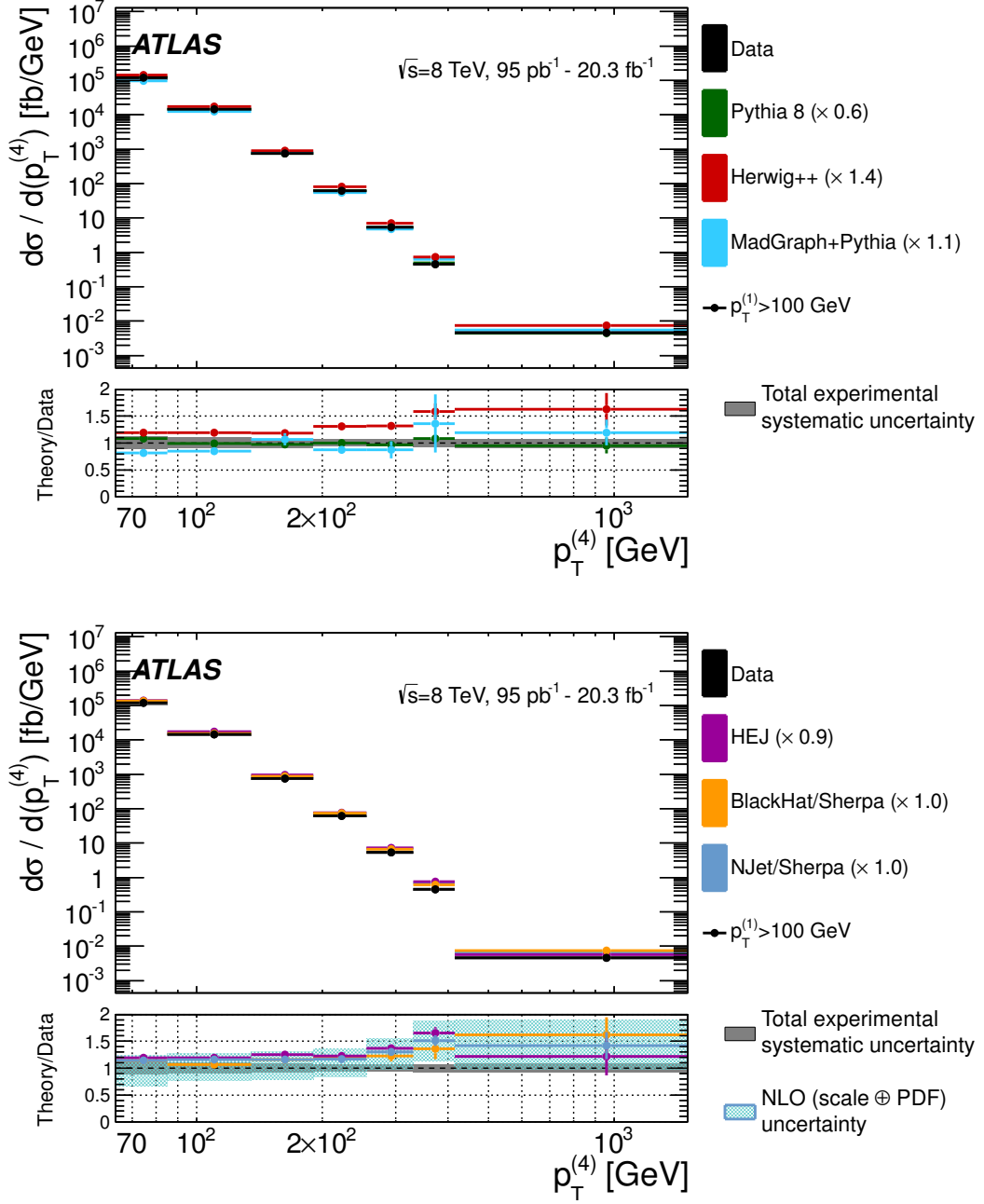


Figure 7: Unfolded four-jet differential cross section as a function of $p_T^{(4)}$, compared to different theoretical predictions. The other details are as for figure 4.

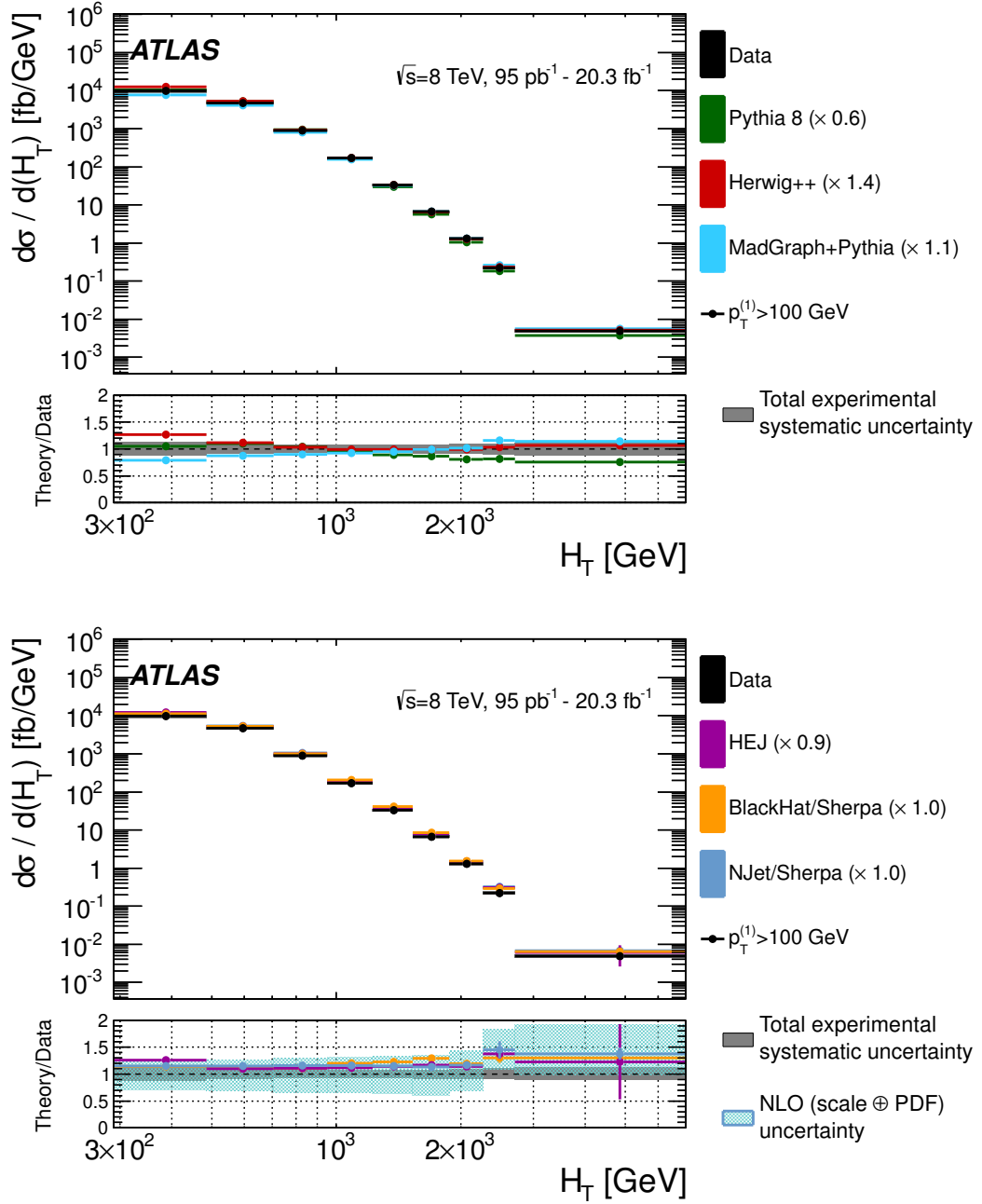


Figure 8: Unfolded four-jet differential cross section as a function of H_T , compared to different theoretical predictions. The other details are as for figure 4.

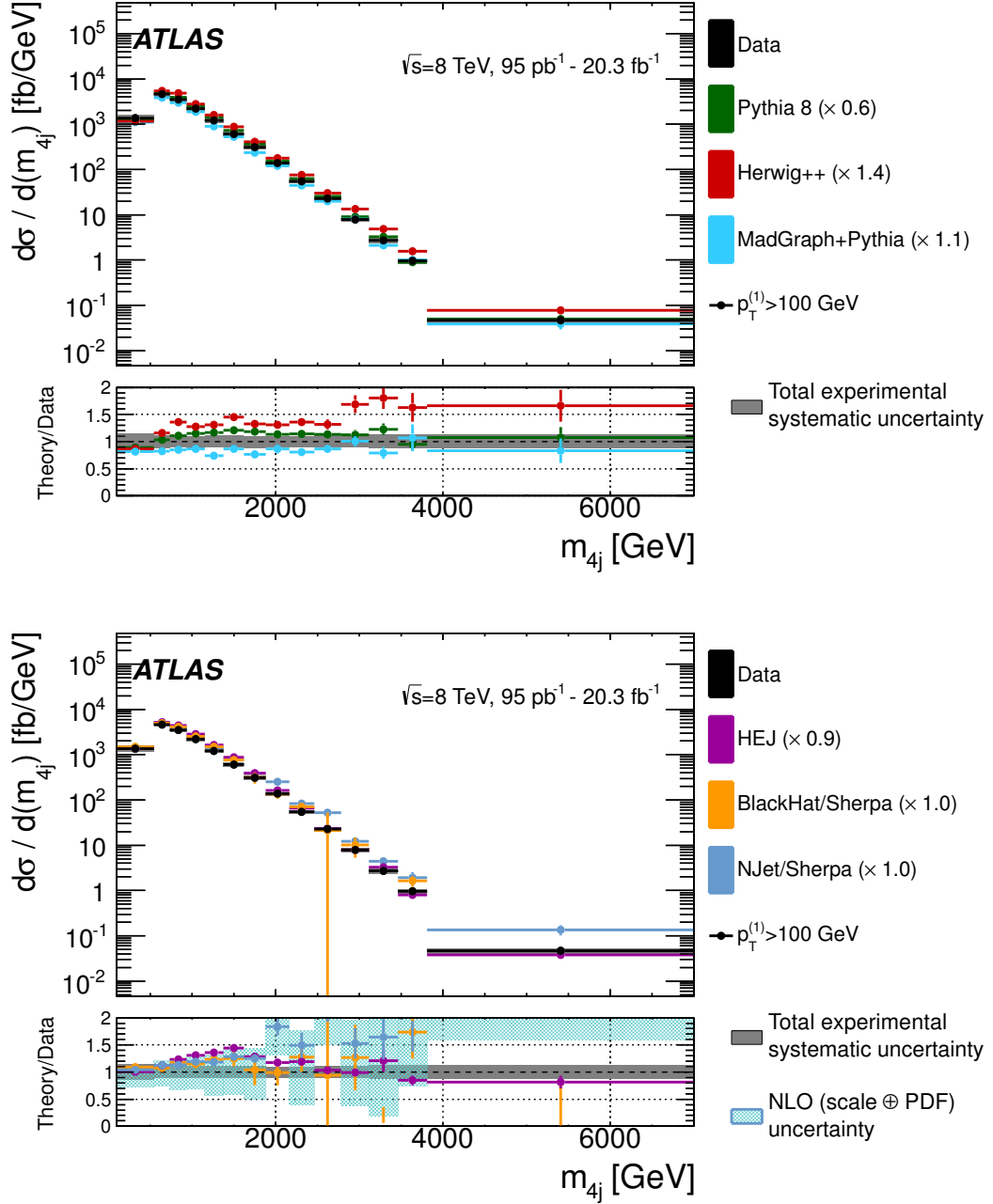


Figure 9: Unfolded four-jet differential cross section as a function of m_{4j} , compared to different theoretical predictions. The other details are as for figure 4. Some points in the ratio curves for NJET/SHERPA fall outside the y -axis range, and thus the NLO uncertainty is shown partially, or not shown, in these particular bins.

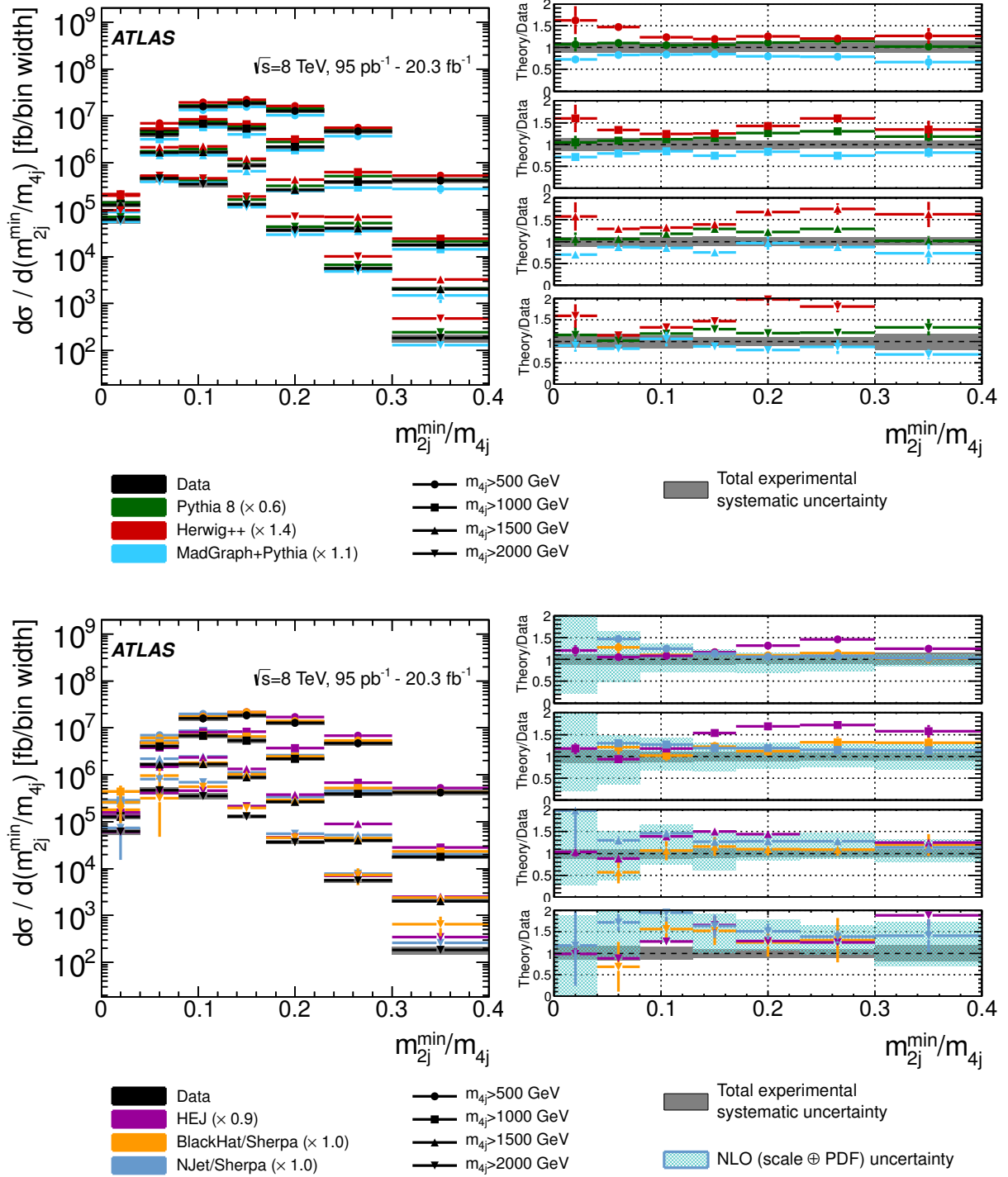


Figure 10: Unfolded four-jet differential cross section as a function of m_{2j}^{\min}/m_{4j} , compared to different theoretical predictions: PYTHIA, HERWIG++ and MADGRAPH+PYTHIA (top), and HEJ, NJET/SHERPA and BLACKHAT/SHERPA (bottom). For better comparison, the predictions are multiplied by the factors indicated in the legend. In each figure, the left panel shows the full spectra and the right panel the ratios of the different predictions to the data, divided according to the selection criterion applied to m_{4j} . The solid band represents the total experimental systematic uncertainty centred at one. The patterned band represents the NLO scale and PDF uncertainties calculated from NJET/SHERPA centred at the nominal NJET/SHERPA values. The scale uncertainties for HEJ (not drawn) are typically $+50\%$ -30% . The ratio curves are formed by the central values and vertical uncertainty lines resulting from the propagation of the statistical uncertainties of the predictions and those of the unfolded data spectrum.

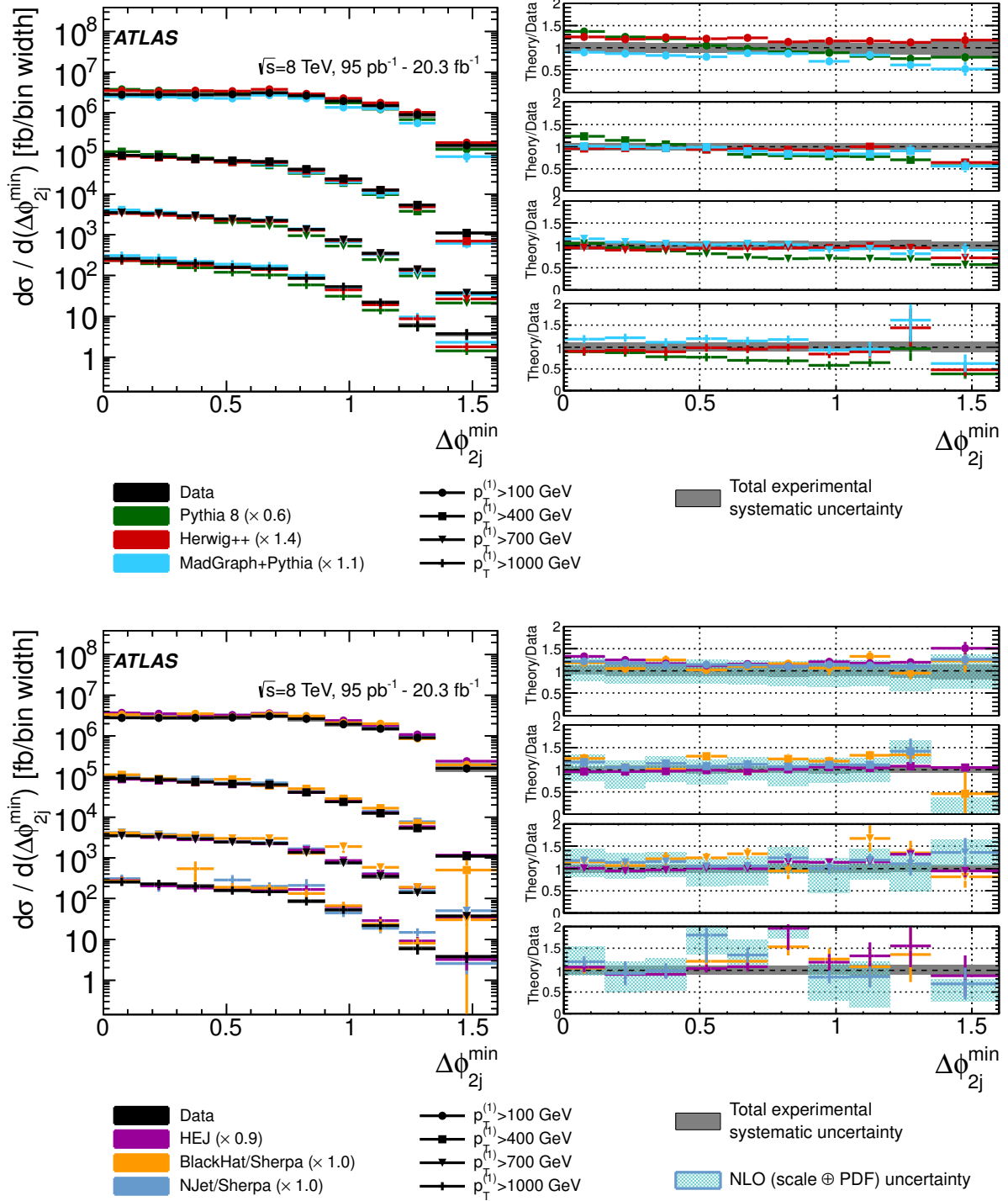


Figure 11: Unfolded four-jet differential cross section as a function of $\Delta\phi_{2j}^{\min}$, compared to different theoretical predictions. The other details are as for figure 10, but here the multiple ratio plots correspond to different selection criteria applied to $p_T^{(1)}$. Some points in the ratio curves for NJET/SHERPA fall outside the y -axis range, and thus the NLO uncertainty is shown partially, or not shown, in these particular bins.

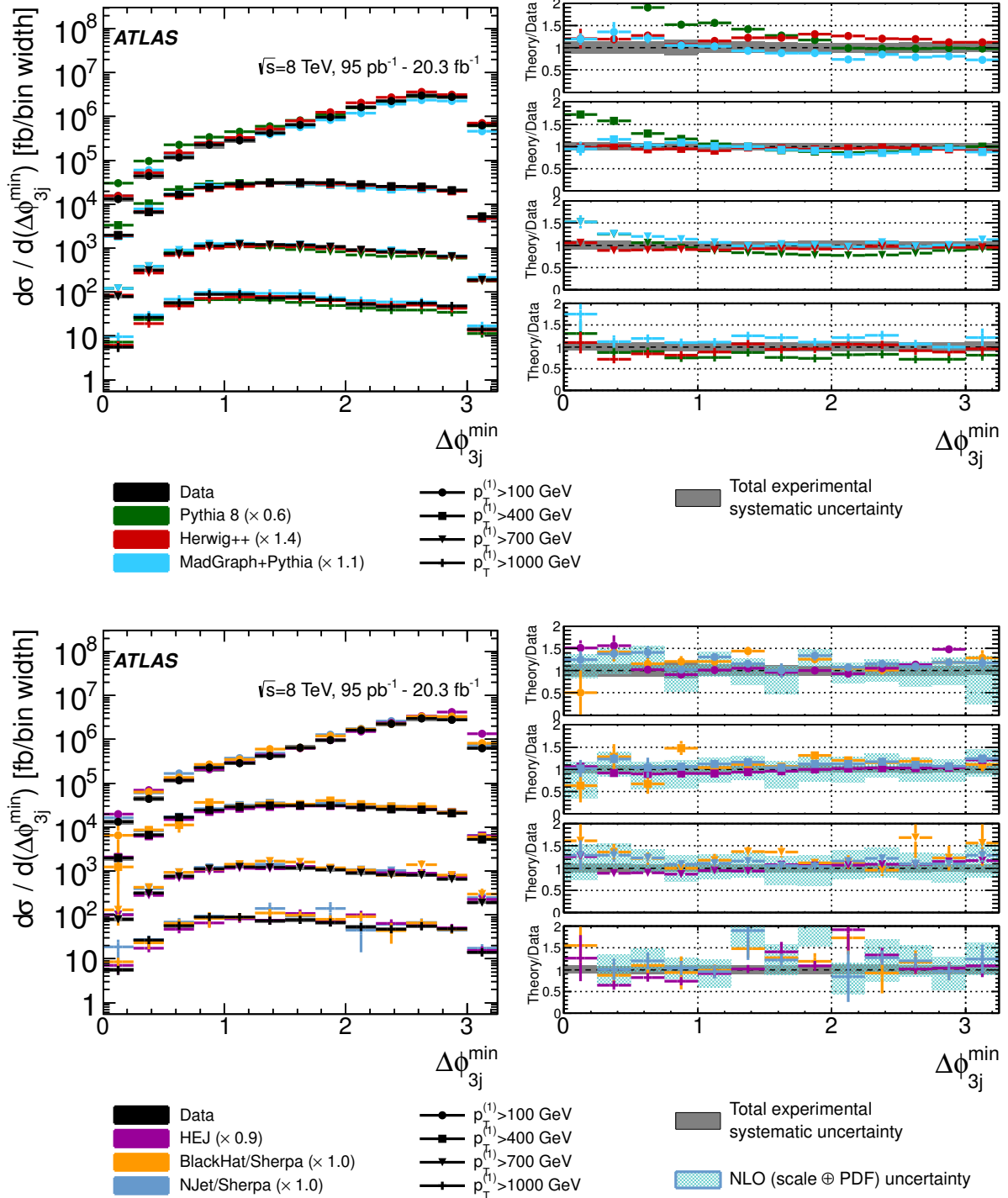


Figure 12: Unfolded four-jet differential cross section as a function of $\Delta\phi_{3j}^{\min}$, compared to different theoretical predictions. The other details are as for figure 11. Some points in the ratio curves for NJET/SHERPA fall outside the y -axis range, and thus the NLO uncertainty is shown partially, or not shown, in these particular bins.

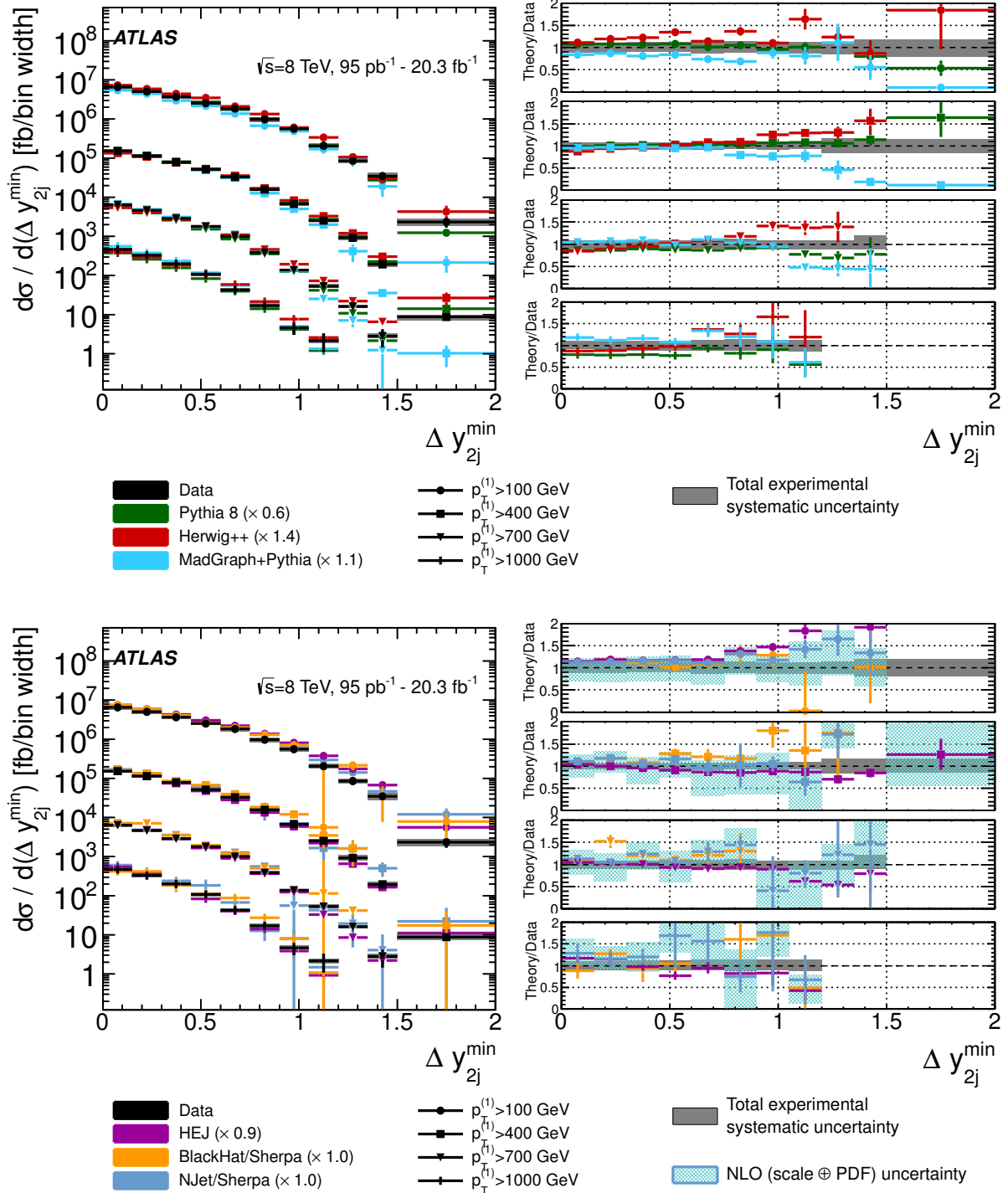


Figure 13: Unfolded four-jet differential cross section as a function of Δy_{2j}^{\min} , compared to different theoretical predictions. The other details are as for figure 11. Some points in the ratio curves for NJET/SHERPA fall outside the y -axis range, and thus the NLO uncertainty is shown partially, or not shown, in these particular bins.

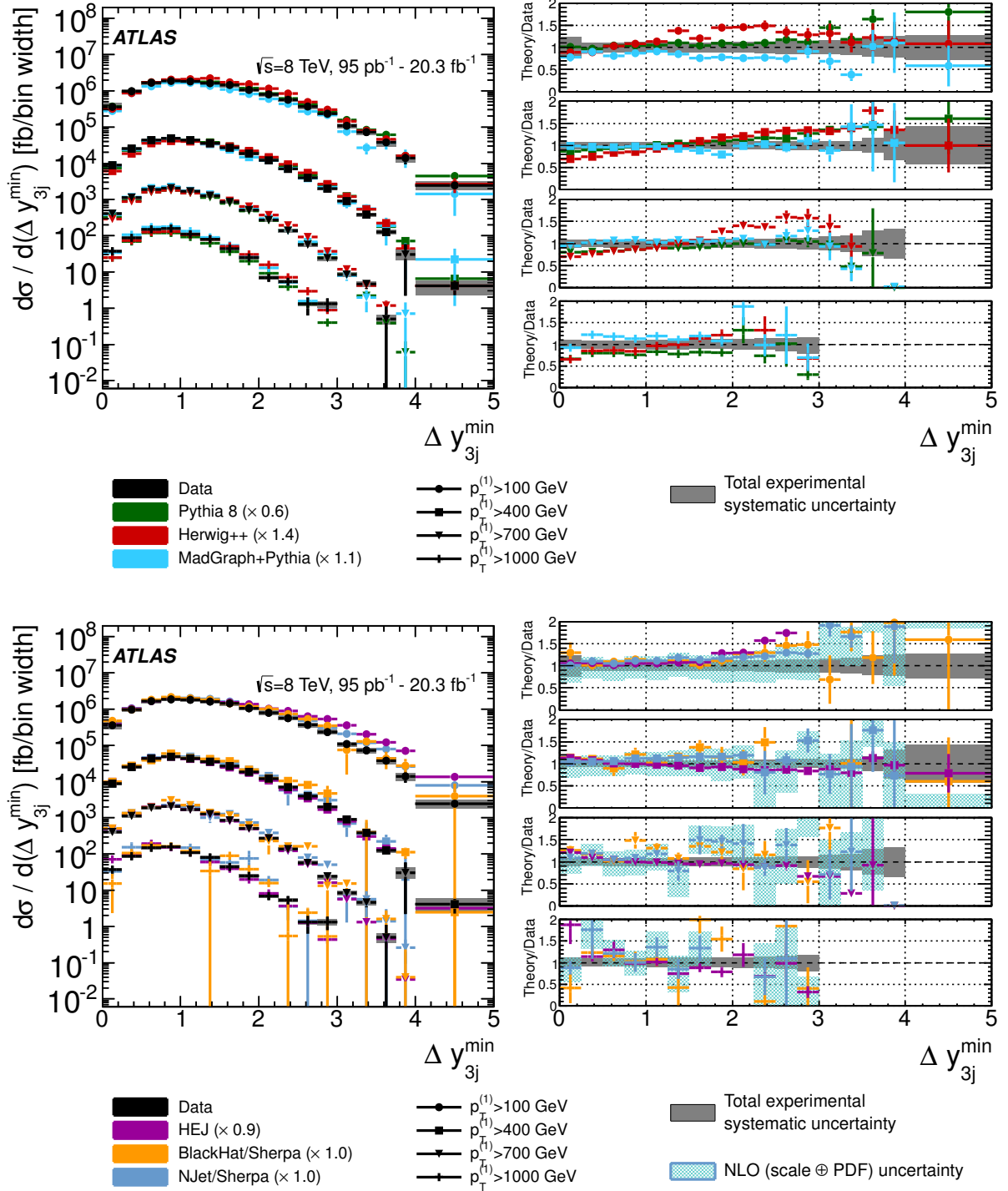


Figure 14: Unfolded four-jet differential cross section as a function of Δy_{3j}^{\min} , compared to different theoretical predictions. The other details are as for figure 11. Some points in the ratio curves for NJET/SHERPA fall outside the y -axis range, and thus the NLO uncertainty is shown partially, or not shown, in these particular bins.

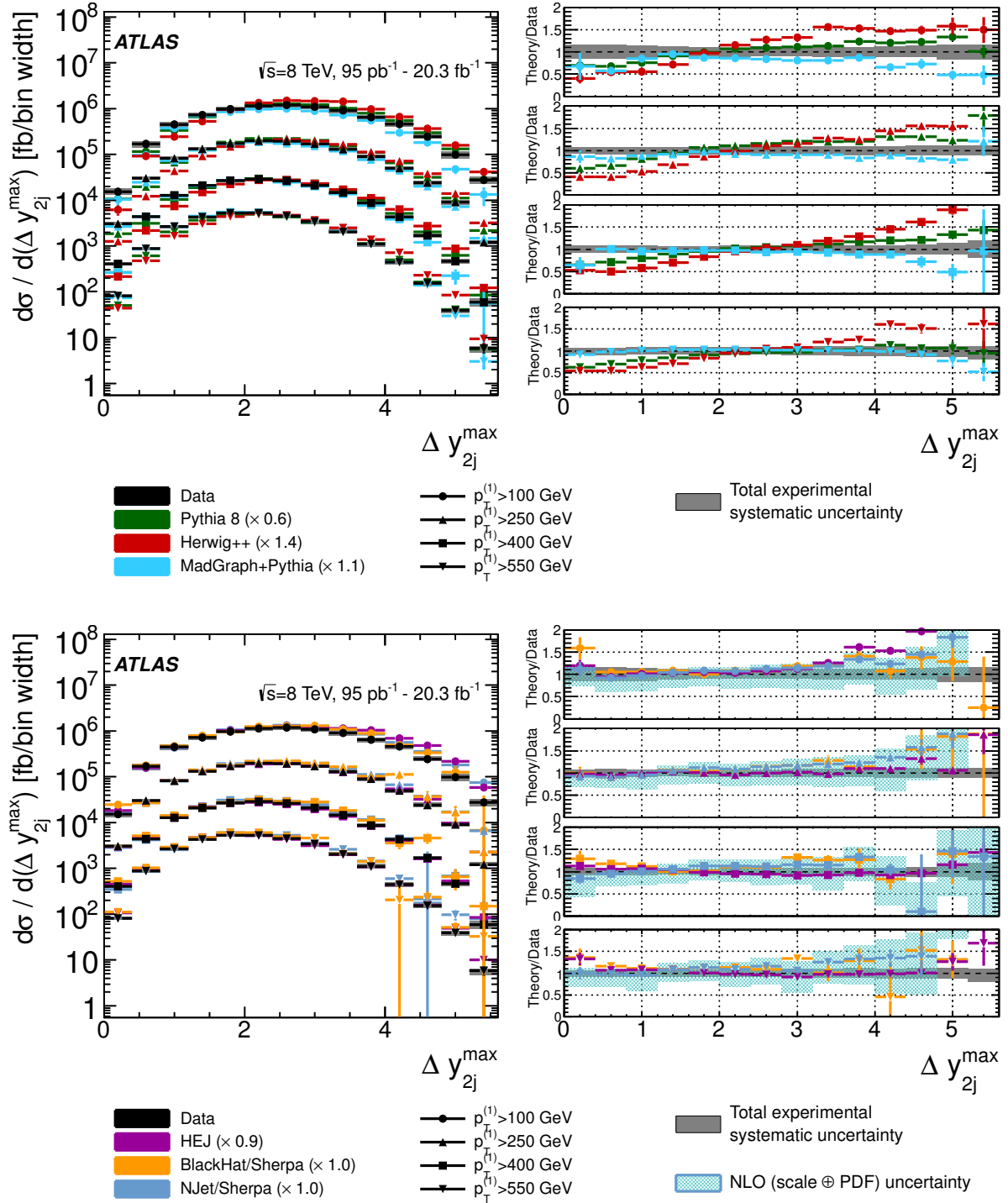


Figure 15: Unfolded four-jet differential cross section as a function of Δy_{2j}^{\max} , compared to different theoretical predictions. The other details are as for figure 11. Some points in the ratio curves for NJET/SHERPA fall outside the y -axis range, and thus the NLO uncertainty is shown partially, or not shown, in these particular bins.

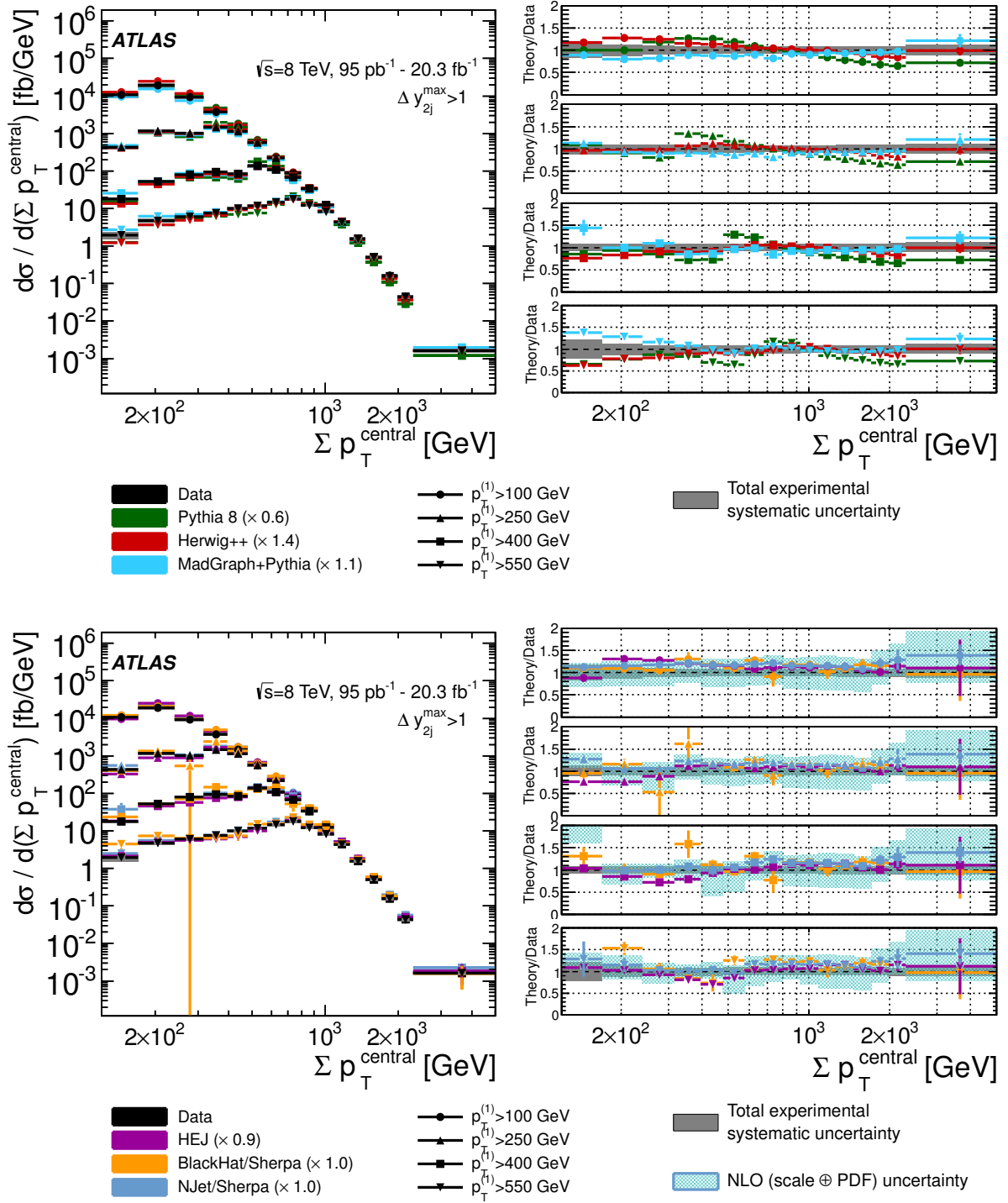


Figure 16: Unfolded four-jet differential cross section as a function of $\Sigma p_T^{\text{central}}$ with $\Delta y_{2j}^{\text{max}} > 1$, compared to different theoretical predictions. The other details are as for figure 11.

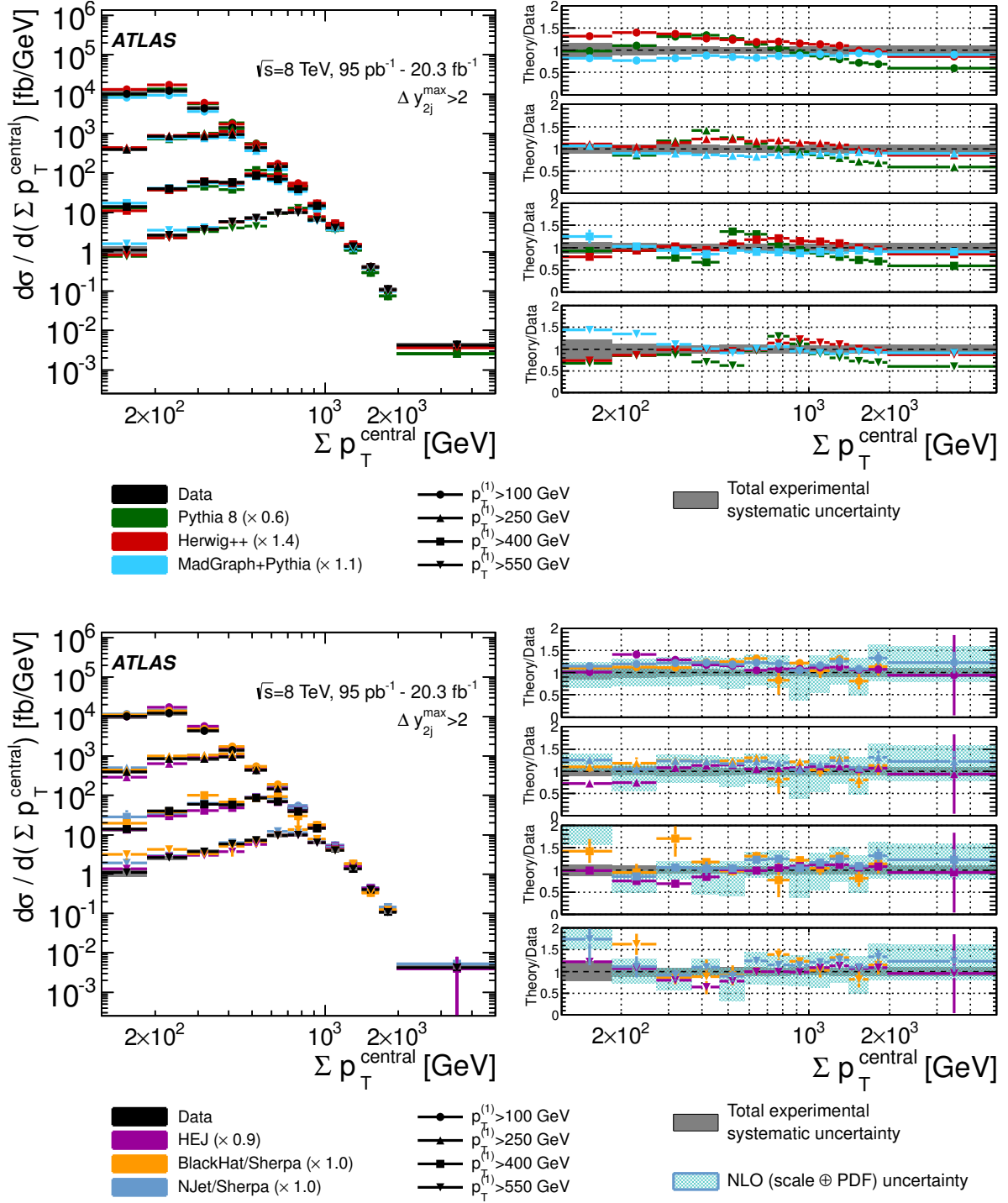


Figure 17: Unfolded four-jet differential cross section as a function of $\Sigma p_T^{\text{central}}$ with $\Delta y_{2j}^{\text{max}} > 2$, compared to different theoretical predictions. The other details are as for figure 11.

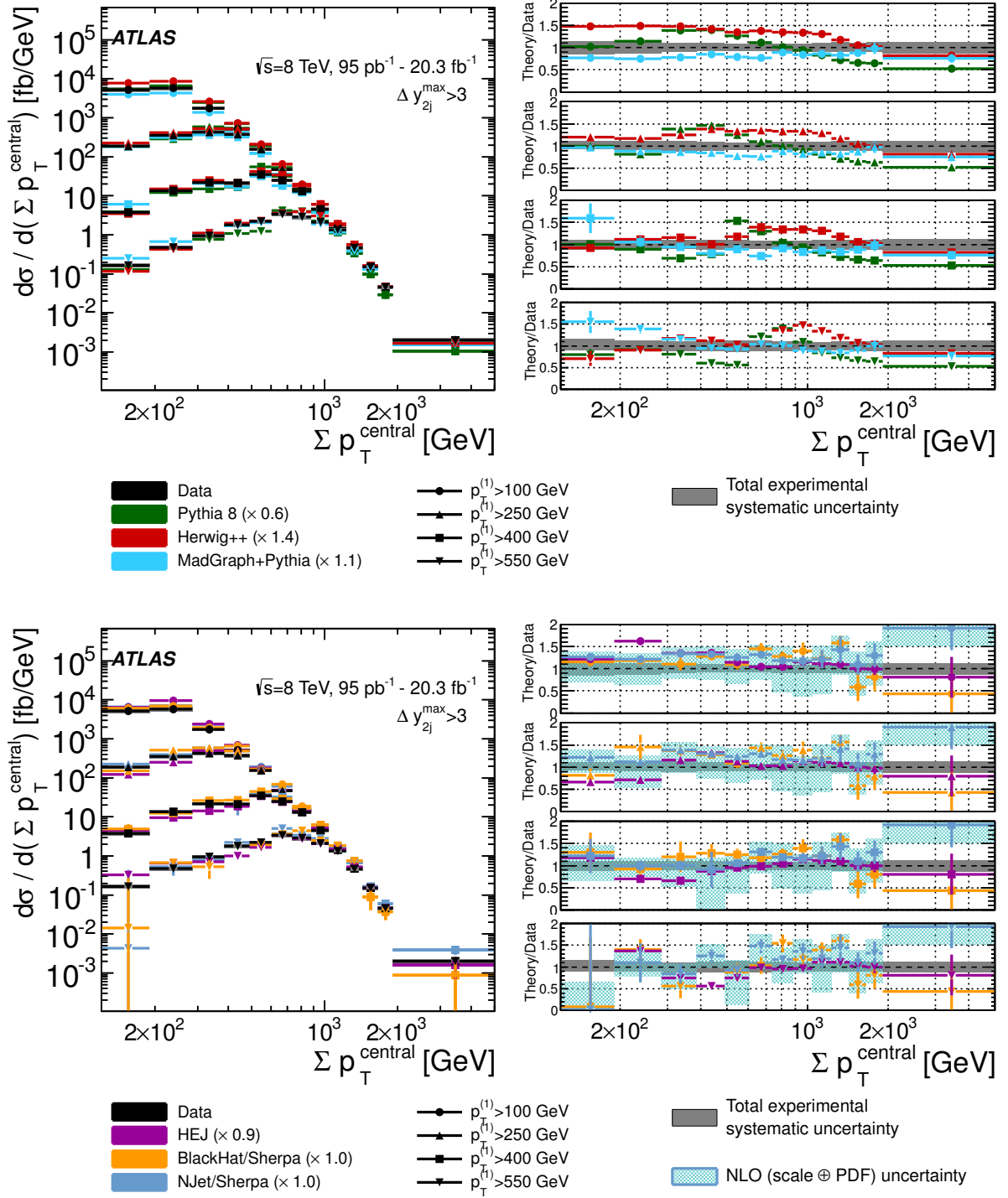


Figure 18: Unfolded four-jet differential cross section as a function of $\Sigma p_{\text{T}}^{\text{central}}$ with $\Delta y_{2j}^{\text{max}} > 3$, compared to different theoretical predictions. The other details are as for figure 11.

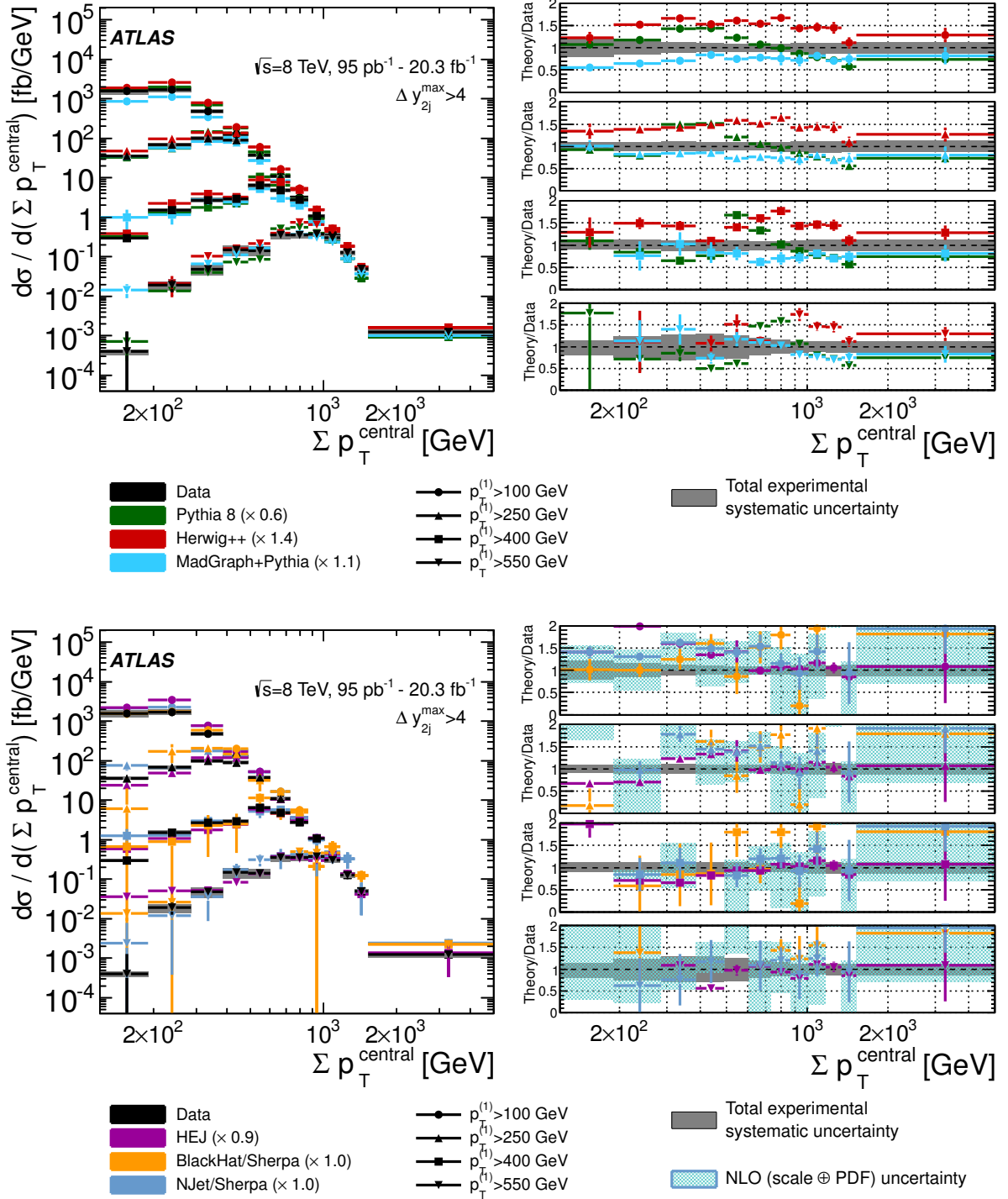


Figure 19: Unfolded four-jet differential cross section as a function of $\Sigma p_T^{\text{central}}$ with $\Delta y_{2j}^{\text{max}} > 4$, compared to different theoretical predictions. The other details are as for figure 11. Some points in the ratio curves for NJET/SHERPA fall outside the y -axis range, and thus the NLO uncertainty is shown partially, or not shown, in these particular bins.

10. Conclusion

This paper presents unfolded differential cross sections of events with at least four jets in pp collisions at 8 TeV centre-of-mass energy. The cross sections are studied as a function of a variety of kinematic and topological variables which include momenta, masses and angles. Events are selected if the four anti- k_t $R = 0.4$ jets with the largest transverse momentum within the rapidity range $|y| < 2.8$ are well separated ($\Delta R_{4j}^{\min} > 0.65$), all have $p_T > 64$ GeV, and include at least one jet with $p_T > 100$ GeV. The results are obtained from the analysis of the full dataset collected by the ATLAS detector at the LHC in 2012, which corresponds to a total integrated luminosity of 20.3 fb^{-1} . The total experimental systematic uncertainty is typically of the order of 10%, and it is dominated by the jet energy scale calibration uncertainty.

The measurements are compared to NLO p QCD predictions provided by BLACKHAT/SHERPA and NJET/SHERPA, as well as the all-orders calculation provided by HEJ. Three leading-order calculations are also considered, including two $2 \rightarrow 2$ PS samples (PYTHIA and HERWIG++) and a multi-leg calculation with up to four partons in the ME matched to a PS generated by PYTHIA (MADGRAPH+PYTHIA).

The LO cross sections and HEJ are normalised by fixed factors to facilitate the comparison of the spectra in the kinematic regions of interest; these factors vary between 0.6 and 1.4 for the different samples, where the MADGRAPH+PYTHIA and HEJ samples are the ones that need the smallest corrections. The NLO predictions, BLACKHAT/SHERPA and NJET/SHERPA, are almost always compatible with the data within their theoretical uncertainties, which are found to be large ($O(30\%)$ at low momenta) and asymmetric. Within the normalisation scheme used, MADGRAPH+PYTHIA also provides a good description of the data, as does HEJ, especially at high leading jet p_T . The $2 \rightarrow 2$ PS calculations generally describe the data relatively poorly, although they are found to provide good predictions in some particular cases: PYTHIA gives a very good prediction of $p_T^{(4)}$ and Δy_{2j}^{\min} , while HERWIG++ performs well in the azimuthal angle variables.

Looking at the individual distributions of the differential cross section, the description of the jet momenta is compatible with previous measurements of the multi-jet cross sections. It should be noted that HEJ, NJET/SHERPA and BLACKHAT/SHERPA give a very good description of the distributions of the leading jets but show some discrepancy with the data for $p_T^{(4)}$. For variables that are particularly sensitive to wide-angle configurations and high- p_T radiation, such as masses or angles, BLACKHAT/SHERPA, NJET/SHERPA and MADGRAPH+PYTHIA do a remarkable job overall. HEJ also provides a good description of the data, the main exception being that it disagrees with the rapidity measurements in events with low $p_T^{(1)}$. At high $p_T^{(1)}$ the prediction is very good. These measurements expose the shortcomings of $2 \rightarrow 2$ parton ME+PS predictions in a variety of scenarios and highlight the importance of the more sophisticated calculations.

Acknowledgements

We thank CERN for the very successful operation of the LHC, as well as the support staff from our institutions without whom ATLAS could not be operated efficiently.

We acknowledge the support of ANPCyT, Argentina; YerPhI, Armenia; ARC, Australia; BMWFW and FWF, Austria; ANAS, Azerbaijan; SSTC, Belarus; CNPq and FAPESP, Brazil; NSERC, NRC and CFI, Canada; CERN; CONICYT, Chile; CAS, MOST and NSFC, China; COLCIENCIAS, Colombia; MSMT CR, MPO CR and VSC CR, Czech Republic; DNRF, DNSRC and Lundbeck Foundation, Denmark; IN2P3-CNRS, CEA-DSM/IRFU, France; GNSF, Georgia; BMBF, HGF, and MPG, Germany; GSRT, Greece; RGC, Hong Kong SAR, China; ISF, I-CORE and Benoziyo Center, Israel; INFN, Italy;

MEXT and JSPS, Japan; CNRST, Morocco; FOM and NWO, Netherlands; RCN, Norway; MNiSW and NCN, Poland; FCT, Portugal; MNE/IFA, Romania; MES of Russia and NRC KI, Russian Federation; JINR; MESTD, Serbia; MSSR, Slovakia; ARRS and MIZŠ, Slovenia; DST/NRF, South Africa; MINECO, Spain; SRC and Wallenberg Foundation, Sweden; SERI, SNSF and Cantons of Bern and Geneva, Switzerland; MOST, Taiwan; TAEK, Turkey; STFC, United Kingdom; DOE and NSF, United States of America. In addition, individual groups and members have received support from BCKDF, the Canada Council, CANARIE, CRC, Compute Canada, FQRNT, and the Ontario Innovation Trust, Canada; EPLANET, ERC, FP7, Horizon 2020 and Marie Skłodowska-Curie Actions, European Union; Investissements d'Avenir Labex and Idex, ANR, Region Auvergne and Fondation Partager le Savoir, France; DFG and AvH Foundation, Germany; Herakleitos, Thales and Aristeia programmes co-financed by EU-ESF and the Greek NSRF; BSF, GIF and Minerva, Israel; BRF, Norway; the Royal Society and Leverhulme Trust, United Kingdom.

The crucial computing support from all WLCG partners is acknowledged gratefully, in particular from CERN and the ATLAS Tier-1 facilities at TRIUMF (Canada), NDGF (Denmark, Norway, Sweden), CC-IN2P3 (France), KIT/GridKA (Germany), INFN-CNAF (Italy), NL-T1 (Netherlands), PIC (Spain), ASGC (Taiwan), RAL (UK) and BNL (USA) and in the Tier-2 facilities worldwide.

A. Tables of the measured cross sections

| Bin | Bin edges [GeV] | $d\sigma/d(p_T^{(1)})$ [fb/GeV] | $\delta_{\text{stat}}^{\text{data}}$ [%] | $\delta_{\text{stat}}^{\text{MC}}$ [%] | u_{JES} [%] | u_{JER} [%] | u_{unfold} [%] | u_{lumi} [%] |
|-----|-----------------|---------------------------------|--|--|----------------------|----------------------|-------------------------|-----------------------|
| 1 | 100–155 | 2.62×10^4 | 0.3 | 1.4 | +9.7 -8.7 | 5.2 | 8.4 | 2.8 |
| 2 | 155–235 | 1.47×10^4 | 0.3 | 0.6 | +8.2 -7.8 | 2.8 | 6.4 | 2.8 |
| 3 | 235–325 | 4.89×10^3 | 0.4 | 0.4 | +6.7 -6.7 | 1.5 | 4.3 | 2.8 |
| 4 | 325–420 | 1.35×10^3 | < 0.1 | 0.3 | +6.0 -6.0 | 1.2 | 2.5 | 2.8 |
| 5 | 420–530 | 3.56×10^2 | 0.1 | 0.2 | +6.4 -6.0 | 1.1 | 1.6 | 2.8 |
| 6 | 530–650 | 9.2×10^1 | 0.2 | 0.3 | +7.0 -6.3 | 1.3 | 1.4 | 2.8 |
| 7 | 650–790 | 2.26×10^1 | 0.4 | 0.3 | +7.5 -7.5 | 1.5 | 1.3 | 2.8 |
| 8 | 790–950 | 5.34 | 0.8 | 0.2 | +8.1 -7.8 | 1.7 | 1.4 | 2.8 |
| 9 | 950–1130 | 1.19 | 2.1 | 0.2 | +8.6 -8.7 | 1.8 | 1.5 | 2.8 |
| 10 | 1130–1350 | 2.27×10^{-1} | 3.8 | 0.3 | +9.7 -9.0 | 2.0 | 1.7 | 2.8 |
| 11 | 1350–1630 | 3.40×10^{-2} | 9.1 | 0.3 | +11.7 -10.7 | 2.1 | 1.8 | 2.8 |
| 12 | 1630–4000 | 6.31×10^{-4} | 21.9 | 0.4 | +14.5 -13.2 | 2.5 | 1.9 | 2.8 |

Table 4: Measured differential four-jet cross section for $R = 0.4$ jets, in bins of $p_T^{(1)}$, along with the uncertainties in the measurement. The events are selected using the inclusive analysis cuts. All uncertainties are given in %. $\delta_{\text{stat}}^{\text{data}}$ ($\delta_{\text{stat}}^{\text{MC}}$) are the statistical uncertainties due to the number of data (MC simulation) events. The other columns correspond to the experimental systematic uncertainties arising from JES, JER, unfolding and luminosity, respectively.

| Bin | Bin edges [GeV] | $d\sigma/d(p_T^{(2)})$ [fb/GeV] | $\delta_{\text{stat}}^{\text{data}}$ [%] | $\delta_{\text{stat}}^{\text{MC}}$ [%] | u_{JES} [%] | u_{JER} [%] | u_{unfold} [%] | u_{lumi} [%] |
|-----|-----------------|---------------------------------|--|--|----------------------|----------------------|-------------------------|-----------------------|
| 1 | 64–145 | 2.85×10^4 | 0.2 | 0.8 | +8.6 -8.1 | 3.7 | 6.4 | 2.8 |
| 2 | 145–255 | 7.43×10^3 | 0.3 | 0.4 | +7.5 -7.1 | 1.7 | 4.2 | 2.8 |
| 3 | 255–385 | 7.61×10^2 | 0.4 | 0.3 | +6.6 -6.8 | 0.8 | 2.5 | 2.8 |
| 4 | 385–535 | 9.71×10^1 | 0.2 | 0.3 | +6.7 -6.9 | 0.7 | 2.0 | 2.8 |
| 5 | 535–715 | 1.36×10^1 | 0.6 | 0.3 | +7.5 -7.5 | 0.8 | 2.1 | 2.8 |
| 6 | 715–930 | 1.88 | 1.2 | 0.3 | +8.4 -8.1 | 0.9 | 2.3 | 2.8 |
| 7 | 930–1175 | 2.44×10^{-1} | 3.1 | 0.4 | +9.3 -8.5 | 1.0 | 2.4 | 2.8 |
| 8 | 1175–3000 | 4.91×10^{-3} | 9.2 | 0.4 | +11.4 -10.5 | 1.0 | 2.4 | 2.8 |

Table 5: Measured differential four-jet cross section for $R = 0.4$ jets, in bins of $p_T^{(2)}$, along with the uncertainties in the measurement. The events are selected using the inclusive analysis cuts. All other details are as for table 4.

| Bin | Bin edges [GeV] | $d\sigma/d(p_T^{(3)})$ [fb/GeV] | $\delta_{\text{stat}}^{\text{data}}$ [%] | $\delta_{\text{stat}}^{\text{MC}}$ [%] | u_{JES} [%] | u_{JER} [%] | u_{unfold} [%] | u_{lumi} [%] |
|-----|-----------------|---------------------------------|--|--|----------------------|----------------------|-------------------------|-----------------------|
| 1 | 64–120 | 4.85×10^4 | 0.2 | 0.7 | +8.6 -8.0 | 3.4 | 5.8 | 2.8 |
| 2 | 120–205 | 5.87×10^3 | 0.3 | 0.6 | +7.3 -7.5 | 1.3 | 2.9 | 2.8 |
| 3 | 205–305 | 3.0×10^2 | 0.6 | 0.7 | +7.0 -6.8 | 0.4 | 1.7 | 2.8 |
| 4 | 305–425 | 1.94×10^1 | 0.5 | 0.8 | +7.4 -6.7 | 0.3 | 1.9 | 2.8 |
| 5 | 425–570 | 1.39 | 1.9 | 1.1 | +7.8 -7.3 | 0.2 | 2.1 | 2.8 |
| 6 | 570–2000 | 1.16×10^{-2} | 6.4 | 1.3 | +10.8 -8.7 | 0.2 | 2.7 | 2.8 |

Table 6: Measured differential four-jet cross section for $R = 0.4$ jets, in bins of $p_T^{(3)}$, along with the uncertainties in the measurement. The events are selected using the inclusive analysis cuts. All other details are as for table 4.

| Bin | Bin edges [GeV] | $d\sigma/d(p_T^{(4)})$ [fb/GeV] | $\delta_{\text{stat}}^{\text{data}}$ [%] | $\delta_{\text{stat}}^{\text{MC}}$ [%] | u_{JES} [%] | u_{JER} [%] | u_{unfold} [%] | u_{lumi} [%] |
|-----|-----------------|---------------------------------|--|--|----------------------|----------------------|-------------------------|-----------------------|
| 1 | 64–85 | 1.18×10^5 | 0.2 | 0.7 | +8.7 -8.0 | 3.6 | 7.0 | 2.8 |
| 2 | 85–135 | 1.45×10^4 | < 0.1 | 0.8 | +8.7 -8.1 | 2.9 | 3.1 | 2.8 |
| 3 | 135–190 | 7.65×10^2 | 0.1 | 1.1 | +7.0 -7.2 | 1.4 | 1.5 | 2.8 |
| 4 | 190–255 | 6.24×10^1 | 0.4 | 2.2 | +5.8 -5.9 | 0.8 | 1.9 | 2.8 |
| 5 | 255–330 | 5.37 | 1.2 | 3.4 | +5.6 -5.8 | 0.7 | 2.1 | 2.8 |
| 6 | 330–415 | 4.58×10^{-1} | 3.7 | 4.3 | +6.1 -6.8 | 0.7 | 2.1 | 2.8 |
| 7 | 415–1500 | 4.65×10^{-3} | 11.9 | 6.4 | +6.3 -7.5 | 0.7 | 2.1 | 2.8 |

Table 7: Measured differential four-jet cross section for $R = 0.4$ jets, in bins of $p_T^{(4)}$, along with the uncertainties in the measurement. The events are selected using the inclusive analysis cuts. All other details are as for table 4.

| Bin | Bin edges [GeV] | $d\sigma/d(H_T)$ [fb/GeV] | $\delta_{\text{stat}}^{\text{data}}$ [%] | $\delta_{\text{stat}}^{\text{MC}}$ [%] | u_{JES} [%] | u_{JER} [%] | u_{unfold} [%] | u_{lumi} [%] |
|-----|-----------------|---------------------------|--|--|----------------------|----------------------|-------------------------|-----------------------|
| 1 | 290–485 | 9.85×10^3 | 0.2 | 1.0 | +8.8 -8.3 | 4.0 | 7.8 | 2.8 |
| 2 | 485–705 | 4.73×10^3 | 0.3 | 0.4 | +7.7 -7.3 | 1.7 | 4.6 | 2.8 |
| 3 | 705–950 | 9.0×10^2 | 0.3 | 0.3 | +6.7 -6.7 | 0.7 | 2.2 | 2.8 |
| 4 | 950–1225 | 1.7×10^2 | 0.1 | 0.2 | +6.6 -6.6 | 0.6 | 1.5 | 2.8 |
| 5 | 1225–1530 | 3.35×10^1 | 0.2 | 0.3 | +6.8 -7.0 | 0.6 | 1.5 | 2.8 |
| 6 | 1530–1875 | 6.62 | 0.6 | 0.2 | +7.3 -7.7 | 0.7 | 1.5 | 2.8 |
| 7 | 1875–2265 | 1.29 | 1.1 | 0.3 | +8.3 -8.2 | 0.8 | 1.7 | 2.8 |
| 8 | 2265–2705 | 2.23×10^{-1} | 2.8 | 0.3 | +9.3 -8.4 | 0.8 | 1.6 | 2.8 |
| 9 | 2705–7000 | 4.88×10^{-3} | 6.4 | 0.3 | +10.9 -10.6 | 1.1 | 1.6 | 2.8 |

Table 8: Measured differential four-jet cross section for $R = 0.4$ jets, in bins of H_T , along with the uncertainties in the measurement. The events are selected using the inclusive analysis cuts. All other details are as for table 4.

| Bin | Bin edges [GeV] | $d\sigma/d(m_{4j})$ [fb/GeV] | $\delta_{\text{stat}}^{\text{data}}$ [%] | $\delta_{\text{stat}}^{\text{MC}}$ [%] | u_{JES} [%] | u_{JER} [%] | u_{unfold} [%] | u_{lumi} [%] |
|-----|-----------------|------------------------------|--|--|----------------------|----------------------|-------------------------|-----------------------|
| 1 | 100–545 | 1.36×10^3 | 0.5 | 2.7 | +8.8 -7.9 | 5.6 | 9.5 | 2.8 |
| 2 | 545–735 | 4.66×10^3 | 0.4 | 1.4 | +8.3 -7.9 | 3.5 | 6.4 | 2.8 |
| 3 | 735–935 | 3.55×10^3 | 0.4 | 1.2 | +8.7 -8.3 | 3.0 | 5.0 | 2.8 |
| 4 | 935–1150 | 2.2×10^3 | 0.4 | 1.6 | +8.7 -9.1 | 2.4 | 4.4 | 2.8 |
| 5 | 1150–1375 | 1.22×10^3 | 0.6 | 1.6 | +9.8 -9.2 | 2.1 | 3.9 | 2.8 |
| 6 | 1375–1620 | 6.09×10^2 | 0.6 | 1.7 | +10.0 -9.1 | 2.1 | 2.9 | 2.8 |
| 7 | 1620–1880 | 3.09×10^2 | 0.7 | 2.2 | +9.0 -9.6 | 2.1 | 2.6 | 2.8 |
| 8 | 1880–2160 | 1.37×10^2 | 1.0 | 2.2 | +8.3 -9.3 | 2.1 | 2.6 | 2.8 |
| 9 | 2160–2460 | 5.53×10^1 | 1.4 | 2.7 | +8.5 -9.0 | 2.1 | 3.1 | 2.8 |
| 10 | 2460–2780 | 2.28×10^1 | 2.0 | 3.0 | +8.8 -8.7 | 2.1 | 4.5 | 2.8 |
| 11 | 2780–3115 | 7.97 | 3.3 | 5.0 | +9.1 -8.8 | 2.1 | 5.3 | 2.8 |
| 12 | 3115–3460 | 2.71 | 3.0 | 4.9 | +10.2 -9.2 | 2.1 | 5.8 | 2.8 |
| 13 | 3460–3810 | 9.55×10^{-1} | 8.4 | 5.5 | +10.6 -9.4 | 2.1 | 6.0 | 2.8 |
| 14 | 3810–7000 | 4.66×10^{-2} | 12.4 | 6.9 | +11.6 -9.4 | 2.1 | 6.0 | 2.8 |

Table 9: Measured differential four-jet cross section for $R = 0.4$ jets, in bins of m_{4j} , along with the uncertainties in the measurement. The events are selected using the inclusive analysis cuts. All other details are as for table 4.

| Bin | Bin edges | $d\sigma/d(m_{2j}^{\min}/m_{4j})$ [fb] | $\delta_{\text{stat}}^{\text{data}}$ [%] | $\delta_{\text{stat}}^{\text{MC}}$ [%] | u_{JES} [%] | u_{JER} [%] | u_{unfold} [%] | u_{lumi} [%] |
|-----|-----------|--|--|--|----------------------|----------------------|-------------------------|-----------------------|
| 1 | 0–0.04 | 1.31×10^5 | 4.7 | 9.8 | $^{+9.5}_{-7.8}$ | 3.3 | 7.0 | 2.8 |
| 2 | 0.04–0.08 | 4.74×10^6 | 0.7 | 2.5 | $^{+9.5}_{-8.1}$ | 3.3 | 7.0 | 2.8 |
| 3 | 0.08–0.13 | 1.58×10^7 | 0.3 | 1.4 | $^{+8.7}_{-8.5}$ | 3.3 | 7.0 | 2.8 |
| 4 | 0.13–0.17 | 1.85×10^7 | 0.3 | 1.3 | $^{+9.4}_{-9.6}$ | 3.3 | 6.0 | 2.8 |
| 5 | 0.17–0.23 | 1.29×10^7 | 0.4 | 1.4 | $^{+8.5}_{-8.1}$ | 3.3 | 4.0 | 2.8 |
| 6 | 0.23–0.3 | 4.69×10^6 | 0.5 | 2.5 | $^{+7.7}_{-8.9}$ | 3.3 | 4.0 | 2.8 |
| 7 | 0.3–0.4 | 4.21×10^5 | 1.4 | 6.2 | $^{+11.0}_{-4.8}$ | 2.0 | 10.2 | 2.8 |

Table 10: Measured differential four-jet cross section for $R = 0.4$ jets, in bins of m_{2j}^{\min}/m_{4j} , along with the uncertainties in the measurement. The events are selected using the inclusive analysis cuts, as well as $m_{4j} > 500$ GeV. All other details are as for table 4.

| Bin | Bin edges | $d\sigma/d(m_{2j}^{\min}/m_{4j})$ [fb] | $\delta_{\text{stat}}^{\text{data}}$ [%] | $\delta_{\text{stat}}^{\text{MC}}$ [%] | u_{JES} [%] | u_{JER} [%] | u_{unfold} [%] | u_{lumi} [%] |
|-----|-----------|--|--|--|----------------------|----------------------|-------------------------|-----------------------|
| 1 | 0–0.04 | 1.34×10^5 | 4.6 | 9.7 | $^{+9.7}_{-8.6}$ | 1.9 | 10.5 | 2.8 |
| 2 | 0.04–0.08 | 4.01×10^6 | 0.7 | 2.2 | $^{+9.8}_{-8.9}$ | 1.9 | 10.5 | 2.8 |
| 3 | 0.08–0.13 | 6.79×10^6 | 0.4 | 1.4 | $^{+8.9}_{-10.4}$ | 1.9 | 5.8 | 2.8 |
| 4 | 0.13–0.17 | 5.35×10^6 | 0.5 | 1.8 | $^{+9.4}_{-7.9}$ | 1.9 | 5.5 | 2.8 |
| 5 | 0.17–0.23 | 2.21×10^6 | 0.6 | 1.8 | $^{+8.2}_{-9.9}$ | 1.9 | 3.1 | 2.8 |
| 6 | 0.23–0.3 | 3.97×10^5 | 1.0 | 2.2 | $^{+7.1}_{-7.5}$ | 1.9 | 3.1 | 2.8 |
| 7 | 0.3–0.4 | 1.78×10^4 | 2.7 | 5.9 | $^{+6.7}_{-7.5}$ | 1.9 | 3.1 | 2.8 |

Table 11: Measured differential four-jet cross section for $R = 0.4$ jets, in bins of m_{2j}^{\min}/m_{4j} , along with the uncertainties in the measurement. The events are selected using the inclusive analysis cuts, as well as $m_{4j} > 1000$ GeV. All other details are as for table 4.

| Bin | Bin edges | $d\sigma/d(m_{2j}^{\min}/m_{4j})$ [fb] | $\delta_{\text{stat}}^{\text{data}}$ [%] | $\delta_{\text{stat}}^{\text{MC}}$ [%] | u_{JES} [%] | u_{JER} [%] | u_{unfold} [%] | u_{lumi} [%] |
|-----|-----------|--|--|--|----------------------|----------------------|-------------------------|-----------------------|
| 1 | 0–0.04 | 1.28×10^5 | 4.6 | 9.6 | $^{+8.2}_{-10.3}$ | 2.1 | 4.8 | 2.8 |
| 2 | 0.04–0.08 | 1.67×10^6 | 1.1 | 2.2 | $^{+8.3}_{-11.1}$ | 2.1 | 4.8 | 2.8 |
| 3 | 0.08–0.13 | 1.68×10^6 | 0.8 | 2.4 | $^{+8.3}_{-9.5}$ | 2.1 | 4.8 | 2.8 |
| 4 | 0.13–0.17 | 8.81×10^5 | 0.9 | 2.5 | $^{+8.7}_{-8.9}$ | 2.1 | 4.8 | 2.8 |
| 5 | 0.17–0.23 | 2.63×10^5 | 0.9 | 1.9 | $^{+8.7}_{-7.7}$ | 2.1 | 5.2 | 2.8 |
| 6 | 0.23–0.3 | 4.04×10^4 | 1.7 | 2.6 | $^{+9.3}_{-7.1}$ | 2.1 | 5.2 | 2.8 |
| 7 | 0.3–0.4 | 2.03×10^3 | 2.2 | 5.9 | $^{+8.9}_{-7.1}$ | 2.1 | 3.1 | 2.8 |

Table 12: Measured differential four-jet cross section for $R = 0.4$ jets, in bins of m_{2j}^{\min}/m_{4j} , along with the uncertainties in the measurement. The events are selected using the inclusive analysis cuts, as well as $m_{4j} > 1500$ GeV. All other details are as for table 4.

| Bin | Bin edges | $d\sigma/d(m_{2j}^{\min}/m_{4j})$ [fb] | $\delta_{\text{stat}}^{\text{data}}$ [%] | $\delta_{\text{stat}}^{\text{MC}}$ [%] | u_{JES} [%] | u_{JER} [%] | u_{unfold} [%] | u_{lumi} [%] |
|-----|-----------|--|--|--|----------------------|----------------------|-------------------------|-----------------------|
| 1 | 0–0.04 | 6.15×10^4 | 5.3 | 13.0 | $^{+9.9}_{-7.1}$ | 1.5 | 13.2 | 2.8 |
| 2 | 0.04–0.08 | 4.66×10^5 | 1.6 | 2.8 | $^{+10.6}_{-10.4}$ | 1.5 | 13.2 | 2.8 |
| 3 | 0.08–0.13 | 3.55×10^5 | 1.2 | 3.3 | $^{+10.6}_{-10.4}$ | 1.5 | 9.7 | 2.8 |
| 4 | 0.13–0.17 | 1.29×10^5 | 0.8 | 3.0 | $^{+8.9}_{-9.0}$ | 1.5 | 4.2 | 2.8 |
| 5 | 0.17–0.23 | 3.64×10^4 | 1.1 | 2.5 | $^{+8.6}_{-9.0}$ | 1.5 | 4.2 | 2.8 |
| 6 | 0.23–0.3 | 5.61×10^3 | 1.3 | 4.0 | $^{+8.6}_{-9.0}$ | 1.5 | 4.2 | 2.8 |
| 7 | 0.3–0.4 | 1.85×10^2 | 5.9 | 11.3 | $^{+8.6}_{-9.0}$ | 1.5 | 16.4 | 2.8 |

Table 13: Measured differential four-jet cross section for $R = 0.4$ jets, in bins of m_{2j}^{\min}/m_{4j} , along with the uncertainties in the measurement. The events are selected using the inclusive analysis cuts, as well as $m_{4j} > 2000$ GeV. All other details are as for table 4.

| Bin | Bin edges | $d\sigma/d(\Delta\phi_{2j}^{\min})$ [fb] | $\delta_{\text{stat}}^{\text{data}}$ [%] | $\delta_{\text{stat}}^{\text{MC}}$ [%] | u_{JES} [%] | u_{JER} [%] | u_{unfold} [%] | u_{lumi} [%] |
|-----|-----------|--|--|--|----------------------|----------------------|-------------------------|-----------------------|
| 1 | 0–0.15 | 2.79×10^6 | 0.5 | 1.8 | +10.6 -6.5 | 3.8 | 2.1 | 2.8 |
| 2 | 0.15–0.3 | 2.81×10^6 | 0.5 | 1.7 | +9.6 -7.7 | 3.8 | 7.7 | 2.8 |
| 3 | 0.3–0.45 | 2.81×10^6 | 0.5 | 1.6 | +7.7 -8.6 | 3.5 | 6.1 | 2.8 |
| 4 | 0.45–0.6 | 2.87×10^6 | 0.5 | 2.0 | +7.2 -8.5 | 3.5 | 6.1 | 2.8 |
| 5 | 0.6–0.75 | 3.12×10^6 | 0.4 | 1.7 | +7.2 -8.4 | 3.5 | 7.6 | 2.8 |
| 6 | 0.75–0.9 | 2.62×10^6 | 0.5 | 2.3 | +8.9 -9.4 | 3.7 | 7.5 | 2.8 |
| 7 | 0.9–1.05 | 1.95×10^6 | 0.6 | 2.5 | +9.5 -8.8 | 3.7 | 6.6 | 2.8 |
| 8 | 1.05–1.2 | 1.52×10^6 | 0.8 | 3.1 | +7.8 -8.6 | 3.7 | 6.6 | 2.8 |
| 9 | 1.2–1.35 | 9.07×10^5 | 1.0 | 4.8 | +7.8 -8.6 | 3.7 | 11.0 | 2.8 |
| 10 | 1.35–1.6 | 1.6×10^5 | 1.9 | 9.1 | +7.5 -14.4 | 3.7 | 11.0 | 2.8 |

Table 14: Measured differential four-jet cross section for $R = 0.4$ jets, in bins of $\Delta\phi_{2j}^{\min}$, along with the uncertainties in the measurement. The events are selected using the inclusive analysis cuts. All other details are as for table 4.

| Bin | Bin edges | $d\sigma/d(\Delta\phi_{2j}^{\min})$ [fb] | $\delta_{\text{stat}}^{\text{data}}$ [%] | $\delta_{\text{stat}}^{\text{MC}}$ [%] | u_{JES} [%] | u_{JER} [%] | u_{unfold} [%] | u_{lumi} [%] |
|-----|-----------|--|--|--|----------------------|----------------------|-------------------------|-----------------------|
| 1 | 0–0.15 | 8.98×10^4 | 0.2 | 0.4 | +6.4 -6.5 | 0.9 | 3.3 | 2.8 |
| 2 | 0.15–0.3 | 8.31×10^4 | 0.2 | 0.5 | +6.4 -6.7 | 0.9 | 3.0 | 2.8 |
| 3 | 0.3–0.45 | 7.37×10^4 | 0.2 | 0.5 | +6.6 -6.2 | 1.5 | 2.4 | 2.8 |
| 4 | 0.45–0.6 | 6.61×10^4 | 0.3 | 0.5 | +5.9 -6.3 | 1.5 | 3.7 | 2.8 |
| 5 | 0.6–0.75 | 6.28×10^4 | 0.3 | 0.6 | +6.1 -6.7 | 1.3 | 2.5 | 2.8 |
| 6 | 0.75–0.9 | 4.07×10^4 | 0.3 | 0.6 | +6.4 -6.4 | 1.3 | 2.2 | 2.8 |
| 7 | 0.9–1.05 | 2.41×10^4 | 0.4 | 0.9 | +5.9 -6.9 | 1.8 | 3.6 | 2.8 |
| 8 | 1.05–1.2 | 1.26×10^4 | 0.7 | 1.3 | +5.9 -6.8 | 1.8 | 2.8 | 2.8 |
| 9 | 1.2–1.35 | 5.47×10^3 | 0.9 | 2.1 | +5.9 -5.6 | 1.8 | 2.8 | 2.8 |
| 10 | 1.35–1.6 | 1.11×10^3 | 1.5 | 3.7 | +6.4 -5.1 | 1.8 | 2.8 | 2.8 |

Table 15: Measured differential four-jet cross section for $R = 0.4$ jets, in bins of $\Delta\phi_{2j}^{\min}$, along with the uncertainties in the measurement. The events are selected using the inclusive analysis cuts, as well as $p_{\text{T}}^{(1)} > 400$ GeV. All other details are as for table 4.

| Bin | Bin edges | $d\sigma/d(\Delta\phi_{2j}^{\min})$ [fb] | $\delta_{\text{stat}}^{\text{data}}$ [%] | $\delta_{\text{stat}}^{\text{MC}}$ [%] | u_{JES} [%] | u_{JER} [%] | u_{unfold} [%] | u_{lumi} [%] |
|-----|-----------|--|--|--|----------------------|----------------------|-------------------------|-----------------------|
| 1 | 0–0.15 | 3.57×10^3 | 1.1 | 0.4 | +7.4 -7.8 | 1.8 | 2.2 | 2.8 |
| 2 | 0.15–0.3 | 3.37×10^3 | 1.2 | 0.4 | +7.8 -7.6 | 1.3 | 3.7 | 2.8 |
| 3 | 0.3–0.45 | 2.94×10^3 | 1.3 | 0.5 | +7.1 -7.4 | 1.7 | 3.3 | 2.8 |
| 4 | 0.45–0.6 | 2.45×10^3 | 1.5 | 0.5 | +7.6 -7.5 | 1.9 | 2.8 | 2.8 |
| 5 | 0.6–0.75 | 2.26×10^3 | 1.3 | 0.6 | +7.6 -7.3 | 2.1 | 2.5 | 2.8 |
| 6 | 0.75–0.9 | 1.37×10^3 | 2.0 | 0.8 | +8.6 -8.1 | 1.6 | 2.7 | 2.8 |
| 7 | 0.9–1.05 | 7.54×10^2 | 2.5 | 0.9 | +6.8 -9.0 | 1.6 | 2.7 | 2.8 |
| 8 | 1.05–1.2 | 3.5×10^2 | 3.4 | 1.6 | +9.0 -7.5 | 1.6 | 5.3 | 2.8 |
| 9 | 1.2–1.35 | 1.4×10^2 | 5.7 | 2.3 | +10.6 -6.4 | 1.6 | 3.2 | 2.8 |
| 10 | 1.35–1.6 | 3.72×10^1 | 9.3 | 4.7 | +8.0 -6.4 | 1.6 | 3.2 | 2.8 |

Table 16: Measured differential four-jet cross section for $R = 0.4$ jets, in bins of $\Delta\phi_{2j}^{\min}$, along with the uncertainties in the measurement. The events are selected using the inclusive analysis cuts, as well as $p_{\text{T}}^{(1)} > 700$ GeV. All other details are as for table 4.

| Bin | Bin edges | $d\sigma/d(\Delta\phi_{2j}^{\min})$ [fb] | $\delta_{\text{stat}}^{\text{data}}$ [%] | $\delta_{\text{stat}}^{\text{MC}}$ [%] | u_{JES} [%] | u_{JER} [%] | u_{unfold} [%] | u_{lumi} [%] |
|-----|-----------|--|--|--|----------------------|----------------------|-------------------------|-----------------------|
| 1 | 0–0.15 | 2.6×10^2 | 4.4 | 0.4 | +8.9 -8.4 | 1.9 | 2.5 | 2.8 |
| 2 | 0.15–0.3 | 2.27×10^2 | 4.4 | 0.6 | +8.6 -8.5 | 2.1 | 3.1 | 2.8 |
| 3 | 0.3–0.45 | 2.02×10^2 | 4.8 | 0.7 | +9.3 -7.9 | 2.1 | 3.6 | 2.8 |
| 4 | 0.45–0.6 | 1.59×10^2 | 5.8 | 0.7 | +9.0 -8.0 | 2.1 | 3.5 | 2.8 |
| 5 | 0.6–0.75 | 1.5×10^2 | 6.2 | 0.7 | +8.6 -8.0 | 2.1 | 3.2 | 2.8 |
| 6 | 0.75–0.9 | 8.7×10^1 | 6.7 | 0.9 | +9.8 -8.3 | 2.8 | 2.5 | 2.8 |
| 7 | 0.9–1.05 | 5.33×10^1 | 8.8 | 1.2 | +10.1 -8.5 | 2.8 | 5.4 | 2.8 |
| 8 | 1.05–1.2 | 2.18×10^1 | 14.4 | 2.2 | +10.0 -10.2 | 2.8 | 4.8 | 2.8 |
| 9 | 1.2–1.35 | 5.96 | 27.4 | 5.6 | +9.5 -7.9 | 4.6 | 4.8 | 2.8 |
| 10 | 1.35–1.6 | 3.71 | 29.4 | 3.5 | +9.5 -7.9 | 4.6 | 6.7 | 2.8 |

Table 17: Measured differential four-jet cross section for $R = 0.4$ jets, in bins of $\Delta\phi_{2j}^{\min}$, along with the uncertainties in the measurement. The events are selected using the inclusive analysis cuts, as well as $p_T^{(1)} > 1000$ GeV. All other details are as for table 4.

| Bin | Bin edges | $d\sigma/d(\Delta\phi_{3j}^{\min})$ [fb] | $\delta_{\text{stat}}^{\text{data}}$ [%] | $\delta_{\text{stat}}^{\text{MC}}$ [%] | u_{JES} [%] | u_{JER} [%] | u_{unfold} [%] | u_{lumi} [%] |
|-----|-----------|--|--|--|----------------------|----------------------|-------------------------|-----------------------|
| 1 | 0–0.25 | 1.31×10^4 | 5.6 | 8.0 | +9.9 -8.0 | 5.2 | 7.9 | 2.8 |
| 2 | 0.25–0.5 | 4.41×10^4 | 3.1 | 3.3 | +10.0 -8.3 | 5.2 | 7.9 | 2.8 |
| 3 | 0.5–0.75 | 1.18×10^5 | 2.0 | 4.4 | +10.0 -8.1 | 5.2 | 7.9 | 2.8 |
| 4 | 0.75–1 | 2.25×10^5 | 1.4 | 2.3 | +10.0 -7.2 | 5.2 | 13.9 | 2.8 |
| 5 | 1–1.25 | 2.89×10^5 | 1.3 | 3.5 | +9.9 -7.4 | 4.1 | 8.0 | 2.8 |
| 6 | 1.25–1.5 | 4.21×10^5 | 1.2 | 2.2 | +9.3 -8.0 | 4.1 | 7.7 | 2.8 |
| 7 | 1.5–1.75 | 6.48×10^5 | 0.9 | 2.4 | +8.9 -8.6 | 4.0 | 6.8 | 2.8 |
| 8 | 1.75–2 | 9.53×10^5 | 0.7 | 2.1 | +8.4 -7.9 | 3.8 | 5.6 | 2.8 |
| 9 | 2–2.25 | 1.62×10^6 | 0.6 | 2.0 | +8.3 -8.4 | 3.7 | 5.6 | 2.8 |
| 10 | 2.25–2.5 | 2.24×10^6 | 0.5 | 1.7 | +8.4 -8.5 | 3.7 | 6.6 | 2.8 |
| 11 | 2.5–2.75 | 3.0×10^6 | 0.4 | 1.6 | +8.1 -7.9 | 3.3 | 8.7 | 2.8 |
| 12 | 2.75–3 | 2.81×10^6 | 0.4 | 1.8 | +8.6 -8.9 | 3.3 | 4.1 | 2.8 |
| 13 | 3–3.25 | 6.3×10^5 | 0.9 | 4.0 | +10.9 -7.8 | 3.3 | 4.1 | 2.8 |

Table 18: Measured differential four-jet cross section for $R = 0.4$ jets, in bins of $\Delta\phi_{3j}^{\min}$, along with the uncertainties in the measurement. The events are selected using the inclusive analysis cuts. All other details are as for table 4.

| Bin | Bin edges | $d\sigma/d(\Delta\phi_{3j}^{\min})$ [fb] | $\delta_{\text{stat}}^{\text{data}}$ [%] | $\delta_{\text{stat}}^{\text{MC}}$ [%] | u_{JES} [%] | u_{JER} [%] | u_{unfold} [%] | u_{lumi} [%] |
|-----|-----------|--|--|--|----------------------|----------------------|-------------------------|-----------------------|
| 1 | 0–0.25 | 1.97×10^3 | 1.2 | 2.3 | +6.2 -6.5 | 0.8 | 5.7 | 2.8 |
| 2 | 0.25–0.5 | 6.68×10^3 | 0.6 | 1.0 | +6.2 -6.3 | 0.8 | 5.7 | 2.8 |
| 3 | 0.5–0.75 | 1.68×10^4 | 0.4 | 0.6 | +6.7 -6.2 | 0.8 | 3.6 | 2.8 |
| 4 | 0.75–1 | 2.46×10^4 | 0.3 | 0.6 | +6.2 -6.0 | 0.8 | 3.2 | 2.8 |
| 5 | 1–1.25 | 2.87×10^4 | 0.3 | 0.6 | +6.5 -6.2 | 0.8 | 4.5 | 2.8 |
| 6 | 1.25–1.5 | 3.07×10^4 | 0.3 | 0.5 | +6.4 -6.2 | 0.9 | 4.0 | 2.8 |
| 7 | 1.5–1.75 | 3.13×10^4 | 0.3 | 0.6 | +6.5 -6.2 | 1.1 | 3.2 | 2.8 |
| 8 | 1.75–2 | 3.08×10^4 | 0.3 | 0.6 | +6.3 -6.4 | 1.8 | 2.5 | 2.8 |
| 9 | 2–2.25 | 2.79×10^4 | 0.3 | 0.6 | +6.2 -6.5 | 1.6 | 2.2 | 2.8 |
| 10 | 2.25–2.5 | 2.55×10^4 | 0.3 | 0.6 | +6.3 -6.6 | 1.4 | 2.2 | 2.8 |
| 11 | 2.5–2.75 | 2.48×10^4 | 0.4 | 0.7 | +5.9 -7.3 | 1.6 | 3.1 | 2.8 |
| 12 | 2.75–3 | 2.1×10^4 | 0.4 | 0.7 | +6.1 -6.2 | 1.6 | 3.3 | 2.8 |
| 13 | 3–3.25 | 5.29×10^3 | 0.7 | 1.4 | +5.5 -7.2 | 1.1 | 2.0 | 2.8 |

Table 19: Measured differential four-jet cross section for $R = 0.4$ jets, in bins of $\Delta\phi_{3j}^{\min}$, along with the uncertainties in the measurement. The events are selected using the inclusive analysis cuts, as well as $p_{\text{T}}^{(1)} > 400$ GeV. All other details are as for table 4.

| Bin | Bin edges | $d\sigma/d(\Delta\phi_{3j}^{\min})$ [fb] | $\delta_{\text{stat}}^{\text{data}}$ [%] | $\delta_{\text{stat}}^{\text{MC}}$ [%] | u_{JES} [%] | u_{JER} [%] | u_{unfold} [%] | u_{lumi} [%] |
|-----|-----------|--|--|--|----------------------|----------------------|-------------------------|-----------------------|
| 1 | 0–0.25 | 8.01×10^1 | 5.8 | 2.1 | +8.3 -7.1 | 2.4 | 5.5 | 2.8 |
| 2 | 0.25–0.5 | 3.1×10^2 | 2.8 | 0.9 | +7.7 -6.7 | 2.4 | 5.5 | 2.8 |
| 3 | 0.5–0.75 | 7.61×10^2 | 2.2 | 0.7 | +7.0 -8.7 | 1.1 | 2.5 | 2.8 |
| 4 | 0.75–1 | 1.11×10^3 | 1.5 | 0.5 | +7.0 -7.3 | 1.1 | 2.3 | 2.8 |
| 5 | 1–1.25 | 1.22×10^3 | 1.5 | 0.6 | +7.4 -7.5 | 1.2 | 2.8 | 2.8 |
| 6 | 1.25–1.5 | 1.22×10^3 | 1.6 | 0.5 | +7.6 -7.4 | 1.5 | 3.2 | 2.8 |
| 7 | 1.5–1.75 | 1.17×10^3 | 1.6 | 0.5 | +7.7 -7.4 | 1.7 | 3.6 | 2.8 |
| 8 | 1.75–2 | 1.07×10^3 | 1.6 | 0.6 | +8.1 -7.6 | 1.8 | 4.4 | 2.8 |
| 9 | 2–2.25 | 9.19×10^2 | 1.8 | 0.6 | +8.3 -8.0 | 2.0 | 3.3 | 2.8 |
| 10 | 2.25–2.5 | 8.33×10^2 | 1.9 | 0.7 | +8.5 -8.1 | 2.6 | 2.4 | 2.8 |
| 11 | 2.5–2.75 | 8.17×10^2 | 1.9 | 0.7 | +7.6 -7.7 | 1.9 | 2.2 | 2.8 |
| 12 | 2.75–3 | 6.6×10^2 | 2.4 | 0.7 | +7.0 -8.0 | 1.9 | 1.9 | 2.8 |
| 13 | 3–3.25 | 1.92×10^2 | 4.0 | 1.4 | +7.1 -6.8 | 3.2 | 1.9 | 2.8 |

Table 20: Measured differential four-jet cross section for $R = 0.4$ jets, in bins of $\Delta\phi_{3j}^{\min}$, along with the uncertainties in the measurement. The events are selected using the inclusive analysis cuts, as well as $p_{\text{T}}^{(1)} > 700$ GeV. All other details are as for table 4.

| Bin | Bin edges | $d\sigma/d(\Delta\phi_{3j}^{\min})$ [fb] | $\delta_{\text{stat}}^{\text{data}}$ [%] | $\delta_{\text{stat}}^{\text{MC}}$ [%] | u_{JES} [%] | u_{JER} [%] | u_{unfold} [%] | u_{lumi} [%] |
|-----|-----------|--|--|--|----------------------|----------------------|-------------------------|-----------------------|
| 1 | 0–0.25 | 5.54 | 21.2 | 2.5 | +9.0 -7.8 | 1.6 | 2.4 | 2.8 |
| 2 | 0.25–0.5 | 2.68×10^1 | 11.6 | 1.3 | +7.6 -8.6 | 1.6 | 2.4 | 2.8 |
| 3 | 0.5–0.75 | 5.75×10^1 | 7.4 | 0.9 | +9.0 -8.6 | 1.6 | 2.3 | 2.8 |
| 4 | 0.75–1 | 8.98×10^1 | 5.7 | 0.7 | +7.9 -8.2 | 1.6 | 2.3 | 2.8 |
| 5 | 1–1.25 | 8.83×10^1 | 6.0 | 0.8 | +8.7 -8.2 | 1.6 | 3.8 | 2.8 |
| 6 | 1.25–1.5 | 7.41×10^1 | 6.3 | 0.6 | +8.9 -8.1 | 1.7 | 3.4 | 2.8 |
| 7 | 1.5–1.75 | 7.68×10^1 | 6.3 | 0.7 | +8.9 -8.4 | 1.7 | 3.5 | 2.8 |
| 8 | 1.75–2 | 6.68×10^1 | 7.0 | 0.7 | +9.4 -8.3 | 2.1 | 3.8 | 2.8 |
| 9 | 2–2.25 | 5.29×10^1 | 7.3 | 1.0 | +10.1 -7.9 | 3.1 | 4.5 | 2.8 |
| 10 | 2.25–2.5 | 4.76×10^1 | 7.9 | 1.0 | +10.3 -8.1 | 3.6 | 3.7 | 2.8 |
| 11 | 2.5–2.75 | 5.53×10^1 | 6.7 | 1.0 | +10.1 -8.1 | 2.8 | 3.3 | 2.8 |
| 12 | 2.75–3 | 4.83×10^1 | 8.4 | 1.0 | +9.1 -9.2 | 2.8 | 3.3 | 2.8 |
| 13 | 3–3.25 | 1.41×10^1 | 15.1 | 1.7 | +10.7 -6.7 | 4.3 | 5.6 | 2.8 |

Table 21: Measured differential four-jet cross section for $R = 0.4$ jets, in bins of $\Delta\phi_{3j}^{\min}$, along with the uncertainties in the measurement. The events are selected using the inclusive analysis cuts, as well as $p_{\text{T}}^{(1)} > 1000$ GeV. All other details are as for table 4.

| Bin | Bin edges | $d\sigma/d(\Delta y_{2j}^{\min})$ [fb] | $\delta_{\text{stat}}^{\text{data}}$ [%] | $\delta_{\text{stat}}^{\text{MC}}$ [%] | u_{JES} [%] | u_{JER} [%] | u_{unfold} [%] | u_{lumi} [%] |
|-----|-----------|--|--|--|----------------------|----------------------|-------------------------|-----------------------|
| 1 | 0–0.15 | 6.61×10^6 | 0.4 | 1.2 | +8.4 -7.2 | 3.5 | 7.4 | 2.8 |
| 2 | 0.15–0.3 | 5.03×10^6 | 0.4 | 1.5 | +8.2 -8.6 | 3.5 | 4.6 | 2.8 |
| 3 | 0.3–0.45 | 3.68×10^6 | 0.4 | 1.5 | +8.9 -8.3 | 3.5 | 4.6 | 2.8 |
| 4 | 0.45–0.6 | 2.58×10^6 | 0.6 | 2.0 | +9.3 -8.3 | 3.7 | 4.6 | 2.8 |
| 5 | 0.6–0.75 | 1.86×10^6 | 0.6 | 2.6 | +10.8 -8.8 | 3.7 | 10.2 | 2.8 |
| 6 | 0.75–0.9 | 9.92×10^5 | 0.9 | 3.7 | +9.6 -8.8 | 3.7 | 7.3 | 2.8 |
| 7 | 0.9–1.05 | 5.56×10^5 | 1.2 | 4.4 | +9.6 -10.2 | 3.7 | 7.3 | 2.8 |
| 8 | 1.05–1.2 | 2.08×10^5 | 1.9 | 9.4 | +9.6 -10.2 | 3.7 | 7.3 | 2.8 |
| 9 | 1.2–1.35 | 8.57×10^4 | 3.0 | 12.6 | +7.9 -10.2 | 6.9 | 7.3 | 2.8 |
| 10 | 1.35–1.5 | 3.49×10^4 | 6.3 | 19.3 | +7.9 -10.2 | 6.9 | 15.9 | 2.8 |
| 11 | 1.5–2 | 2.33×10^3 | 10.9 | 22.6 | +7.9 -10.2 | 6.9 | 15.9 | 2.8 |

Table 22: Measured differential four-jet cross section for $R = 0.4$ jets, in bins of Δy_{2j}^{\min} , along with the uncertainties in the measurement. The events are selected using the inclusive analysis cuts. All other details are as for table 4.

| Bin | Bin edges | $d\sigma/d(\Delta y_{2j}^{\min})$ [fb] | $\delta_{\text{stat}}^{\text{data}}$ [%] | $\delta_{\text{stat}}^{\text{MC}}$ [%] | u_{JES} [%] | u_{JER} [%] | u_{unfold} [%] | u_{lumi} [%] |
|-----|-----------|--|--|--|----------------------|----------------------|-------------------------|-----------------------|
| 1 | 0–0.15 | 1.54×10^5 | 0.2 | 0.3 | +6.4 -6.3 | 1.4 | 2.7 | 2.8 |
| 2 | 0.15–0.3 | 1.15×10^5 | 0.2 | 0.3 | +6.2 -6.3 | 0.9 | 2.5 | 2.8 |
| 3 | 0.3–0.45 | 7.96×10^4 | 0.2 | 0.4 | +6.3 -6.2 | 0.9 | 3.2 | 2.8 |
| 4 | 0.45–0.6 | 5.23×10^4 | 0.3 | 0.6 | +6.3 -6.3 | 1.7 | 3.1 | 2.8 |
| 5 | 0.6–0.75 | 3.27×10^4 | 0.4 | 0.7 | +6.0 -7.0 | 1.0 | 2.4 | 2.8 |
| 6 | 0.75–0.9 | 1.59×10^4 | 0.5 | 0.9 | +6.2 -6.5 | 1.0 | 2.8 | 2.8 |
| 7 | 0.9–1.05 | 6.68×10^3 | 0.8 | 1.5 | +7.3 -6.5 | 1.0 | 2.8 | 2.8 |
| 8 | 1.05–1.2 | 2.57×10^3 | 1.4 | 2.6 | +7.6 -6.5 | 1.0 | 2.8 | 2.8 |
| 9 | 1.2–1.35 | 9.3×10^2 | 2.5 | 5.5 | +8.3 -7.0 | 1.0 | 14.0 | 2.8 |
| 10 | 1.35–1.5 | 1.97×10^2 | 4.6 | 8.3 | +8.3 -7.0 | 1.0 | 12.9 | 2.8 |
| 11 | 1.5–2 | 8.66 | 9.9 | 20.2 | +8.3 -7.0 | 1.0 | 12.9 | 2.8 |

Table 23: Measured differential four-jet cross section for $R = 0.4$ jets, in bins of Δy_{2j}^{\min} , along with the uncertainties in the measurement. The events are selected using the inclusive analysis cuts, as well as $p_{\text{T}}^{(1)} > 400$ GeV. All other details are as for table 4.

| Bin | Bin edges | $d\sigma/d(\Delta y_{2j}^{\min})$ [fb] | $\delta_{\text{stat}}^{\text{data}}$ [%] | $\delta_{\text{stat}}^{\text{MC}}$ [%] | u_{JES} [%] | u_{JER} [%] | u_{unfold} [%] | u_{lumi} [%] |
|-----|-----------|--|--|--|----------------------|----------------------|-------------------------|-----------------------|
| 1 | 0–0.15 | 6.37×10^3 | 0.8 | 0.3 | $^{+7.3}_{-7.4}$ | 1.4 | 2.7 | 2.8 |
| 2 | 0.15–0.3 | 4.64×10^3 | 1.1 | 0.3 | $^{+7.6}_{-7.4}$ | 1.6 | 2.9 | 2.8 |
| 3 | 0.3–0.45 | 2.89×10^3 | 1.4 | 0.6 | $^{+7.7}_{-7.8}$ | 1.9 | 3.3 | 2.8 |
| 4 | 0.45–0.6 | 1.77×10^3 | 1.8 | 0.6 | $^{+7.7}_{-7.9}$ | 1.9 | 2.8 | 2.8 |
| 5 | 0.6–0.75 | 9.97×10^2 | 2.4 | 0.8 | $^{+7.9}_{-8.3}$ | 2.6 | 3.3 | 2.8 |
| 6 | 0.75–0.9 | 3.91×10^2 | 3.5 | 1.4 | $^{+10.1}_{-9.3}$ | 2.6 | 5.8 | 2.8 |
| 7 | 0.9–1.05 | 1.38×10^2 | 6.0 | 2.3 | $^{+7.5}_{-9.7}$ | 0.8 | 4.6 | 2.8 |
| 8 | 1.05–1.2 | 5.34×10^1 | 9.5 | 4.7 | $^{+7.5}_{-9.7}$ | 0.8 | 4.6 | 2.8 |
| 9 | 1.2–1.35 | 1.6×10^1 | 20.9 | 6.6 | $^{+7.5}_{-8.8}$ | 0.8 | 4.6 | 2.8 |
| 10 | 1.35–1.5 | 2.82 | 45.2 | 17.5 | $^{+20.3}_{-8.8}$ | 0.8 | 4.6 | 2.8 |

Table 24: Measured differential four-jet cross section for $R = 0.4$ jets, in bins of Δy_{2j}^{\min} , along with the uncertainties in the measurement. The events are selected using the inclusive analysis cuts, as well as $p_{\text{T}}^{(1)} > 700$ GeV. All other details are as for table 4.

| Bin | Bin edges | $d\sigma/d(\Delta y_{2j}^{\min})$ [fb] | $\delta_{\text{stat}}^{\text{data}}$ [%] | $\delta_{\text{stat}}^{\text{MC}}$ [%] | u_{JES} [%] | u_{JER} [%] | u_{unfold} [%] | u_{lumi} [%] |
|-----|-----------|--|--|--|----------------------|----------------------|-------------------------|-----------------------|
| 1 | 0–0.15 | 4.69×10^2 | 3.2 | 0.4 | $^{+8.6}_{-7.7}$ | 1.7 | 2.5 | 2.8 |
| 2 | 0.15–0.3 | 3.33×10^2 | 4.1 | 0.5 | $^{+8.7}_{-8.5}$ | 2.5 | 2.7 | 2.8 |
| 3 | 0.3–0.45 | 1.98×10^2 | 5.0 | 0.7 | $^{+9.0}_{-8.1}$ | 2.1 | 5.3 | 2.8 |
| 4 | 0.45–0.6 | 1.08×10^2 | 6.8 | 0.8 | $^{+9.3}_{-9.2}$ | 2.1 | 3.9 | 2.8 |
| 5 | 0.6–0.75 | 4.24×10^1 | 10.3 | 1.3 | $^{+11.7}_{-8.7}$ | 4.1 | 4.3 | 2.8 |
| 6 | 0.75–0.9 | 1.72×10^1 | 16.8 | 2.5 | $^{+13.0}_{-9.5}$ | 4.1 | 3.8 | 2.8 |
| 7 | 0.9–1.05 | 4.62 | 34.1 | 4.0 | $^{+12.3}_{-9.6}$ | 1.0 | 3.8 | 2.8 |
| 8 | 1.05–1.2 | 2.17 | 50.6 | 7.0 | $^{+12.3}_{-11.3}$ | 1.0 | 3.8 | 2.8 |

Table 25: Measured differential four-jet cross section for $R = 0.4$ jets, in bins of Δy_{2j}^{\min} , along with the uncertainties in the measurement. The events are selected using the inclusive analysis cuts, as well as $p_{\text{T}}^{(1)} > 1000$ GeV. All other details are as for table 4.

| Bin | Bin edges | $d\sigma/d(\Delta y_{3j}^{\min})$ [fb] | $\delta_{\text{stat}}^{\text{data}}$ [%] | $\delta_{\text{stat}}^{\text{MC}}$ [%] | u_{JES} [%] | u_{JER} [%] | u_{unfold} [%] | u_{lumi} [%] |
|-----|-----------|--|--|--|----------------------|----------------------|-------------------------|-----------------------|
| 1 | 0–0.25 | 3.61×10^5 | 1.3 | 4.6 | +7.5 -7.1 | 3.4 | 23.0 | 2.8 |
| 2 | 0.25–0.5 | 9.65×10^5 | 0.7 | 2.6 | +7.6 -7.3 | 3.4 | 6.9 | 2.8 |
| 3 | 0.5–0.75 | 1.64×10^6 | 0.5 | 1.9 | +7.6 -7.4 | 3.4 | 6.9 | 2.8 |
| 4 | 0.75–1 | 1.89×10^6 | 0.5 | 1.9 | +8.8 -7.9 | 3.4 | 6.9 | 2.8 |
| 5 | 1–1.25 | 1.83×10^6 | 0.5 | 1.6 | +9.0 -8.7 | 2.8 | 6.6 | 2.8 |
| 6 | 1.25–1.5 | 1.62×10^6 | 0.5 | 2.3 | +9.3 -8.4 | 2.8 | 6.6 | 2.8 |
| 7 | 1.5–1.75 | 1.42×10^6 | 0.5 | 1.9 | +8.8 -8.1 | 2.8 | 6.6 | 2.8 |
| 8 | 1.75–2 | 1.07×10^6 | 0.7 | 2.7 | +8.7 -8.3 | 2.8 | 7.3 | 2.8 |
| 9 | 2–2.25 | 7.88×10^5 | 0.8 | 2.8 | +9.0 -8.8 | 3.7 | 7.6 | 2.8 |
| 10 | 2.25–2.5 | 5.6×10^5 | 1.0 | 3.4 | +9.3 -9.4 | 6.1 | 6.8 | 2.8 |
| 11 | 2.5–2.75 | 3.67×10^5 | 1.1 | 4.3 | +9.6 -10.7 | 7.0 | 6.5 | 2.8 |
| 12 | 2.75–3 | 2.35×10^5 | 1.4 | 5.0 | +10.2 -11.1 | 7.0 | 6.5 | 2.8 |
| 13 | 3–3.25 | 1.09×10^5 | 2.2 | 9.9 | +11.0 -11.4 | 7.0 | 6.6 | 2.8 |
| 14 | 3.25–3.5 | 7.17×10^4 | 2.6 | 6.5 | +11.8 -11.6 | 7.0 | 9.4 | 2.8 |
| 15 | 3.5–3.75 | 3.72×10^4 | 3.4 | 7.1 | +12.0 -11.1 | 7.0 | 16.9 | 2.8 |
| 16 | 3.75–4 | 1.4×10^4 | 5.9 | 32.0 | +12.0 -10.9 | 7.0 | 19.7 | 2.8 |
| 17 | 4–5 | 2.46×10^3 | 7.8 | 23.2 | +12.0 -10.9 | 15.2 | 19.9 | 2.8 |

Table 26: Measured differential four-jet cross section for $R = 0.4$ jets, in bins of Δy_{3j}^{\min} , along with the uncertainties in the measurement. The events are selected using the inclusive analysis cuts. All other details are as for table 4.

| Bin | Bin edges | $d\sigma/d(\Delta y_{3j}^{\min})$ [fb] | $\delta_{\text{stat}}^{\text{data}}$ [%] | $\delta_{\text{stat}}^{\text{MC}}$ [%] | u_{JES} [%] | u_{JER} [%] | u_{unfold} [%] | u_{lumi} [%] |
|-----|-----------|--|--|--|----------------------|----------------------|-------------------------|-----------------------|
| 1 | 0–0.25 | 8.7×10^3 | 0.6 | 0.8 | +6.1 -6.2 | 1.7 | 2.8 | 2.8 |
| 2 | 0.25–0.5 | 2.49×10^4 | 0.3 | 0.7 | +6.3 -6.3 | 1.7 | 3.0 | 2.8 |
| 3 | 0.5–0.75 | 4.28×10^4 | 0.3 | 0.5 | +5.9 -6.5 | 1.0 | 2.0 | 2.8 |
| 4 | 0.75–1 | 4.83×10^4 | 0.2 | 0.4 | +6.3 -5.7 | 1.0 | 2.4 | 2.8 |
| 5 | 1–1.25 | 4.34×10^4 | 0.3 | 0.4 | +6.2 -6.3 | 1.2 | 3.1 | 2.8 |
| 6 | 1.25–1.5 | 3.58×10^4 | 0.3 | 0.5 | +6.1 -6.3 | 1.2 | 3.3 | 2.8 |
| 7 | 1.5–1.75 | 2.69×10^4 | 0.4 | 0.6 | +6.0 -6.4 | 1.4 | 3.1 | 2.8 |
| 8 | 1.75–2 | 1.86×10^4 | 0.4 | 0.7 | +6.4 -6.9 | 1.4 | 3.1 | 2.8 |
| 9 | 2–2.25 | 1.21×10^4 | 0.5 | 0.9 | +7.1 -7.1 | 1.3 | 4.0 | 2.8 |
| 10 | 2.25–2.5 | 7.08×10^3 | 0.5 | 1.2 | +7.7 -7.0 | 1.2 | 4.4 | 2.8 |
| 11 | 2.5–2.75 | 4.01×10^3 | 0.8 | 1.7 | +8.3 -7.5 | 1.2 | 3.6 | 2.8 |
| 12 | 2.75–3 | 2.0×10^3 | 1.3 | 2.3 | +8.7 -8.2 | 1.2 | 3.2 | 2.8 |
| 13 | 3–3.25 | 9.06×10^2 | 1.7 | 3.1 | +8.7 -9.1 | 1.2 | 3.2 | 2.8 |
| 14 | 3.25–3.5 | 3.88×10^2 | 2.9 | 4.7 | +9.0 -10.1 | 1.2 | 3.6 | 2.8 |
| 15 | 3.5–3.75 | 1.26×10^2 | 4.6 | 9.0 | +11.0 -11.1 | 1.2 | 11.1 | 2.8 |
| 16 | 3.75–4 | 3.24×10^1 | 10.1 | 16.6 | +11.8 -11.5 | 1.2 | 30.3 | 2.8 |
| 17 | 4–5 | 4.08 | 17.1 | 37.0 | +11.8 -11.5 | 1.2 | 40.7 | 2.8 |

Table 27: Measured differential four-jet cross section for $R = 0.4$ jets, in bins of Δy_{3j}^{\min} , along with the uncertainties in the measurement. The events are selected using the inclusive analysis cuts, as well as $p_T^{(1)} > 400$ GeV. All other details are as for table 4.

| Bin | Bin edges | $d\sigma/d(\Delta y_{3j}^{\min})$ [fb] | $\delta_{\text{stat}}^{\text{data}}$ [%] | $\delta_{\text{stat}}^{\text{MC}}$ [%] | u_{JES} [%] | u_{JER} [%] | u_{unfold} [%] | u_{lumi} [%] |
|-----|-----------|--|--|--|----------------------|----------------------|-------------------------|-----------------------|
| 1 | 0–0.25 | 4.06×10^2 | 2.3 | 1.1 | +6.7 -7.6 | 1.5 | 3.9 | 2.8 |
| 2 | 0.25–0.5 | 1.14×10^3 | 1.6 | 0.5 | +6.6 -7.1 | 1.5 | 3.2 | 2.8 |
| 3 | 0.5–0.75 | 1.91×10^3 | 1.4 | 0.5 | +7.3 -6.9 | 1.5 | 3.7 | 2.8 |
| 4 | 0.75–1 | 2.06×10^3 | 1.0 | 0.4 | +7.5 -7.3 | 1.3 | 2.3 | 2.8 |
| 5 | 1–1.25 | 1.71×10^3 | 1.3 | 0.5 | +7.4 -8.0 | 1.5 | 2.9 | 2.8 |
| 6 | 1.25–1.5 | 1.28×10^3 | 1.4 | 0.6 | +7.7 -7.8 | 2.0 | 2.9 | 2.8 |
| 7 | 1.5–1.75 | 8.57×10^2 | 1.7 | 0.7 | +8.4 -8.0 | 2.2 | 2.6 | 2.8 |
| 8 | 1.75–2 | 5.06×10^2 | 2.7 | 0.8 | +9.0 -8.1 | 2.4 | 2.1 | 2.8 |
| 9 | 2–2.25 | 2.69×10^2 | 3.4 | 1.3 | +8.9 -9.3 | 2.5 | 1.9 | 2.8 |
| 10 | 2.25–2.5 | 1.39×10^2 | 5.0 | 1.9 | +9.2 -10.6 | 2.6 | 2.6 | 2.8 |
| 11 | 2.5–2.75 | 5.72×10^1 | 8.0 | 2.7 | +9.6 -11.0 | 2.6 | 4.7 | 2.8 |
| 12 | 2.75–3 | 2.39×10^1 | 12.0 | 4.6 | +10.9 -12.4 | 2.6 | 5.5 | 2.8 |
| 13 | 3–3.25 | 8.54 | 16.3 | 8.3 | +13.7 -14.0 | 2.6 | 5.8 | 2.8 |
| 14 | 3.25–3.5 | 4.60 | 24.3 | 9.2 | +14.7 -14.2 | 2.6 | 10.9 | 2.8 |
| 15 | 3.5–3.75 | 4.97×10^{-1} | 80.2 | 88.5 | +14.7 -14.2 | 2.6 | 24.9 | 2.8 |
| 16 | 3.75–4 | 3.03×10^1 | 82.6 | 81.5 | +14.7 -14.1 | 2.6 | 30.0 | 2.8 |

Table 28: Measured differential four-jet cross section for $R = 0.4$ jets, in bins of Δy_{3j}^{\min} , along with the uncertainties in the measurement. The events are selected using the inclusive analysis cuts, as well as $p_{\text{T}}^{(1)} > 700$ GeV. All other details are as for table 4.

| Bin | Bin edges | $d\sigma/d(\Delta y_{3j}^{\min})$ [fb] | $\delta_{\text{stat}}^{\text{data}}$ [%] | $\delta_{\text{stat}}^{\text{MC}}$ [%] | u_{JES} [%] | u_{JER} [%] | u_{unfold} [%] | u_{lumi} [%] |
|-----|-----------|--|--|--|----------------------|----------------------|-------------------------|-----------------------|
| 1 | 0–0.25 | 3.74×10^1 | 8.2 | 1.4 | +9.7 -6.5 | 1.5 | 4.0 | 2.8 |
| 2 | 0.25–0.5 | 8.69×10^1 | 5.1 | 0.7 | +8.3 -7.4 | 1.5 | 2.2 | 2.8 |
| 3 | 0.5–0.75 | 1.48×10^2 | 4.8 | 0.5 | +8.1 -8.0 | 1.5 | 2.2 | 2.8 |
| 4 | 0.75–1 | 1.56×10^2 | 4.4 | 0.5 | +8.1 -8.0 | 1.9 | 2.9 | 2.8 |
| 5 | 1–1.25 | 1.11×10^2 | 6.2 | 0.6 | +9.7 -8.8 | 2.2 | 3.8 | 2.8 |
| 6 | 1.25–1.5 | 8.07×10^1 | 6.5 | 0.7 | +10.0 -8.8 | 2.7 | 4.0 | 2.8 |
| 7 | 1.5–1.75 | 4.44×10^1 | 8.2 | 1.0 | +10.8 -8.9 | 3.4 | 4.2 | 2.8 |
| 8 | 1.75–2 | 2.48×10^1 | 10.3 | 1.3 | +10.8 -9.5 | 3.8 | 3.6 | 2.8 |
| 9 | 2–2.25 | 6.87 | 22.3 | 2.3 | +11.6 -10.0 | 3.8 | 3.3 | 2.8 |
| 10 | 2.25–2.5 | 5.32 | 23.6 | 3.0 | +12.8 -11.1 | 3.6 | 3.3 | 2.8 |
| 11 | 2.5–2.75 | 1.31 | 50.7 | 6.8 | +14.3 -13.8 | 3.5 | 3.3 | 2.8 |
| 12 | 2.75–3 | 1.32 | 39.5 | 7.9 | +16.5 -20.0 | 3.4 | 3.3 | 2.8 |

Table 29: Measured differential four-jet cross section for $R = 0.4$ jets, in bins of Δy_{3j}^{\min} , along with the uncertainties in the measurement. The events are selected using the inclusive analysis cuts, as well as $p_{\text{T}}^{(1)} > 1000$ GeV. All other details are as for table 4.

| Bin | Bin edges | $d\sigma/d(\Delta y_{2j}^{\max})$ [fb] | $\delta_{\text{stat}}^{\text{data}}$ [%] | $\delta_{\text{stat}}^{\text{MC}}$ [%] | u_{JES} [%] | u_{JER} [%] | u_{unfold} [%] | u_{lumi} [%] |
|-----|-----------|--|--|--|----------------------|----------------------|-------------------------|-----------------------|
| 1 | 0–0.4 | 1.55×10^4 | 4.4 | 10.2 | +8.3 -8.4 | 3.3 | 11.8 | 2.8 |
| 2 | 0.4–0.8 | 1.69×10^5 | 1.6 | 5.5 | +8.4 -9.1 | 3.3 | 11.8 | 2.8 |
| 3 | 0.8–1.2 | 4.44×10^5 | 0.9 | 3.3 | +8.4 -8.5 | 3.3 | 10.8 | 2.8 |
| 4 | 1.2–1.6 | 7.29×10^5 | 0.6 | 2.6 | +8.1 -7.5 | 3.3 | 8.4 | 2.8 |
| 5 | 1.6–2 | 9.77×10^5 | 0.5 | 2.2 | +7.1 -7.1 | 3.3 | 5.7 | 2.8 |
| 6 | 2–2.4 | 1.15×10^6 | 0.6 | 1.7 | +7.1 -7.3 | 3.4 | 4.9 | 2.8 |
| 7 | 2.4–2.8 | 1.18×10^6 | 0.5 | 1.7 | +8.5 -7.4 | 3.7 | 4.7 | 2.8 |
| 8 | 2.8–3.2 | 1.09×10^6 | 0.6 | 2.0 | +9.9 -8.0 | 3.8 | 5.1 | 2.8 |
| 9 | 3.2–3.6 | 9.05×10^5 | 0.7 | 2.0 | +9.5 -9.4 | 3.7 | 5.9 | 2.8 |
| 10 | 3.6–4 | 6.39×10^5 | 0.6 | 2.5 | +9.1 -9.8 | 3.6 | 5.4 | 2.8 |
| 11 | 4–4.4 | 4.55×10^5 | 0.7 | 3.3 | +10.4 -9.5 | 3.5 | 5.1 | 2.8 |
| 12 | 4.4–4.8 | 2.46×10^5 | 1.0 | 4.2 | +11.7 -10.3 | 3.5 | 5.1 | 2.8 |
| 13 | 4.8–5.2 | 9.91×10^4 | 1.8 | 5.2 | +13.3 -13.3 | 3.5 | 8.9 | 2.8 |
| 14 | 5.2–5.6 | 2.78×10^4 | 3.7 | 10.3 | +13.3 -13.3 | 3.5 | 8.9 | 2.8 |

Table 30: Measured differential four-jet cross section for $R = 0.4$ jets, in bins of Δy_{2j}^{\max} , along with the uncertainties in the measurement. The events are selected using the inclusive analysis cuts. All other details are as for table 4.

| Bin | Bin edges | $d\sigma/d(\Delta y_{2j}^{\max})$ [fb] | $\delta_{\text{stat}}^{\text{data}}$ [%] | $\delta_{\text{stat}}^{\text{MC}}$ [%] | u_{JES} [%] | u_{JER} [%] | u_{unfold} [%] | u_{lumi} [%] |
|-----|-----------|--|--|--|----------------------|----------------------|-------------------------|-----------------------|
| 1 | 0–0.4 | 3.08×10^3 | 6.4 | 7.6 | +6.2 -3.8 | 1.5 | 4.0 | 2.8 |
| 2 | 0.4–0.8 | 3.0×10^4 | 2.2 | 2.4 | +6.2 -5.5 | 1.5 | 4.0 | 2.8 |
| 3 | 0.8–1.2 | 8.29×10^4 | 1.4 | 1.3 | +6.5 -6.0 | 1.5 | 4.0 | 2.8 |
| 4 | 1.2–1.6 | 1.33×10^5 | 0.9 | 0.8 | +6.4 -5.9 | 1.5 | 4.0 | 2.8 |
| 5 | 1.6–2 | 1.73×10^5 | 0.8 | 0.7 | +6.0 -6.0 | 1.5 | 4.0 | 2.8 |
| 6 | 2–2.4 | 1.99×10^5 | 0.9 | 0.8 | +5.9 -6.3 | 1.5 | 4.0 | 2.8 |
| 7 | 2.4–2.8 | 1.92×10^5 | 0.8 | 0.7 | +6.0 -6.4 | 1.5 | 4.1 | 2.8 |
| 8 | 2.8–3.2 | 1.68×10^5 | 0.9 | 0.8 | +6.8 -6.7 | 1.5 | 4.2 | 2.8 |
| 9 | 3.2–3.6 | 1.29×10^5 | 1.0 | 0.9 | +7.7 -6.7 | 1.6 | 4.1 | 2.8 |
| 10 | 3.6–4 | 9.03×10^4 | 1.4 | 1.1 | +8.3 -7.0 | 1.9 | 4.1 | 2.8 |
| 11 | 4–4.4 | 4.93×10^4 | 1.8 | 1.4 | +8.1 -7.7 | 2.0 | 5.2 | 2.8 |
| 12 | 4.4–4.8 | 2.43×10^4 | 3.0 | 2.3 | +7.9 -8.3 | 2.0 | 6.1 | 2.8 |
| 13 | 4.8–5.2 | 9.11×10^3 | 5.1 | 3.0 | +9.2 -7.9 | 2.0 | 6.4 | 2.8 |
| 14 | 5.2–5.6 | 1.22×10^3 | 13.8 | 11.9 | +8.9 -8.2 | 2.0 | 5.0 | 2.8 |

Table 31: Measured differential four-jet cross section for $R = 0.4$ jets, in bins of Δy_{2j}^{\max} , along with the uncertainties in the measurement. The events are selected using the inclusive analysis cuts, as well as $p_{\text{T}}^{(1)} > 250$ GeV. All other details are as for table 4.

| Bin | Bin edges | $d\sigma/d(\Delta y_{2j}^{\max})$ [fb] | $\delta_{\text{stat}}^{\text{data}}$ [%] | $\delta_{\text{stat}}^{\text{MC}}$ [%] | u_{JES} [%] | u_{JER} [%] | u_{unfold} [%] | u_{lumi} [%] |
|-----|-----------|--|--|--|----------------------|----------------------|-------------------------|-----------------------|
| 1 | 0–0.4 | 4.07×10^2 | 2.2 | 4.2 | +6.5 -6.5 | 0.8 | 3.6 | 2.8 |
| 2 | 0.4–0.8 | 4.4×10^3 | 0.7 | 1.0 | +6.5 -6.5 | 0.8 | 3.6 | 2.8 |
| 3 | 0.8–1.2 | 1.28×10^4 | 0.4 | 0.6 | +6.0 -6.5 | 0.8 | 3.2 | 2.8 |
| 4 | 1.2–1.6 | 2.12×10^4 | 0.3 | 0.5 | +5.9 -5.5 | 0.8 | 2.6 | 2.8 |
| 5 | 1.6–2 | 2.73×10^4 | 0.3 | 0.4 | +5.7 -5.7 | 0.8 | 2.6 | 2.8 |
| 6 | 2–2.4 | 2.88×10^4 | 0.2 | 0.4 | +5.9 -6.1 | 1.1 | 3.2 | 2.8 |
| 7 | 2.4–2.8 | 2.66×10^4 | 0.3 | 0.4 | +6.3 -6.3 | 1.8 | 3.1 | 2.8 |
| 8 | 2.8–3.2 | 2.13×10^4 | 0.3 | 0.5 | +6.4 -6.3 | 1.7 | 2.9 | 2.8 |
| 9 | 3.2–3.6 | 1.46×10^4 | 0.4 | 0.6 | +7.0 -6.3 | 1.2 | 2.2 | 2.8 |
| 10 | 3.6–4 | 8.75×10^3 | 0.4 | 0.8 | +7.6 -6.9 | 1.0 | 2.1 | 2.8 |
| 11 | 4–4.4 | 4.32×10^3 | 0.7 | 1.2 | +8.3 -7.7 | 1.0 | 2.6 | 2.8 |
| 12 | 4.4–4.8 | 1.69×10^3 | 1.0 | 1.8 | +9.1 -8.5 | 1.0 | 4.1 | 2.8 |
| 13 | 4.8–5.2 | 4.64×10^2 | 2.0 | 3.3 | +9.4 -9.1 | 1.0 | 9.2 | 2.8 |
| 14 | 5.2–5.6 | 5.92×10^1 | 5.4 | 12.6 | +9.4 -8.3 | 1.0 | 16.9 | 2.8 |

Table 32: Measured differential four-jet cross section for $R = 0.4$ jets, in bins of Δy_{2j}^{\max} , along with the uncertainties in the measurement. The events are selected using the inclusive analysis cuts, as well as $p_{\text{T}}^{(1)} > 400$ GeV. All other details are as for table 4.

| Bin | Bin edges | $d\sigma/d(\Delta y_{2j}^{\max})$ [fb] | $\delta_{\text{stat}}^{\text{data}}$ [%] | $\delta_{\text{stat}}^{\text{MC}}$ [%] | u_{JES} [%] | u_{JER} [%] | u_{unfold} [%] | u_{lumi} [%] |
|-----|-----------|--|--|--|----------------------|----------------------|-------------------------|-----------------------|
| 1 | 0–0.4 | 8.16×10^1 | 5.1 | 4.5 | +5.5 -6.1 | 1.9 | 3.0 | 2.8 |
| 2 | 0.4–0.8 | 8.85×10^2 | 1.6 | 1.3 | +5.6 -6.8 | 1.9 | 3.0 | 2.8 |
| 3 | 0.8–1.2 | 2.65×10^3 | 0.8 | 0.8 | +6.1 -6.3 | 1.9 | 2.9 | 2.8 |
| 4 | 1.2–1.6 | 4.34×10^3 | 0.7 | 0.6 | +6.6 -6.6 | 1.7 | 2.8 | 2.8 |
| 5 | 1.6–2 | 5.3×10^3 | 0.6 | 0.5 | +6.6 -6.7 | 1.7 | 2.4 | 2.8 |
| 6 | 2–2.4 | 5.3×10^3 | 0.6 | 0.5 | +6.9 -6.7 | 1.6 | 2.6 | 2.8 |
| 7 | 2.4–2.8 | 4.5×10^3 | 0.7 | 0.5 | +7.2 -7.0 | 1.8 | 2.8 | 2.8 |
| 8 | 2.8–3.2 | 3.4×10^3 | 0.7 | 0.7 | +7.6 -7.8 | 2.0 | 3.0 | 2.8 |
| 9 | 3.2–3.6 | 2.06×10^3 | 0.9 | 0.8 | +8.2 -8.4 | 2.0 | 3.8 | 2.8 |
| 10 | 3.6–4 | 1.1×10^3 | 1.2 | 1.2 | +9.6 -9.1 | 1.9 | 4.8 | 2.8 |
| 11 | 4–4.4 | 4.47×10^2 | 2.0 | 1.6 | +10.1 -10.1 | 2.1 | 4.2 | 2.8 |
| 12 | 4.4–4.8 | 1.54×10^2 | 3.5 | 3.1 | +9.4 -11.4 | 2.4 | 3.9 | 2.8 |
| 13 | 4.8–5.2 | 3.92×10^1 | 6.9 | 8.4 | +9.1 -12.0 | 2.6 | 3.9 | 2.8 |
| 14 | 5.2–5.6 | 5.91 | 17.1 | 13.9 | +9.1 -17.7 | 2.6 | 3.9 | 2.8 |

Table 33: Measured differential four-jet cross section for $R = 0.4$ jets, in bins of Δy_{2j}^{\max} , along with the uncertainties in the measurement. The events are selected using the inclusive analysis cuts, as well as $p_{\text{T}}^{(1)} > 550$ GeV. All other details are as for table 4.

| Bin | Bin edges [GeV] | $d\sigma/d(\Sigma p_T^{\text{central}})$ [fb/GeV] | $\delta_{\text{stat}}^{\text{data}}$ [%] | $\delta_{\text{stat}}^{\text{MC}}$ [%] | u_{JES} [%] | u_{JER} [%] | u_{unfold} [%] | u_{lumi} [%] |
|-----|-----------------|---|--|--|----------------------|----------------------|-------------------------|-----------------------|
| 1 | 120–170 | 1.07×10^4 | 0.6 | 2.4 | +9.9 -7.7 | 5.6 | 13.5 | 2.8 |
| 2 | 170–240 | 1.93×10^4 | 0.3 | 1.2 | +9.2 -8.3 | 4.6 | 8.4 | 2.8 |
| 3 | 240–315 | 9.21×10^3 | 0.4 | 1.0 | +7.8 -8.0 | 1.9 | 5.5 | 2.8 |
| 4 | 315–395 | 3.76×10^3 | 0.4 | 0.7 | +7.2 -7.3 | 0.8 | 4.6 | 2.8 |
| 5 | 395–480 | 1.46×10^3 | 0.5 | 0.7 | +6.4 -6.5 | 0.7 | 4.2 | 2.8 |
| 6 | 480–575 | 5.75×10^2 | 0.6 | 0.5 | +6.3 -6.1 | 0.7 | 2.6 | 2.8 |
| 7 | 575–680 | 2.23×10^2 | 0.5 | 0.5 | +6.6 -6.2 | 0.7 | 2.1 | 2.8 |
| 8 | 680–795 | 8.73×10^1 | 0.2 | 0.4 | +6.3 -6.7 | 0.7 | 2.0 | 2.8 |
| 9 | 795–930 | 3.4×10^1 | 0.4 | 0.5 | +6.6 -7.0 | 0.7 | 2.0 | 2.8 |
| 10 | 930–1085 | 1.25×10^1 | 0.6 | 0.5 | +6.8 -7.2 | 0.8 | 2.2 | 2.8 |
| 11 | 1085–1260 | 4.48 | 1.0 | 0.7 | +7.2 -7.6 | 1.1 | 2.5 | 2.8 |
| 12 | 1260–1465 | 1.56 | 1.4 | 0.5 | +8.0 -7.8 | 1.2 | 2.6 | 2.8 |
| 13 | 1465–1705 | 5.07×10^{-1} | 2.1 | 0.5 | +8.0 -7.9 | 1.2 | 2.8 | 2.8 |
| 14 | 1705–1980 | 1.59×10^{-1} | 3.7 | 0.6 | +8.2 -8.0 | 1.3 | 2.6 | 2.8 |
| 15 | 1980–2300 | 4.43×10^{-2} | 7.0 | 0.7 | +8.5 -8.5 | 1.3 | 2.4 | 2.8 |
| 16 | 2300–5000 | 1.64×10^{-3} | 11.7 | 0.6 | +11.2 -9.6 | 1.3 | 3.7 | 2.8 |

Table 34: Measured differential four-jet cross section for $R = 0.4$ jets, in bins of $\Sigma p_T^{\text{central}}$, along with the uncertainties in the measurement. The events are selected using the inclusive analysis cuts and $\Delta y_{2j}^{\text{max}} > 1$. All other details are as for table 4.

| Bin | Bin edges [GeV] | $d\sigma/d(\Sigma p_T^{\text{central}})$ [fb/GeV] | $\delta_{\text{stat}}^{\text{data}}$ [%] | $\delta_{\text{stat}}^{\text{MC}}$ [%] | u_{JES} [%] | u_{JER} [%] | u_{unfold} [%] | u_{lumi} [%] |
|-----|-----------------|---|--|--|----------------------|----------------------|-------------------------|-----------------------|
| 1 | 120–170 | 4.3×10^2 | 2.5 | 2.3 | +5.9 -4.9 | 2.4 | 9.2 | 2.8 |
| 2 | 170–240 | 1.15×10^3 | 0.9 | 0.9 | +6.4 -6.3 | 2.2 | 5.8 | 2.8 |
| 3 | 240–315 | 1.01×10^3 | 0.8 | 0.8 | +6.3 -6.8 | 1.6 | 4.5 | 2.8 |
| 4 | 315–395 | 1.48×10^3 | 0.7 | 0.7 | +6.8 -6.9 | 1.4 | 6.3 | 2.8 |
| 5 | 395–480 | 1.13×10^3 | 0.6 | 0.5 | +6.6 -6.6 | 1.3 | 6.5 | 2.8 |
| 6 | 480–575 | 5.73×10^2 | 0.6 | 0.5 | +6.6 -6.2 | 1.0 | 3.7 | 2.8 |
| 7 | 575–680 | 2.25×10^2 | 0.5 | 0.5 | +6.7 -6.3 | 0.9 | 2.3 | 2.8 |
| 8 | 680–795 | 8.79×10^1 | 0.3 | 0.4 | +6.4 -6.8 | 0.9 | 2.0 | 2.8 |
| 9 | 795–930 | 3.42×10^1 | 0.4 | 0.5 | +6.7 -7.1 | 1.1 | 2.0 | 2.8 |
| 10 | 930–1085 | 1.26×10^1 | 0.6 | 0.5 | +6.9 -7.2 | 1.4 | 2.2 | 2.8 |
| 11 | 1085–1260 | 4.51 | 1.0 | 0.7 | +7.3 -7.6 | 1.6 | 2.5 | 2.8 |
| 12 | 1260–1465 | 1.57 | 1.4 | 0.5 | +8.1 -7.9 | 1.5 | 2.6 | 2.8 |
| 13 | 1465–1705 | 5.10×10^{-1} | 2.1 | 0.5 | +8.1 -7.9 | 1.6 | 2.8 | 2.8 |
| 14 | 1705–1980 | 1.60×10^{-1} | 3.6 | 0.6 | +8.3 -8.0 | 1.8 | 2.6 | 2.8 |
| 15 | 1980–2300 | 4.45×10^{-2} | 7.0 | 0.7 | +8.6 -8.5 | 1.5 | 2.4 | 2.8 |
| 16 | 2300–5000 | 1.65×10^{-3} | 11.7 | 0.6 | +11.3 -9.7 | 1.3 | 3.7 | 2.8 |

Table 35: Measured differential four-jet cross section for $R = 0.4$ jets, in bins of $\Sigma p_T^{\text{central}}$, along with the uncertainties in the measurement. The events are selected using the inclusive analysis cuts and $\Delta y_{2j}^{\text{max}} > 1$, as well as $p_T^{(1)} > 250$ GeV. All other details are as for table 4.

| Bin | Bin edges [GeV] | $d\sigma/d(\Sigma p_T^{\text{central}})$ [fb/GeV] | $\delta_{\text{stat}}^{\text{data}}$ [%] | $\delta_{\text{stat}}^{\text{MC}}$ [%] | u_{JES} [%] | u_{JER} [%] | u_{unfold} [%] | u_{lumi} [%] |
|-----|-----------------|---|--|--|----------------------|----------------------|-------------------------|-----------------------|
| 1 | 120–170 | 1.78×10^1 | 0.8 | 2.5 | +6.2 -6.6 | 1.4 | 3.3 | 2.8 |
| 2 | 170–240 | 5.29×10^1 | 0.5 | 1.0 | +5.9 -6.6 | 1.4 | 3.8 | 2.8 |
| 3 | 240–315 | 7.88×10^1 | 0.3 | 0.7 | +5.8 -6.5 | 1.4 | 4.6 | 2.8 |
| 4 | 315–395 | 9.39×10^1 | 0.3 | 0.7 | +6.3 -6.3 | 1.4 | 4.3 | 2.8 |
| 5 | 395–480 | 8.49×10^1 | 0.3 | 0.8 | +6.4 -6.3 | 1.4 | 4.9 | 2.8 |
| 6 | 480–575 | 1.37×10^2 | 0.2 | 0.4 | +6.2 -6.3 | 1.2 | 4.1 | 2.8 |
| 7 | 575–680 | 1.09×10^2 | 0.2 | 0.4 | +6.7 -6.3 | 1.1 | 3.6 | 2.8 |
| 8 | 680–795 | 6.76×10^1 | 0.3 | 0.4 | +6.5 -6.8 | 1.2 | 3.4 | 2.8 |
| 9 | 795–930 | 3.39×10^1 | 0.4 | 0.5 | +6.7 -7.0 | 1.2 | 2.4 | 2.8 |
| 10 | 930–1085 | 1.24×10^1 | 0.6 | 0.5 | +6.9 -7.1 | 1.5 | 2.2 | 2.8 |
| 11 | 1085–1260 | 4.47 | 1.0 | 0.7 | +7.2 -7.6 | 1.6 | 2.5 | 2.8 |
| 12 | 1260–1465 | 1.56 | 1.4 | 0.5 | +8.0 -7.8 | 1.5 | 2.6 | 2.8 |
| 13 | 1465–1705 | 5.06×10^{-1} | 2.1 | 0.5 | +8.1 -7.8 | 1.6 | 2.8 | 2.8 |
| 14 | 1705–1980 | 1.59×10^{-1} | 3.7 | 0.6 | +8.2 -7.9 | 1.9 | 2.6 | 2.8 |
| 15 | 1980–2300 | 4.41×10^{-2} | 7.0 | 0.7 | +8.5 -8.4 | 1.6 | 2.4 | 2.8 |
| 16 | 2300–5000 | 1.63×10^{-3} | 11.8 | 0.6 | +11.2 -9.6 | 1.3 | 3.7 | 2.8 |

Table 36: Measured differential four-jet cross section for $R = 0.4$ jets, in bins of $\Sigma p_T^{\text{central}}$, along with the uncertainties in the measurement. The events are selected using the inclusive analysis cuts and $\Delta y_{2j}^{\text{max}} > 1$, as well as $p_T^{(1)} > 400$ GeV. All other details are as for table 4.

| Bin | Bin edges [GeV] | $d\sigma/d(\Sigma p_T^{\text{central}})$ [fb/GeV] | $\delta_{\text{stat}}^{\text{data}}$ [%] | $\delta_{\text{stat}}^{\text{MC}}$ [%] | u_{JES} [%] | u_{JER} [%] | u_{unfold} [%] | u_{lumi} [%] |
|-----|-----------------|---|--|--|----------------------|----------------------|-------------------------|-----------------------|
| 1 | 120–170 | 1.94 | 2.6 | 3.5 | +11.7 -5.8 | 10.1 | 16.8 | 2.8 |
| 2 | 170–240 | 4.79 | 1.5 | 1.6 | +8.0 -6.6 | 5.5 | 8.6 | 2.8 |
| 3 | 240–315 | 6.03 | 1.4 | 1.4 | +6.5 -7.3 | 3.2 | 4.8 | 2.8 |
| 4 | 315–395 | 7.51 | 1.1 | 1.2 | +7.3 -7.7 | 2.2 | 3.9 | 2.8 |
| 5 | 395–480 | 9.99 | 0.9 | 1.0 | +6.8 -7.7 | 1.9 | 3.7 | 2.8 |
| 6 | 480–575 | 1.19×10^1 | 0.8 | 0.9 | +7.1 -7.1 | 1.9 | 3.7 | 2.8 |
| 7 | 575–680 | 1.49×10^1 | 0.6 | 0.8 | +7.3 -6.8 | 1.8 | 3.6 | 2.8 |
| 8 | 680–795 | 1.81×10^1 | 0.6 | 0.5 | +7.4 -7.1 | 1.6 | 3.3 | 2.8 |
| 9 | 795–930 | 1.21×10^1 | 0.6 | 0.5 | +7.3 -7.0 | 1.4 | 3.4 | 2.8 |
| 10 | 930–1085 | 8.24 | 0.8 | 0.6 | +7.2 -7.2 | 1.3 | 3.3 | 2.8 |
| 11 | 1085–1260 | 4.41 | 1.0 | 0.7 | +7.9 -7.6 | 1.3 | 2.9 | 2.8 |
| 12 | 1260–1465 | 1.54 | 1.4 | 0.5 | +7.7 -7.9 | 1.4 | 2.8 | 2.8 |
| 13 | 1465–1705 | 5.01×10^{-1} | 2.1 | 0.5 | +7.9 -7.8 | 1.5 | 2.9 | 2.8 |
| 14 | 1705–1980 | 1.57×10^{-1} | 3.7 | 0.6 | +8.0 -8.2 | 1.8 | 2.6 | 2.8 |
| 15 | 1980–2300 | 4.38×10^{-2} | 7.1 | 0.7 | +8.3 -8.3 | 1.5 | 2.4 | 2.8 |
| 16 | 2300–5000 | 1.62×10^{-3} | 11.8 | 0.6 | +11.1 -9.5 | 1.2 | 3.7 | 2.8 |

Table 37: Measured differential four-jet cross section for $R = 0.4$ jets, in bins of $\Sigma p_T^{\text{central}}$, along with the uncertainties in the measurement. The events are selected using the inclusive analysis cuts and $\Delta y_{2j}^{\text{max}} > 1$, as well as $p_T^{(1)} > 550$ GeV. All other details are as for table 4.

| Bin | Bin edges [GeV] | $d\sigma/d(\Sigma p_T^{\text{central}})$ [fb/GeV] | $\delta_{\text{stat}}^{\text{data}}$ [%] | $\delta_{\text{stat}}^{\text{MC}}$ [%] | u_{JES} [%] | u_{JER} [%] | u_{unfold} [%] | u_{lumi} [%] |
|-----|-----------------|---|--|--|----------------------|----------------------|-------------------------|-----------------------|
| 1 | 120–185 | 1.01×10^4 | 0.5 | 2.2 | +10.9 -8.3 | 4.6 | 11.1 | 2.8 |
| 2 | 185–270 | 1.23×10^4 | 0.3 | 1.1 | +8.9 -8.9 | 3.9 | 6.7 | 2.8 |
| 3 | 270–365 | 4.38×10^3 | 0.4 | 1.1 | +8.0 -7.5 | 1.7 | 4.4 | 2.8 |
| 4 | 365–465 | 1.39×10^3 | 0.6 | 0.7 | +6.8 -6.6 | 0.8 | 3.9 | 2.8 |
| 5 | 465–575 | 4.43×10^2 | 0.7 | 0.5 | +6.2 -6.4 | 0.8 | 2.5 | 2.8 |
| 6 | 575–700 | 1.44×10^2 | 0.6 | 0.5 | +6.5 -6.5 | 0.8 | 2.0 | 2.8 |
| 7 | 700–845 | 4.56×10^1 | 0.3 | 0.5 | +6.8 -7.1 | 0.8 | 1.9 | 2.8 |
| 8 | 845–1005 | 1.46×10^1 | 0.6 | 0.5 | +7.3 -7.1 | 0.8 | 2.2 | 2.8 |
| 9 | 1005–1195 | 4.58 | 0.9 | 0.8 | +7.6 -7.6 | 0.8 | 2.9 | 2.8 |
| 10 | 1195–1410 | 1.38 | 1.6 | 0.7 | +8.3 -7.8 | 0.8 | 3.6 | 2.8 |
| 11 | 1410–1665 | 4.12×10^{-1} | 2.4 | 0.6 | +8.0 -8.0 | 0.9 | 3.6 | 2.8 |
| 12 | 1665–1960 | 1.10×10^{-1} | 4.4 | 0.7 | +9.0 -8.4 | 1.3 | 3.4 | 2.8 |
| 13 | 1960–5000 | 4.31×10^{-3} | 7.5 | 0.7 | +8.4 -9.3 | 1.6 | 3.0 | 2.8 |

Table 38: Measured differential four-jet cross section for $R = 0.4$ jets, in bins of $\Sigma p_T^{\text{central}}$, along with the uncertainties in the measurement. The events are selected using the inclusive analysis cuts and $\Delta y_{2j}^{\text{max}} > 2$. All other details are as for table 4.

| Bin | Bin edges [GeV] | $d\sigma/d(\Sigma p_T^{\text{central}})$ [fb/GeV] | $\delta_{\text{stat}}^{\text{data}}$ [%] | $\delta_{\text{stat}}^{\text{MC}}$ [%] | u_{JES} [%] | u_{JER} [%] | u_{unfold} [%] | u_{lumi} [%] |
|-----|-----------------|---|--|--|----------------------|----------------------|-------------------------|-----------------------|
| 1 | 120–185 | 3.96×10^2 | 2.1 | 1.9 | +5.7 -6.5 | 1.8 | 8.4 | 2.8 |
| 2 | 185–270 | 8.47×10^2 | 0.9 | 0.8 | +6.8 -6.6 | 1.7 | 6.1 | 2.8 |
| 3 | 270–365 | 8.57×10^2 | 0.9 | 1.0 | +7.1 -6.8 | 1.3 | 7.3 | 2.8 |
| 4 | 365–465 | 9.37×10^2 | 0.7 | 0.5 | +7.0 -6.8 | 1.1 | 6.9 | 2.8 |
| 5 | 465–575 | 4.35×10^2 | 0.7 | 0.5 | +6.6 -6.5 | 1.1 | 3.8 | 2.8 |
| 6 | 575–700 | 1.45×10^2 | 0.6 | 0.5 | +6.7 -6.6 | 1.1 | 2.4 | 2.8 |
| 7 | 700–845 | 4.59×10^1 | 0.3 | 0.5 | +6.7 -6.9 | 1.3 | 2.0 | 2.8 |
| 8 | 845–1005 | 1.46×10^1 | 0.6 | 0.5 | +7.4 -7.2 | 1.4 | 2.2 | 2.8 |
| 9 | 1005–1195 | 4.61 | 0.9 | 0.7 | +7.8 -7.6 | 1.4 | 2.9 | 2.8 |
| 10 | 1195–1410 | 1.39 | 1.6 | 0.7 | +8.2 -7.8 | 1.5 | 3.6 | 2.8 |
| 11 | 1410–1665 | 4.14×10^{-1} | 2.4 | 0.6 | +8.8 -8.0 | 1.5 | 3.6 | 2.8 |
| 12 | 1665–1960 | 1.11×10^{-1} | 4.4 | 0.6 | +9.1 -8.4 | 1.8 | 3.4 | 2.8 |
| 13 | 1960–5000 | 4.33×10^{-3} | 7.4 | 0.7 | +8.9 -9.3 | 2.0 | 3.0 | 2.8 |

Table 39: Measured differential four-jet cross section for $R = 0.4$ jets, in bins of $\Sigma p_T^{\text{central}}$, along with the uncertainties in the measurement. The events are selected using the inclusive analysis cuts and $\Delta y_{2j}^{\text{max}} > 2$, as well as $p_T^{(1)} > 250$ GeV. All other details are as for table 4.

| Bin | Bin edges [GeV] | $d\sigma/d(\Sigma p_T^{\text{central}})$ [fb/GeV] | $\delta_{\text{stat}}^{\text{data}}$ [%] | $\delta_{\text{stat}}^{\text{MC}}$ [%] | u_{JES} [%] | u_{JER} [%] | u_{unfold} [%] | u_{lumi} [%] |
|-----|-----------------|---|--|--|----------------------|----------------------|-------------------------|-----------------------|
| 1 | 120–185 | 1.38×10^1 | 0.9 | 2.1 | +7.1 -7.1 | 5.1 | 8.3 | 2.8 |
| 2 | 185–270 | 3.96×10^1 | 0.5 | 1.0 | +6.8 -7.0 | 2.8 | 5.7 | 2.8 |
| 3 | 270–365 | 5.95×10^1 | 0.4 | 0.8 | +6.3 -7.0 | 1.8 | 4.2 | 2.8 |
| 4 | 365–465 | 5.75×10^1 | 0.3 | 0.8 | +6.6 -6.9 | 1.6 | 3.5 | 2.8 |
| 5 | 465–575 | 8.69×10^1 | 0.3 | 0.5 | +6.4 -6.5 | 1.3 | 3.7 | 2.8 |
| 6 | 575–700 | 6.98×10^1 | 0.3 | 0.5 | +6.9 -6.4 | 1.2 | 3.7 | 2.8 |
| 7 | 700–845 | 3.85×10^1 | 0.3 | 0.5 | +6.9 -7.0 | 1.3 | 3.5 | 2.8 |
| 8 | 845–1005 | 1.45×10^1 | 0.6 | 0.5 | +7.4 -7.2 | 1.3 | 2.8 | 2.8 |
| 9 | 1005–1195 | 4.58 | 0.9 | 0.8 | +7.8 -7.5 | 1.4 | 3.0 | 2.8 |
| 10 | 1195–1410 | 1.38 | 1.6 | 0.7 | +8.2 -7.8 | 1.5 | 3.6 | 2.8 |
| 11 | 1410–1665 | 4.11×10^{-1} | 2.4 | 0.6 | +8.8 -7.9 | 1.6 | 3.6 | 2.8 |
| 12 | 1665–1960 | 1.10×10^{-1} | 4.4 | 0.6 | +9.0 -8.3 | 1.8 | 3.4 | 2.8 |
| 13 | 1960–5000 | 4.30×10^{-3} | 7.5 | 0.7 | +8.9 -9.2 | 2.0 | 3.0 | 2.8 |

Table 40: Measured differential four-jet cross section for $R = 0.4$ jets, in bins of $\Sigma p_T^{\text{central}}$, along with the uncertainties in the measurement. The events are selected using the inclusive analysis cuts and $\Delta y_{2j}^{\text{max}} > 2$, as well as $p_T^{(1)} > 400$ GeV. All other details are as for table 4.

| Bin | Bin edges [GeV] | $d\sigma/d(\Sigma p_T^{\text{central}})$ [fb/GeV] | $\delta_{\text{stat}}^{\text{data}}$ [%] | $\delta_{\text{stat}}^{\text{MC}}$ [%] | u_{JES} [%] | u_{JER} [%] | u_{unfold} [%] | u_{lumi} [%] |
|-----|-----------------|---|--|--|----------------------|----------------------|-------------------------|-----------------------|
| 1 | 120–185 | 1.12 | 3.4 | 3.7 | +8.1 -7.5 | 3.6 | 20.8 | 2.8 |
| 2 | 185–270 | 2.62 | 1.7 | 1.9 | +7.8 -7.3 | 3.3 | 8.7 | 2.8 |
| 3 | 270–365 | 3.75 | 1.3 | 1.4 | +7.6 -8.2 | 2.5 | 3.6 | 2.8 |
| 4 | 365–465 | 5.76 | 1.1 | 1.3 | +6.9 -8.7 | 2.2 | 3.5 | 2.8 |
| 5 | 465–575 | 7.27 | 0.9 | 1.0 | +7.7 -7.7 | 2.2 | 5.1 | 2.8 |
| 6 | 575–700 | 9.64 | 0.8 | 0.8 | +7.8 -7.2 | 2.1 | 5.5 | 2.8 |
| 7 | 700–845 | 9.83 | 0.6 | 0.6 | +7.6 -7.3 | 1.7 | 4.5 | 2.8 |
| 8 | 845–1005 | 6.31 | 0.9 | 0.7 | +7.6 -7.4 | 1.4 | 3.7 | 2.8 |
| 9 | 1005–1195 | 3.99 | 1.0 | 0.7 | +7.6 -7.6 | 1.3 | 3.5 | 2.8 |
| 10 | 1195–1410 | 1.37 | 1.6 | 0.7 | +8.0 -7.7 | 1.3 | 3.9 | 2.8 |
| 11 | 1410–1665 | 4.07×10^{-1} | 2.5 | 0.6 | +8.5 -7.9 | 1.4 | 3.7 | 2.8 |
| 12 | 1665–1960 | 1.09×10^{-1} | 4.4 | 0.6 | +8.8 -8.3 | 1.7 | 3.4 | 2.8 |
| 13 | 1960–5000 | 4.26×10^{-3} | 7.5 | 0.7 | +8.8 -9.0 | 1.9 | 3.0 | 2.8 |

Table 41: Measured differential four-jet cross section for $R = 0.4$ jets, in bins of $\Sigma p_T^{\text{central}}$, along with the uncertainties in the measurement. The events are selected using the inclusive analysis cuts and $\Delta y_{2j}^{\text{max}} > 2$, as well as $p_T^{(1)} > 550$ GeV. All other details are as for table 4.

| Bin | Bin edges [GeV] | $d\sigma/d(\Sigma p_T^{\text{central}})$ [fb/GeV] | $\delta_{\text{stat}}^{\text{data}}$ [%] | $\delta_{\text{stat}}^{\text{MC}}$ [%] | u_{JES} [%] | u_{JER} [%] | u_{unfold} [%] | u_{lumi} [%] |
|-----|-----------------|---|--|--|----------------------|----------------------|-------------------------|-----------------------|
| 1 | 120–190 | 5.25×10^3 | 0.7 | 3.2 | +10.4 -10.1 | 5.4 | 8.0 | 2.8 |
| 2 | 190–285 | 5.85×10^3 | 0.4 | 1.3 | +9.7 -9.7 | 4.6 | 6.5 | 2.8 |
| 3 | 285–385 | 1.77×10^3 | 0.7 | 1.1 | +8.8 -8.0 | 2.2 | 4.5 | 2.8 |
| 4 | 385–490 | 5.1×10^2 | 1.0 | 0.9 | +8.0 -6.4 | 1.2 | 3.4 | 2.8 |
| 5 | 490–605 | 1.55×10^2 | 1.1 | 0.8 | +7.1 -6.2 | 1.2 | 2.3 | 2.8 |
| 6 | 605–735 | 4.7×10^1 | 0.6 | 0.9 | +7.1 -6.6 | 1.2 | 2.4 | 2.8 |
| 7 | 735–880 | 1.45×10^1 | 0.5 | 0.8 | +7.6 -7.3 | 1.2 | 3.5 | 2.8 |
| 8 | 880–1040 | 4.49 | 0.9 | 1.0 | +8.1 -7.8 | 1.2 | 3.6 | 2.8 |
| 9 | 1040–1225 | 1.44 | 1.4 | 1.2 | +8.6 -7.9 | 1.2 | 4.0 | 2.8 |
| 10 | 1225–1430 | 4.69×10^{-1} | 2.9 | 1.1 | +9.1 -7.9 | 1.2 | 5.1 | 2.8 |
| 11 | 1430–1655 | 1.52×10^{-1} | 4.5 | 1.3 | +9.2 -8.6 | 1.2 | 4.5 | 2.8 |
| 12 | 1655–1905 | 4.60×10^{-2} | 7.4 | 1.3 | +9.6 -8.9 | 1.5 | 4.5 | 2.8 |
| 13 | 1905–5000 | 2.01×10^{-3} | 10.7 | 1.2 | +10.1 -10.7 | 1.6 | 6.8 | 2.8 |

Table 42: Measured differential four-jet cross section for $R = 0.4$ jets, in bins of $\Sigma p_T^{\text{central}}$, along with the uncertainties in the measurement. The events are selected using the inclusive analysis cuts and $\Delta y_{2j}^{\text{max}} > 3$. All other details are as for table 4.

| Bin | Bin edges [GeV] | $d\sigma/d(\Sigma p_T^{\text{central}})$ [fb/GeV] | $\delta_{\text{stat}}^{\text{data}}$ [%] | $\delta_{\text{stat}}^{\text{MC}}$ [%] | u_{JES} [%] | u_{JER} [%] | u_{unfold} [%] | u_{lumi} [%] |
|-----|-----------------|---|--|--|----------------------|----------------------|-------------------------|-----------------------|
| 1 | 120–190 | 1.86×10^2 | 3.0 | 2.4 | +9.1 -5.3 | 2.0 | 4.1 | 2.8 |
| 2 | 190–285 | 3.54×10^2 | 1.3 | 1.2 | +8.6 -8.0 | 2.0 | 5.4 | 2.8 |
| 3 | 285–385 | 4.27×10^2 | 1.2 | 1.3 | +7.4 -7.7 | 2.0 | 7.8 | 2.8 |
| 4 | 385–490 | 3.77×10^2 | 0.9 | 0.8 | +7.1 -7.2 | 1.9 | 5.2 | 2.8 |
| 5 | 490–605 | 1.56×10^2 | 1.1 | 0.8 | +6.6 -6.2 | 1.5 | 2.8 | 2.8 |
| 6 | 605–735 | 4.75×10^1 | 0.6 | 0.9 | +7.2 -6.7 | 1.4 | 2.6 | 2.8 |
| 7 | 735–880 | 1.46×10^1 | 0.5 | 0.8 | +7.6 -7.4 | 1.4 | 3.5 | 2.8 |
| 8 | 880–1040 | 4.53 | 0.9 | 0.9 | +7.9 -8.0 | 1.4 | 3.6 | 2.8 |
| 9 | 1040–1225 | 1.45 | 1.4 | 1.1 | +8.6 -8.1 | 1.4 | 4.0 | 2.8 |
| 10 | 1225–1430 | 4.73×10^{-1} | 2.9 | 1.1 | +9.3 -8.1 | 1.4 | 5.1 | 2.8 |
| 11 | 1430–1655 | 1.53×10^{-1} | 4.5 | 1.3 | +9.2 -8.8 | 1.5 | 4.5 | 2.8 |
| 12 | 1655–1905 | 4.63×10^{-2} | 7.4 | 1.3 | +9.3 -9.2 | 1.9 | 4.5 | 2.8 |
| 13 | 1905–5000 | 2.02×10^{-3} | 10.6 | 1.2 | +9.9 -10.9 | 2.1 | 6.8 | 2.8 |

Table 43: Measured differential four-jet cross section for $R = 0.4$ jets, in bins of $\Sigma p_T^{\text{central}}$, along with the uncertainties in the measurement. The events are selected using the inclusive analysis cuts and $\Delta y_{2j}^{\text{max}} > 3$, as well as $p_T^{(1)} > 250$ GeV. All other details are as for table 4.

| Bin | Bin edges [GeV] | $d\sigma/d(\Sigma p_T^{\text{central}})$ [fb/GeV] | $\delta_{\text{stat}}^{\text{data}}$ [%] | $\delta_{\text{stat}}^{\text{MC}}$ [%] | u_{JES} [%] | u_{JER} [%] | u_{unfold} [%] | u_{lumi} [%] |
|-----|-----------------|---|--|--|----------------------|----------------------|-------------------------|-----------------------|
| 1 | 120–190 | 3.81 | 1.6 | 4.0 | +9.3 -9.8 | 1.4 | 3.6 | 2.8 |
| 2 | 190–285 | 1.35×10^1 | 0.8 | 1.5 | +8.1 -8.5 | 1.4 | 4.6 | 2.8 |
| 3 | 285–385 | 2.17×10^1 | 0.6 | 1.1 | +7.0 -7.3 | 1.4 | 6.1 | 2.8 |
| 4 | 385–490 | 2.12×10^1 | 0.6 | 1.5 | +7.1 -6.9 | 1.4 | 7.9 | 2.8 |
| 5 | 490–605 | 3.56×10^1 | 0.4 | 0.8 | +7.3 -6.9 | 1.4 | 5.1 | 2.8 |
| 6 | 605–735 | 2.46×10^1 | 0.5 | 0.8 | +6.9 -7.0 | 1.4 | 3.5 | 2.8 |
| 7 | 735–880 | 1.32×10^1 | 0.6 | 0.9 | +7.2 -7.5 | 1.5 | 3.0 | 2.8 |
| 8 | 880–1040 | 4.49 | 0.9 | 1.0 | +7.8 -7.9 | 1.9 | 3.1 | 2.8 |
| 9 | 1040–1225 | 1.43 | 1.4 | 1.1 | +8.3 -8.0 | 2.0 | 3.9 | 2.8 |
| 10 | 1225–1430 | 4.69×10^{-1} | 2.9 | 1.1 | +9.2 -8.1 | 2.0 | 5.1 | 2.8 |
| 11 | 1430–1655 | 1.51×10^{-1} | 4.5 | 1.3 | +9.1 -8.7 | 2.0 | 4.5 | 2.8 |
| 12 | 1655–1905 | 4.59×10^{-2} | 7.4 | 1.3 | +9.4 -9.1 | 2.0 | 4.5 | 2.8 |
| 13 | 1905–5000 | 2.00×10^{-3} | 10.7 | 1.2 | +9.9 -10.8 | 1.7 | 6.8 | 2.8 |

Table 44: Measured differential four-jet cross section for $R = 0.4$ jets, in bins of $\Sigma p_T^{\text{central}}$, along with the uncertainties in the measurement. The events are selected using the inclusive analysis cuts and $\Delta y_{2j}^{\text{max}} > 3$, as well as $p_T^{(1)} > 400$ GeV. All other details are as for table 4.

| Bin | Bin edges [GeV] | $d\sigma/d(\Sigma p_T^{\text{central}})$ [fb/GeV] | $\delta_{\text{stat}}^{\text{data}}$ [%] | $\delta_{\text{stat}}^{\text{MC}}$ [%] | u_{JES} [%] | u_{JER} [%] | u_{unfold} [%] | u_{lumi} [%] |
|-----|-----------------|---|--|--|----------------------|----------------------|-------------------------|-----------------------|
| 1 | 120–190 | 1.63×10^{-1} | 7.7 | 10.2 | +12.8 -7.5 | 5.6 | 3.8 | 2.8 |
| 2 | 190–285 | 4.76×10^{-1} | 4.0 | 4.0 | +9.6 -8.2 | 5.6 | 3.8 | 2.8 |
| 3 | 285–385 | 9.39×10^{-1} | 2.6 | 2.8 | +8.5 -8.8 | 5.6 | 4.2 | 2.8 |
| 4 | 385–490 | 1.79 | 2.2 | 2.8 | +8.7 -9.8 | 5.5 | 5.3 | 2.8 |
| 5 | 490–605 | 2.21 | 1.8 | 2.1 | +9.6 -10.2 | 4.9 | 6.2 | 2.8 |
| 6 | 605–735 | 3.43 | 1.2 | 1.3 | +8.9 -9.1 | 3.0 | 7.3 | 2.8 |
| 7 | 735–880 | 2.86 | 1.2 | 1.0 | +8.3 -8.7 | 2.2 | 6.1 | 2.8 |
| 8 | 880–1040 | 2.10 | 1.4 | 1.3 | +8.1 -8.0 | 2.1 | 3.8 | 2.8 |
| 9 | 1040–1225 | 1.34 | 1.4 | 1.1 | +8.1 -7.9 | 1.8 | 3.7 | 2.8 |
| 10 | 1225–1430 | 4.64×10^{-1} | 2.9 | 1.1 | +9.0 -9.0 | 1.7 | 5.1 | 2.8 |
| 11 | 1430–1655 | 1.50×10^{-1} | 4.5 | 1.3 | +8.6 -8.8 | 1.7 | 4.6 | 2.8 |
| 12 | 1655–1905 | 4.54×10^{-2} | 7.4 | 1.3 | +9.9 -9.7 | 1.7 | 4.5 | 2.8 |
| 13 | 1905–5000 | 1.98×10^{-3} | 10.7 | 1.2 | +9.7 -10.5 | 1.7 | 6.8 | 2.8 |

Table 45: Measured differential four-jet cross section for $R = 0.4$ jets, in bins of $\Sigma p_T^{\text{central}}$, along with the uncertainties in the measurement. The events are selected using the inclusive analysis cuts and $\Delta y_{2j}^{\text{max}} > 3$, as well as $p_T^{(1)} > 550$ GeV. All other details are as for table 4.

| Bin | Bin edges [GeV] | $d\sigma/d(\Sigma p_T^{\text{central}})$ [fb/GeV] | $\delta_{\text{stat}}^{\text{data}}$ [%] | $\delta_{\text{stat}}^{\text{MC}}$ [%] | u_{JES} [%] | u_{JER} [%] | u_{unfold} [%] | u_{lumi} [%] |
|-----|-----------------|---|--|--|----------------------|----------------------|-------------------------|-----------------------|
| 1 | 120–190 | 1.56×10^3 | 1.1 | 6.6 | +10.3 -8.7 | 4.2 | 18.1 | 2.8 |
| 2 | 190–285 | 1.72×10^3 | 0.8 | 2.7 | +10.1 -8.8 | 4.2 | 11.0 | 2.8 |
| 3 | 285–385 | 4.81×10^2 | 1.3 | 2.0 | +9.5 -8.7 | 3.7 | 5.6 | 2.8 |
| 4 | 385–490 | 1.26×10^2 | 2.1 | 2.2 | +8.7 -8.2 | 2.4 | 4.0 | 2.8 |
| 5 | 490–605 | 3.72×10^1 | 2.7 | 1.7 | +6.9 -7.9 | 1.9 | 3.2 | 2.8 |
| 6 | 605–730 | 1.09×10^1 | 1.8 | 1.9 | +6.4 -7.8 | 1.8 | 2.9 | 2.8 |
| 7 | 730–865 | 3.18 | 1.1 | 1.9 | +7.2 -8.3 | 1.8 | 3.5 | 2.8 |
| 8 | 865–1010 | 1.07 | 2.0 | 2.6 | +8.1 -9.8 | 1.8 | 5.5 | 2.8 |
| 9 | 1010–1170 | 3.49×10^{-1} | 3.7 | 3.2 | +8.9 -12.0 | 1.8 | 5.9 | 2.8 |
| 10 | 1170–1340 | 1.29×10^{-1} | 5.6 | 3.6 | +9.1 -11.5 | 1.8 | 4.9 | 2.8 |
| 11 | 1340–1525 | 4.99×10^{-2} | 9.8 | 3.3 | +9.1 -11.1 | 1.8 | 4.5 | 2.8 |
| 12 | 1525–5000 | 1.25×10^{-3} | 12.0 | 2.6 | +11.7 -11.8 | 1.8 | 4.5 | 2.8 |

Table 46: Measured differential four-jet cross section for $R = 0.4$ jets, in bins of $\Sigma p_T^{\text{central}}$, along with the uncertainties in the measurement. The events are selected using the inclusive analysis cuts and $\Delta y_{2j}^{\text{max}} > 4$. All other details are as for table 4.

| Bin | Bin edges [GeV] | $d\sigma/d(\Sigma p_T^{\text{central}})$ [fb/GeV] | $\delta_{\text{stat}}^{\text{data}}$ [%] | $\delta_{\text{stat}}^{\text{MC}}$ [%] | u_{JES} [%] | u_{JER} [%] | u_{unfold} [%] | u_{lumi} [%] |
|-----|-----------------|---|--|--|----------------------|----------------------|-------------------------|-----------------------|
| 1 | 120–190 | 3.57×10^1 | 7.3 | 5.7 | +5.6 -6.9 | 2.0 | 5.4 | 2.8 |
| 2 | 190–285 | 6.91×10^1 | 3.0 | 2.8 | +7.5 -7.7 | 2.0 | 6.1 | 2.8 |
| 3 | 285–385 | 9.82×10^1 | 3.1 | 2.4 | +8.1 -8.5 | 2.0 | 7.0 | 2.8 |
| 4 | 385–490 | 9.06×10^1 | 2.0 | 1.7 | +9.7 -9.2 | 2.0 | 4.4 | 2.8 |
| 5 | 490–605 | 3.75×10^1 | 2.6 | 1.8 | +7.4 -8.1 | 2.0 | 3.1 | 2.8 |
| 6 | 605–730 | 1.1×10^1 | 1.7 | 1.8 | +7.8 -8.1 | 2.0 | 3.5 | 2.8 |
| 7 | 730–865 | 3.21 | 1.1 | 1.9 | +8.1 -9.1 | 2.0 | 5.0 | 2.8 |
| 8 | 865–1010 | 1.09 | 2.0 | 2.5 | +8.5 -10.2 | 2.0 | 5.8 | 2.8 |
| 9 | 1010–1170 | 3.53×10^{-1} | 3.6 | 3.2 | +9.2 -10.6 | 2.0 | 6.5 | 2.8 |
| 10 | 1170–1340 | 1.30×10^{-1} | 5.6 | 3.5 | +9.4 -11.0 | 2.0 | 6.3 | 2.8 |
| 11 | 1340–1525 | 5.03×10^{-2} | 9.7 | 3.3 | +9.5 -11.2 | 2.0 | 4.9 | 2.8 |
| 12 | 1525–5000 | 1.27×10^{-3} | 11.9 | 2.5 | +12.0 -12.1 | 2.0 | 4.1 | 2.8 |

Table 47: Measured differential four-jet cross section for $R = 0.4$ jets, in bins of $\Sigma p_T^{\text{central}}$, along with the uncertainties in the measurement. The events are selected using the inclusive analysis cuts and $\Delta y_{2j}^{\text{max}} > 4$, as well as $p_T^{(1)} > 250$ GeV. All other details are as for table 4.

| Bin | Bin edges [GeV] | $d\sigma/d(\Sigma p_T^{\text{central}})$ [fb/GeV] | $\delta_{\text{stat}}^{\text{data}}$ [%] | $\delta_{\text{stat}}^{\text{MC}}$ [%] | u_{JES} [%] | u_{JER} [%] | u_{unfold} [%] | u_{lumi} [%] |
|-----|-----------------|---|--|--|----------------------|----------------------|-------------------------|-----------------------|
| 1 | 120–190 | 2.99×10^{-1} | 5.3 | 13.9 | $^{+9.6}_{-6.3}$ | 2.3 | 5.6 | 2.8 |
| 2 | 190–285 | 1.53 | 2.3 | 4.9 | $^{+9.7}_{-8.5}$ | 2.3 | 5.6 | 2.8 |
| 3 | 285–385 | 2.72 | 1.7 | 3.5 | $^{+9.7}_{-9.9}$ | 2.3 | 6.3 | 2.8 |
| 4 | 385–490 | 2.92 | 1.5 | 4.3 | $^{+9.5}_{-8.8}$ | 2.3 | 8.2 | 2.8 |
| 5 | 490–605 | 6.36 | 1.0 | 1.7 | $^{+8.6}_{-8.9}$ | 2.3 | 7.9 | 2.8 |
| 6 | 605–730 | 4.84 | 1.1 | 1.9 | $^{+7.8}_{-8.6}$ | 2.3 | 4.9 | 2.8 |
| 7 | 730–865 | 2.80 | 1.2 | 1.8 | $^{+7.9}_{-8.9}$ | 2.3 | 3.7 | 2.8 |
| 8 | 865–1010 | 1.08 | 2.0 | 2.6 | $^{+9.1}_{-9.7}$ | 2.3 | 4.2 | 2.8 |
| 9 | 1010–1170 | 3.49×10^{-1} | 3.7 | 3.3 | $^{+9.6}_{-11.4}$ | 2.3 | 6.0 | 2.8 |
| 10 | 1170–1340 | 1.29×10^{-1} | 5.6 | 3.5 | $^{+9.6}_{-11.9}$ | 2.3 | 6.2 | 2.8 |
| 11 | 1340–1525 | 4.99×10^{-2} | 9.8 | 3.3 | $^{+9.4}_{-11.7}$ | 2.3 | 4.9 | 2.8 |
| 12 | 1525–5000 | 1.25×10^{-3} | 12.0 | 2.5 | $^{+11.1}_{-12.7}$ | 2.3 | 4.1 | 2.8 |

Table 48: Measured differential four-jet cross section for $R = 0.4$ jets, in bins of $\Sigma p_T^{\text{central}}$, along with the uncertainties in the measurement. The events are selected using the inclusive analysis cuts and $\Delta y_{2j}^{\text{max}} > 4$, as well as $p_T^{(1)} > 400$ GeV. All other details are as for table 4.

| Bin | Bin edges [GeV] | $d\sigma/d(\Sigma p_T^{\text{central}})$ [fb/GeV] | $\delta_{\text{stat}}^{\text{data}}$ [%] | $\delta_{\text{stat}}^{\text{MC}}$ [%] | u_{JES} [%] | u_{JER} [%] | u_{unfold} [%] | u_{lumi} [%] |
|-----|-----------------|---|--|--|----------------------|----------------------|-------------------------|-----------------------|
| 1 | 120–190 | 4.02×10^{-4} | 103.7 | 141.7 | $^{+13.0}_{-18.5}$ | 3.2 | 4.8 | 2.8 |
| 2 | 190–285 | 1.92×10^{-2} | 20.4 | 30.3 | $^{+14.8}_{-18.6}$ | 3.2 | 17.8 | 2.8 |
| 3 | 285–385 | 4.80×10^{-2} | 11.4 | 14.6 | $^{+16.1}_{-18.2}$ | 3.2 | 23.4 | 2.8 |
| 4 | 385–490 | 1.51×10^{-1} | 6.8 | 9.1 | $^{+16.2}_{-17.0}$ | 3.2 | 23.9 | 2.8 |
| 5 | 490–605 | 1.42×10^{-1} | 6.6 | 8.0 | $^{+15.2}_{-15.6}$ | 3.2 | 21.6 | 2.8 |
| 6 | 605–730 | 3.53×10^{-1} | 3.6 | 3.7 | $^{+12.5}_{-12.4}$ | 3.2 | 14.8 | 2.8 |
| 7 | 730–865 | 3.55×10^{-1} | 3.8 | 2.7 | $^{+10.2}_{-11.1}$ | 3.2 | 10.7 | 2.8 |
| 8 | 865–1010 | 3.75×10^{-1} | 2.9 | 3.4 | $^{+9.6}_{-11.2}$ | 3.2 | 6.6 | 2.8 |
| 9 | 1010–1170 | 3.03×10^{-1} | 4.0 | 3.1 | $^{+9.6}_{-11.5}$ | 3.2 | 5.0 | 2.8 |
| 10 | 1170–1340 | 1.28×10^{-1} | 5.6 | 3.5 | $^{+9.7}_{-11.7}$ | 3.2 | 4.9 | 2.8 |
| 11 | 1340–1525 | 4.95×10^{-2} | 9.8 | 3.3 | $^{+10.0}_{-12.0}$ | 3.2 | 4.9 | 2.8 |
| 12 | 1525–5000 | 1.24×10^{-3} | 12.1 | 2.6 | $^{+10.2}_{-12.6}$ | 3.2 | 3.7 | 2.8 |

Table 49: Measured differential four-jet cross section for $R = 0.4$ jets, in bins of $\Sigma p_T^{\text{central}}$, along with the uncertainties in the measurement. The events are selected using the inclusive analysis cuts and $\Delta y_{2j}^{\text{max}} > 4$, as well as $p_T^{(1)} > 550$ GeV. All other details are as for table 4.

References

- [1] L. Evans (ed.) and P. Bryant (ed.), *LHC Machine*, *JINST* **3** (2008) S08001.
- [2] C. Berger et al., *An Automated Implementation of On-Shell Methods for One-Loop Amplitudes*, *Phys. Rev.* **D78** (2008) 036003, and we thank Dr D. Maître (Durham University, UK) for providing the BlackHat histograms that were compared with the data, arXiv:0803.4180 [hep-ph].
- [3] Z. Bern et al., *Four-Jet Production at the Large Hadron Collider at Next-to-Leading Order in QCD*, *Phys. Rev. Lett.* **109** (2012) 042001, arXiv:1112.3940 [hep-ph].
- [4] S. Hoeche et al., *QCD matrix elements + parton showers: The NLO case*, *JHEP* **1304** (2013) 027, arXiv:1207.5030 [hep-ph].
- [5] T. Sjöstrand, S. Mrenna and P. Z. Skands, *A Brief Introduction to PYTHIA 8.1*, *Comput. Phys. Commun.* **178** (2008) 852–867, arXiv:0710.3820 [hep-ph].
- [6] M. Bähr et al., *Herwig++ physics and manual*, *Eur. Phys. J.* **C58** (2008) 639, arXiv:0803.0883 [hep-ph].
- [7] T. Gleisberg et al., *Event generation with SHERPA 1.1*, *JHEP* **02** (2009) 007, arXiv:0811.4622 [hep-ph].
- [8] J. Alwall et al., *The automated computation of tree-level and next-to-leading order differential cross sections, and their matching to parton shower simulations*, *JHEP* **1407** (2014) 079, arXiv:1405.0301 [hep-ph].
- [9] ATLAS Collaboration, *Measurement of multi-jet cross sections in proton-proton collisions at a 7 TeV center-of-mass energy*, *Eur. Phys. J.* **C71** (2011) 1763, arXiv:1107.2092 [hep-ex].
- [10] S. Badger et al., *Next-to-leading order QCD corrections to five jet production at the LHC*, *Phys. Rev.* **D89** (2014) 034019, arXiv:1309.6585 [hep-ph].
- [11] ATLAS Collaboration, *Search for new phenomena in final states with large jet multiplicities and missing transverse momentum at $\sqrt{s}=8$ TeV proton-proton collisions using the ATLAS experiment*, *JHEP* **1310** (2013) 130, arXiv:1308.1841 [hep-ex].
- [12] R. Brandelik et al., (TASSO Collaboration), *Evidence for Planar Events in e^+e^- Annihilation at High-Energies*, *Phys. Lett.* **B86** (1979) 243.
- [13] D. Barber et al., *Discovery of Three Jet Events and a Test of Quantum Chromodynamics at PETRA Energies*, *Phys. Rev. Lett.* **43** (1979) 830.
- [14] W. Bartel et al., (JADE Collaboration), *Observation of planar three-jet events in e^+e^- annihilation and evidence for gluon bremsstrahlung*, *Phys. Lett.* **B91** (Mar. 1980) 142–147.
- [15] C. Berger et al., (PLUTO Collaboration), *Evidence for gluon bremsstrahlung in e^+e^- annihilations at high energies*, *Phys. Lett.* **B86** (Oct. 1979) 418–425.
- [16] ATLAS Collaboration, *Measurement of three-jet production cross sections in pp collisions at 7 TeV centre-of-mass energy using the ATLAS detector*, *Eur. Phys. J.* **C75** (2015) 228, arXiv:1411.1855 [hep-ex].

- [17] CMS Collaboration, *Measurement of the ratio of the inclusive 3-jet cross section to the inclusive 2-jet cross section in pp collisions at $\sqrt{s} = 7$ TeV and first determination of the strong coupling constant in the TeV range*, *Eur. Phys. J.* **C73** (2013) 2604, arXiv:1304.7498 [hep-ex].
- [18] ATLAS Collaboration, *Measurement of event shapes at large momentum transfer with the ATLAS detector in pp collisions at $\sqrt{s} = 7$ TeV*, *Eur. Phys. J.* **C72** (2012) 2211, arXiv:1206.2135 [hep-ex].
- [19] CMS Collaboration, *Study of hadronic event-shape variables in multijet final states in pp collisions at $\sqrt{s} = 7$ TeV*, *JHEP* **1410** (2014) 87, arXiv:1407.2856 [hep-ex].
- [20] CMS Collaboration, *Distributions of topological observables in inclusive three- and four-jet events in pp collisions at $\sqrt{s} = 7$ TeV*, *Eur. Phys. J.* **C75** (2015) 302, arXiv:1502.04785 [hep-ex].
- [21] D. Acosta et al., (CDF Collaboration), *Comparison of three-jet events in $p\bar{p}$ collisions at $\sqrt{s} = 1.8$ TeV to predictions from a next-to-leading order QCD calculation*, *Phys. Rev.* **D71** (2005) 032002, arXiv:hep-ex/0410018.
- [22] F. Abe et al., (CDF collaboration), *Study of four jet events and evidence for double parton interactions in $p\bar{p}$ collisions at $\sqrt{s} = 1.8$ TeV*, *Phys. Rev.* **D47** (1993) 4857–4871.
- [23] V. Abazov et al., (D0 Collaboration), *Multiple jet production at low transverse energies in $p\bar{p}$ collisions at $\sqrt{s} = 1.8$ TeV*, *Phys. Rev.* **D67** (2003) 052001, arXiv:hep-ex/0207046.
- [24] B. Abbott et al., (D0 Collaboration), *Ratios of multijet cross sections in $p\bar{p}$ collisions at $\sqrt{s} = 1.8$ TeV*, *Phys. Rev. Lett.* **86** (2001) 1955–1960, arXiv:hep-ex/0009012.
- [25] ATLAS Collaboration, *The ATLAS Experiment at the CERN Large Hadron Collider*, *JINST* **3** (2008) S08003.
- [26] ATLAS Collaboration, *Performance of the ATLAS Trigger System in 2010*, *Eur. Phys. J.* **C72** (2012) 1849, arXiv:1110.1530 [hep-ex].
- [27] M. Cacciari, G. P. Salam and G. Soyez, *The anti- k_t jet clustering algorithm*, *JHEP* **04** (2008) 063, arXiv:0802.1189 [hep-ph].
- [28] M. Cacciari, G. P. Salam and G. Soyez, *FastJet User Manual (for version 3.0.2)*, *Eur. Phys. J.* **C72** (2012) 1896, arXiv:1111.6097 [hep-ph], URL: <http://fastjet.fr/>.
- [29] T. Sjöstrand, S. Mrenna and P. Z. Skands, *PYTHIA 6.4 physics and manual*, *JHEP* **05** (2006) 026, arXiv:hep-ph/0603175.
- [30] S. Hoeche et al., *Matching parton showers and matrix elements* (2006), arXiv:hep-ph/0602031.
- [31] G. Corcella et al., *HERWIG 6.5 release note* (2002), arXiv:hep-ph/0210213.
- [32] H.-L. Lai et al., *New parton distributions for collider physics*, *Phys. Rev.* **D82** (2010) 074024, arXiv:1007.2241 [hep-ph].
- [33] J. Pumplin et al., *New generation of parton distributions with uncertainties from global QCD analysis*, *JHEP* **07** (2002) 012, arXiv:hep-ph/0201195.
- [34] ATLAS Collaboration, *Summary of ATLAS Pythia 8 tunes*, ATL-PHYS-PUB-2012-003 (2012), URL: <https://cds.cern.ch/record/1474107>.

- [35] ATLAS Collaboration, *ATLAS tunes of PYTHIA 6 and Pythia 8 for MC11*, ATL-PHYS-PUB-2011-009 (2011), URL: <https://cds.cern.ch/record/1363300>.
- [36] S. Gieseke, C. Rohr and A. Siodmok, *Colour reconnections in Herwig++*, *Eur. Phys. J. C* **72** (2012) 2225, arXiv:1206.0041 [hep-ph].
- [37] S. Agostinelli et al., *GEANT4: A simulation toolkit*, *Nucl. Instrum. Meth. A* **506** (2003) 250.
- [38] ATLAS Collaboration, *The ATLAS Simulation Infrastructure*, *Eur. Phys. J. C* **70** (2010) 823, arXiv:1005.4568 [physics.ins-det].
- [39] S. Badger et al., *Numerical evaluation of virtual corrections to multi-jet production in massless QCD*, *Comput. Phys. Commun.* **184** (2013) 1981–1998, and we thank Dr S. Badger (Niels Bohr Institute, DK) for providing the NJet prediction, arXiv:1209.0100 [hep-ph].
- [40] S. Badger et al., *NLO QCD corrections to multi-jet production at the LHC with a centre-of-mass energy of $\sqrt{s} = 8$ TeV*, *Phys. Lett. B* **718.3** (2013) 965–978, arXiv:1209.0098 [hep-ph].
- [41] ATLAS Collaboration, *Measurements of the W production cross sections in association with jets with the ATLAS detector*, *Eur. Phys. J. C* **75** (2015) 82, arXiv:1409.8639 [hep-ex].
- [42] ATLAS Collaboration, *Measurement of the inclusive jet cross section in proton-proton collisions at $\sqrt{s} = 7$ TeV using 4.5 fb^{-1} of data with the ATLAS detector*, *JHEP* **1502** (2015) 153, arXiv:1410.8857 [hep-ex].
- [43] F. Krauss, R. Kuhn and G. Soff, *AMEGIC++ 1.0: A Matrix element generator in C++*, *JHEP* **0202** (2002) 044, arXiv:hep-ph/0109036.
- [44] T. Gleisberg and F. Krauss, *Automating dipole subtraction for QCD NLO calculations*, *Eur. Phys. J. C* **53** (2008) 501–523, arXiv:0709.2881 [hep-ph].
- [45] T. Gleisberg and S. Hoeche, *Comix, a new matrix element generator*, *JHEP* **12** (2008) 039, arXiv:0808.3674.
- [46] S. Hoeche, ‘Efficient dipole subtraction with Comix’, in preparation.
- [47] J. R. Andersen and J. M. Smillie, *Constructing All-Order Corrections to Multi-Jet Rates*, *JHEP* **1001** (2010) 039, and we thank Dr J. Andersen and Dr T. Hapola (Durham University, UK) for providing the histograms for the HEJ predictions, arXiv:0908.2786 [hep-ph].
- [48] J. R. Andersen and J. M. Smillie, *The Factorisation of the t-channel Pole in Quark-Gluon Scattering*, *Phys. Rev. D* **81** (2010) 114021, arXiv:0910.5113 [hep-ph].
- [49] J. R. Andersen and J. M. Smillie, *Multiple Jets at the LHC with High Energy Jets*, *JHEP* **06** (2011) 010, arXiv:1101.5394 [hep-ph].
- [50] A. Buckley et al., *LHAPDF6: parton density access in the LHC precision era*, *Eur. Phys. J. C* **75** (2015) 132, arXiv:1412.7420 [hep-ph].
- [51] M. Botje et al., *The PDF4LHC Working Group Interim Recommendations* (2011), arXiv:1101.0538 [hep-ph].
- [52] W. Lampl et al., *Calorimeter Clustering Algorithms: Description and Performance*, ATL-LARG-PUB-2008-002. ATL-COM-LARG-2008-003 (2008), URL: <https://cds.cern.ch/record/1099735>.

- [53] ATLAS Collaboration, ‘Expected performance of the ATLAS experiment - detector, trigger and physics’, [CERN-OPEN-2008-020](#), arXiv:[0901.0512](#) [[hep-ex](#)].
- [54] ATLAS Collaboration, *Jet energy measurement and its systematic uncertainty in proton-proton collisions at $\sqrt{s} = 7$ TeV with the ATLAS detector*, [Eur. Phys. J. C75 \(2015\) 17](#), arXiv:[1406.0076](#) [[hep-ex](#)].
- [55] ATLAS Collaboration, *Jet global sequential corrections with the ATLAS detector in proton-proton collisions at $\sqrt{s} = 8$ TeV*, ATLAS-CONF-2015-002 (2015), URL: <https://cds.cern.ch/record/2001682>.
- [56] ATLAS Collaboration, *Data-driven determination of the energy scale and resolution of jets reconstructed in the ATLAS calorimeters using dijet and multijet events at $\sqrt{s} = 8$ TeV*, ATLAS-CONF-2015-017 (2015), URL: <https://cds.cern.ch/record/2008678>.
- [57] M. Cacciari and G. P. Salam, *Pileup subtraction using jet areas*, [Phys. Lett. B659 \(2008\) 119](#), arXiv:[0707.1378](#) [[hep-ph](#)].
- [58] G. D’Agostini, *A Multidimensional unfolding method based on Bayes’ theorem*, [Nucl. Instrum. Meth. A362 \(1995\) 487–498](#).
- [59] G. D’Agostini, *Improved iterative Bayesian unfolding* (2010), arXiv:[1010.0632](#) [[physics.data-an](#)].
- [60] Abye, Tim, ‘*Unfolding algorithms and tests using RooUnfold*’, in the proceedings of the *PHYSTAT 2011 Workshop on Statistical Issues Related to Discovery Claims in Search Experiments and Unfolding*, CERN, Geneva, Switzerland, January 17-20 2011, 2011 313–318, arXiv:[1105.1160](#) [[physics.data-an](#)], URL: <http://inspirehep.net/record/898599/files/arXiv:1105.1160.pdf>.
- [61] ATLAS Collaboration, *Measurement of dijet cross sections in pp collisions at 7 TeV centre-of-mass energy using the ATLAS detector*, [JHEP 1405 \(2014\) 059](#), arXiv:[1312.3524](#) [[hep-ex](#)].
- [62] ATLAS Collaboration, *Jet energy resolution in proton-proton collisions at $\sqrt{s} = 7$ TeV recorded in 2010 with the ATLAS detector*, [Eur. Phys. J. C73 \(2013\) 2306](#), arXiv:[1210.6210](#) [[hep-ex](#)].
- [63] ATLAS Collaboration, *Improved luminosity determination in pp collisions at $\sqrt{s} = 7$ TeV using the ATLAS detector at the LHC*, [Eur. Phys. J. C73 \(2013\) 2518](#), arXiv:[1302.4393](#) [[hep-ex](#)].
- [64] ATLAS Collaboration, *Measurements of jet vetoes and azimuthal decorrelations in dijet events produced in pp collisions at $\sqrt{s} = 7$ TeV using the ATLAS detector*, [Eur. Phys. J. C74 \(2014\) 3117](#), arXiv:[1407.5756](#) [[hep-ex](#)].

The ATLAS Collaboration

G. Aad⁸⁵, B. Abbott¹¹³, J. Abdallah¹⁵¹, O. Abdinov¹¹, R. Aben¹⁰⁷, M. Abolins⁹⁰, O.S. AbouZeid¹⁵⁸, H. Abramowicz¹⁵³, H. Abreu¹⁵², R. Abreu¹¹⁶, Y. Abulaiti^{146a,146b}, B.S. Acharya^{164a,164b,a}, L. Adamczyk^{38a}, D.L. Adams²⁵, J. Adelman¹⁰⁸, S. Adomeit¹⁰⁰, T. Adye¹³¹, A.A. Affolder⁷⁴, T. Agatonovic-Jovin¹³, J. Agricola⁵⁴, J.A. Aguilar-Saavedra^{126a,126f}, S.P. Ahlen²², F. Ahmadov^{65,b}, G. Aielli^{133a,133b}, H. Akerstedt^{146a,146b}, T.P.A. Åkesson⁸¹, A.V. Akimov⁹⁶, G.L. Alberghi^{20a,20b}, J. Albert¹⁶⁹, S. Albrand⁵⁵, M.J. Alconada Verzini⁷¹, M. Aleksa³⁰, I.N. Aleksandrov⁶⁵, C. Alexa^{26a}, G. Alexander¹⁵³, T. Alexopoulos¹⁰, M. Alhroob¹¹³, G. Alimonti^{91a}, L. Alio⁸⁵, J. Alison³¹, S.P. Alkire³⁵, B.M.M. Allbrooke¹⁴⁹, P.P. Allport⁷⁴, A. Aloisio^{104a,104b}, A. Alonso³⁶, F. Alonso⁷¹, C. Alpigiani⁷⁶, A. Altheimer³⁵, B. Alvarez Gonzalez³⁰, D. Álvarez Piqueras¹⁶⁷, M.G. Alviggi^{104a,104b}, B.T. Amadio¹⁵, K. Amako⁶⁶, Y. Amaral Coutinho^{24a}, C. Amelung²³, D. Amidei⁸⁹, S.P. Amor Dos Santos^{126a,126c}, A. Amorim^{126a,126b}, S. Amoroso⁴⁸, N. Amram¹⁵³, G. Amundsen²³, C. Anastopoulos¹³⁹, L.S. Ancu⁴⁹, N. Andari¹⁰⁸, T. Andeen³⁵, C.F. Anders^{58b}, G. Anders³⁰, J.K. Anders⁷⁴, K.J. Anderson³¹, A. Andreazza^{91a,91b}, V. Andrei^{58a}, S. Angelidakis⁹, I. Angelozzi¹⁰⁷, P. Anger⁴⁴, A. Angerami³⁵, F. Anghinolfi³⁰, A.V. Anisenkov^{109,c}, N. Anjos¹², A. Annovi^{124a,124b}, M. Antonelli⁴⁷, A. Antonov⁹⁸, J. Antos^{144b}, F. Anulli^{132a}, M. Aoki⁶⁶, L. Aperio Bella¹⁸, G. Arabidze⁹⁰, Y. Arai⁶⁶, J.P. Araque^{126a}, A.T.H. Arce⁴⁵, F.A. Arduh⁷¹, J-F. Arguin⁹⁵, S. Argyropoulos⁶³, M. Arik^{19a}, A.J. Armbruster³⁰, O. Arnaez³⁰, V. Arnal⁸², H. Arnold⁴⁸, M. Arratia²⁸, O. Arslan²¹, A. Artamonov⁹⁷, G. Artoni²³, S. Asai¹⁵⁵, N. Asbah⁴², A. Ashkenazi¹⁵³, B. Åsman^{146a,146b}, L. Asquith¹⁴⁹, K. Assamagan²⁵, R. Astalos^{144a}, M. Atkinson¹⁶⁵, N.B. Atlay¹⁴¹, K. Augsten¹²⁸, M. Aurousseau^{145b}, G. Avolio³⁰, B. Axen¹⁵, M.K. Ayoub¹¹⁷, G. Azuelos^{95,d}, M.A. Baak³⁰, A.E. Baas^{58a}, M.J. Baca¹⁸, C. Bacci^{134a,134b}, H. Bachacou¹³⁶, K. Bachas¹⁵⁴, M. Backes³⁰, M. Backhaus³⁰, P. Bagiachi^{132a,132b}, P. Bagnaia^{132a,132b}, Y. Bai^{33a}, T. Bain³⁵, J.T. Baines¹³¹, O.K. Baker¹⁷⁶, E.M. Baldin^{109,c}, P. Balek¹²⁹, T. Balestri¹⁴⁸, F. Balli⁸⁴, E. Banas³⁹, Sw. Banerjee¹⁷³, A.A.E. Bannoura¹⁷⁵, H.S. Bansil¹⁸, L. Barak³⁰, E.L. Barberio⁸⁸, D. Barberis^{50a,50b}, M. Barbero⁸⁵, T. Barillari¹⁰¹, M. Barisonzi^{164a,164b}, T. Barklow¹⁴³, N. Barlow²⁸, S.L. Barnes⁸⁴, B.M. Barnett¹³¹, R.M. Barnett¹⁵, Z. Barnovska⁵, A. Baroncelli^{134a}, G. Barone²³, A.J. Barr¹²⁰, F. Barreiro⁸², J. Barreiro Guimarães da Costa⁵⁷, R. Bartoldus¹⁴³, A.E. Barton⁷², P. Bartos^{144a}, A. Basalaev¹²³, A. Bassalat¹¹⁷, A. Basye¹⁶⁵, R.L. Bates⁵³, S.J. Batista¹⁵⁸, J.R. Batley²⁸, M. Battaglia¹³⁷, M. Bauce^{132a,132b}, F. Bauer¹³⁶, H.S. Bawa^{143,e}, J.B. Beacham¹¹¹, M.D. Beattie⁷², T. Beau⁸⁰, P.H. Beauchemin¹⁶¹, R. Beccherle^{124a,124b}, P. Bechtel²¹, H.P. Beck^{17,f}, K. Becker¹²⁰, M. Becker⁸³, M. Beckingham¹⁷⁰, C. Becot¹¹⁷, A.J. Beddall^{19b}, A. Beddall^{19b}, V.A. Bednyakov⁶⁵, C.P. Bee¹⁴⁸, L.J. Beamster¹⁰⁷, T.A. Beermann³⁰, M. Begel²⁵, J.K. Behr¹²⁰, C. Belanger-Champagne⁸⁷, W.H. Bell⁴⁹, G. Bella¹⁵³, L. Bellagamba^{20a}, A. Bellerive²⁹, M. Bellomo⁸⁶, K. Belotskiy⁹⁸, O. Beltramello³⁰, O. Benary¹⁵³, D. Benckekroun^{135a}, M. Bender¹⁰⁰, K. Bendtz^{146a,146b}, N. Benekos¹⁰, Y. Benhammou¹⁵³, E. Benhar Nocchioli⁴⁹, J.A. Benitez Garcia^{159b}, D.P. Benjamin⁴⁵, J.R. Bensinger²³, S. Bentvelsen¹⁰⁷, L. Beresford¹²⁰, M. Beretta⁴⁷, D. Berge¹⁰⁷, E. Bergeas Kuutmann¹⁶⁶, N. Berger⁵, F. Berghaus¹⁶⁹, J. Beringer¹⁵, C. Bernard²², N.R. Bernard⁸⁶, C. Bernius¹¹⁰, F.U. Bernlochner²¹, T. Berry⁷⁷, P. Berta¹²⁹, C. Bertella⁸³, G. Bertoli^{146a,146b}, F. Bertolucci^{124a,124b}, C. Bertsche¹¹³, D. Bertsche¹¹³, M.I. Besana^{91a}, G.J. Besjes³⁶, O. Bessidskaia Bylund^{146a,146b}, M. Bessner⁴², N. Besson¹³⁶, C. Betancourt⁴⁸, S. Bethke¹⁰¹, A.J. Bevan⁷⁶, W. Bhimji¹⁵, R.M. Bianchi¹²⁵, L. Bianchini²³, M. Bianco³⁰, O. Biebel¹⁰⁰, D. Biedermann¹⁶, S.P. Bieniek⁷⁸, M. Biglietti^{134a}, J. Bilbao De Mendizabal⁴⁹, H. Bilokon⁴⁷, M. Bindi⁵⁴, S. Binet¹¹⁷, A. Bingul^{19b}, C. Bini^{132a,132b}, S. Biondi^{20a,20b}, C.W. Black¹⁵⁰, J.E. Black¹⁴³, K.M. Black²², D. Blackburn¹³⁸, R.E. Blair⁶, J.-B. Blanchard¹³⁶, J.E. Blanco⁷⁷, T. Blazek^{144a}, I. Bloch⁴², C. Blocker²³, W. Blum^{83,*}, U. Blumenschein⁵⁴, G.J. Bobbink¹⁰⁷, V.S. Bobrovnikov^{109,c}, S.S. Bocchetta⁸¹, A. Bocci⁴⁵, C. Bock¹⁰⁰,

M. Boehler⁴⁸, J.A. Bogaerts³⁰, D. Bogavac¹³, A.G. Bogdanchikov¹⁰⁹, C. Bohm^{146a}, V. Boisvert⁷⁷,
T. Bold^{38a}, V. Boldea^{26a}, A.S. Boldyrev⁹⁹, M. Bomben⁸⁰, M. Bona⁷⁶, M. Boonekamp¹³⁶, A. Borisov¹³⁰,
G. Borissov⁷², S. Borroni⁴², J. Bortfeldt¹⁰⁰, V. Bortolotto^{60a,60b,60c}, K. Bos¹⁰⁷, D. Boscherini^{20a},
M. Bosman¹², J. Boudreau¹²⁵, J. Bouffard², E.V. Bouhova-Thacker⁷², D. Boumediene³⁴,
C. Bourdarios¹¹⁷, N. Bousson¹¹⁴, A. Boveia³⁰, J. Boyd³⁰, I.R. Boyko⁶⁵, I. Bozic¹³, J. Bracinik¹⁸,
A. Brandt⁸, G. Brandt⁵⁴, O. Brandt^{58a}, U. Bratzler¹⁵⁶, B. Brau⁸⁶, J.E. Brau¹¹⁶, H.M. Braun^{175,*},
S.F. Brazzale^{164a,164c}, W.D. Breaden Madden⁵³, K. Brendlinger¹²², A.J. Brennan⁸⁸, L. Brenner¹⁰⁷,
R. Brenner¹⁶⁶, S. Bressler¹⁷², K. Bristow^{145c}, T.M. Bristow⁴⁶, D. Britton⁵³, D. Britzger⁴²,
F.M. Brochu²⁸, I. Brock²¹, R. Brock⁹⁰, J. Bronner¹⁰¹, G. Brooijmans³⁵, T. Brooks⁷⁷, W.K. Brooks^{32b},
J. Brosamer¹⁵, E. Brost¹¹⁶, J. Brown⁵⁵, P.A. Bruckman de Renstrom³⁹, D. Bruncko^{144b}, R. Bruneliere⁴⁸,
A. Bruni^{20a}, G. Bruni^{20a}, M. Bruschi^{20a}, N. Bruscinò²¹, L. Bryngemark⁸¹, T. Buanes¹⁴, Q. Buat¹⁴²,
P. Buchholz¹⁴¹, A.G. Buckley⁵³, S.I. Buda^{26a}, I.A. Budagov⁶⁵, F. Buehrer⁴⁸, L. Bugge¹¹⁹,
M.K. Bugge¹¹⁹, O. Bulekov⁹⁸, D. Bullock⁸, H. Burckhart³⁰, S. Burdin⁷⁴, C.D. Burgard⁴⁸,
B. Burghgrave¹⁰⁸, S. Burke¹³¹, I. Burmeister⁴³, E. Busato³⁴, D. Büscher⁴⁸, V. Büscher⁸³, P. Bussey⁵³,
J.M. Butler²², A.I. Butt³, C.M. Buttar⁵³, J.M. Butterworth⁷⁸, P. Butti¹⁰⁷, W. Buttinger²⁵, A. Buzatu⁵³,
A.R. Buzykaev^{109,c}, S. Cabrera Urbán¹⁶⁷, D. Caforio¹²⁸, V.M. Cairo^{37a,37b}, O. Cakir^{4a}, N. Calace⁴⁹,
P. Calafiura¹⁵, A. Calandri¹³⁶, G. Calderini⁸⁰, P. Calfayan¹⁰⁰, L.P. Caloba^{24a}, D. Calvet³⁴, S. Calvet³⁴,
R. Camacho Toro³¹, S. Camarda⁴², P. Camarri^{133a,133b}, D. Cameron¹¹⁹, R. Caminal Armadans¹⁶⁵,
S. Campana³⁰, M. Campanelli⁷⁸, A. Campoverde¹⁴⁸, V. Canale^{104a,104b}, A. Canepa^{159a}, M. Cano Bret^{33e},
J. Cantero⁸², R. Cantrill^{126a}, T. Cao⁴⁰, M.D.M. Capeans Garrido³⁰, I. Caprini^{26a}, M. Caprini^{26a},
M. Capua^{37a,37b}, R. Caputo⁸³, R. Cardarelli^{133a}, F. Cardillo⁴⁸, T. Carli³⁰, G. Carlino^{104a},
L. Carminati^{91a,91b}, S. Caron¹⁰⁶, E. Carquin^{32a}, G.D. Carrillo-Montoya³⁰, J.R. Carter²⁸,
J. Carvalho^{126a,126c}, D. Casadei⁷⁸, M.P. Casado¹², M. Casolino¹², E. Castaneda-Miranda^{145a},
A. Castelli¹⁰⁷, V. Castillo Gimenez¹⁶⁷, N.F. Castro^{126a,g}, P. Catastini⁵⁷, A. Catinaccio³⁰, J.R. Catmore¹¹⁹,
A. Cattai³⁰, J. Caudron⁸³, V. Cavaliere¹⁶⁵, D. Cavalli^{91a}, M. Cavalli-Sforza¹², V. Cavasinni^{124a,124b},
F. Ceradini^{134a,134b}, B.C. Cerio⁴⁵, K. Cerny¹²⁹, A.S. Cerqueira^{24b}, A. Cerri¹⁴⁹, L. Cerrito⁷⁶, F. Cerutti¹⁵,
M. Cerv³⁰, A. Cervelli¹⁷, S.A. Cetin^{19c}, A. Chafaq^{135a}, D. Chakraborty¹⁰⁸, I. Chalupkova¹²⁹,
P. Chang¹⁶⁵, J.D. Chapman²⁸, D.G. Charlton¹⁸, C.C. Chau¹⁵⁸, C.A. Chavez Barajas¹⁴⁹, S. Cheatham¹⁵²,
A. Chegwidden⁹⁰, S. Chekanov⁶, S.V. Chekulaev^{159a}, G.A. Chelkov^{65,h}, M.A. Chelstowska⁸⁹,
C. Chen⁶⁴, H. Chen²⁵, K. Chen¹⁴⁸, L. Chen^{33d,i}, S. Chen^{33c}, X. Chen^{33f}, Y. Chen⁶⁷, H.C. Cheng⁸⁹,
Y. Cheng³¹, A. Cheplakov⁶⁵, E. Cheremushkina¹³⁰, R. Cherkaoui El Moursli^{135e}, V. Chernyatin^{25,*},
E. Cheu⁷, L. Chevalier¹³⁶, V. Chiarella⁴⁷, G. Chiarelli^{124a,124b}, G. Chiodini^{73a}, A.S. Chisholm¹⁸,
R.T. Chislett⁷⁸, A. Chitan^{26a}, M.V. Chizhov⁶⁵, K. Choi⁶¹, S. Chouridou⁹, B.K.B. Chow¹⁰⁰,
V. Christodoulou⁷⁸, D. Chromek-Burckhart³⁰, J. Chudoba¹²⁷, A.J. Chuinard⁸⁷, J.J. Chwastowski³⁹,
L. Chytka¹¹⁵, G. Ciapetti^{132a,132b}, A.K. Ciftci^{4a}, D. Cinca⁵³, V. Cindro⁷⁵, I.A. Cioara²¹, A. Ciocio¹⁵,
F. Ciotto^{104a,104b}, Z.H. Citron¹⁷², M. Ciubancan^{26a}, A. Clark⁴⁹, B.L. Clark⁵⁷, P.J. Clark⁴⁶,
R.N. Clarke¹⁵, W. Cleland¹²⁵, C. Clement^{146a,146b}, Y. Coadou⁸⁵, M. Cobal^{164a,164c}, A. Coccaro⁴⁹,
J. Cochran⁶⁴, L. Coffey²³, J.G. Cogan¹⁴³, L. Colasurdo¹⁰⁶, B. Cole³⁵, S. Cole¹⁰⁸, A.P. Colijn¹⁰⁷,
J. Collot⁵⁵, T. Colombo^{58c}, G. Compostella¹⁰¹, P. Conde Muiño^{126a,126b}, E. Coniavitis⁴⁸,
S.H. Connell^{145b}, I.A. Connelly⁷⁷, V. Consorti⁴⁸, S. Constantinescu^{26a}, C. Conta^{121a,121b}, G. Conti³⁰,
F. Conventi^{104a,j}, M. Cooke¹⁵, B.D. Cooper⁷⁸, A.M. Cooper-Sarkar¹²⁰, T. Cornelissen¹⁷⁵, M. Corradi^{20a},
F. Corriveau^{87,k}, A. Corso-Radu¹⁶³, A. Cortes-Gonzalez¹², G. Cortiana¹⁰¹, G. Costa^{91a}, M.J. Costa¹⁶⁷,
D. Costanzo¹³⁹, D. Côte⁸, G. Cottin²⁸, G. Cowan⁷⁷, B.E. Cox⁸⁴, K. Cranmer¹¹⁰, G. Cree²⁹,
S. Crépe-Renaudin⁵⁵, F. Crescioli⁸⁰, W.A. Cribbs^{146a,146b}, M. Crispin Ortuzar¹²⁰, M. Cristinziani²¹,
V. Croft¹⁰⁶, G. Crosetti^{37a,37b}, T. Cuhadar Donszelmann¹³⁹, J. Cummings¹⁷⁶, M. Curatolo⁴⁷,
C. Cuthbert¹⁵⁰, H. Cziri¹⁴¹, P. Czodrowski³, S. D'Auria⁵³, M. D'Onofrio⁷⁴,
M.J. Da Cunha Sargedas De Sousa^{126a,126b}, C. Da Via⁸⁴, W. Dabrowski^{38a}, A. Dafinca¹²⁰, T. Dai⁸⁹,

O. Dale¹⁴, F. Dallaire⁹⁵, C. Dallapiccola⁸⁶, M. Dam³⁶, J.R. Dandoy³¹, N.P. Dang⁴⁸, A.C. Daniells¹⁸, M. Danninger¹⁶⁸, M. Dano Hoffmann¹³⁶, V. Dao⁴⁸, G. Darbo^{50a}, S. Darmora⁸, J. Dassoulas³, A. Dattagupta⁶¹, W. Davey²¹, C. David¹⁶⁹, T. Davidek¹²⁹, E. Davies^{120,l}, M. Davies¹⁵³, P. Davison⁷⁸, Y. Davygora^{58a}, E. Dawe⁸⁸, I. Dawson¹³⁹, R.K. Daya-Ishmukhametova⁸⁶, K. De⁸, R. de Asmundis^{104a}, A. De Benedetti¹¹³, S. De Castro^{20a,20b}, S. De Cecco⁸⁰, N. De Groot¹⁰⁶, P. de Jong¹⁰⁷, H. De la Torre⁸², F. De Lorenzi⁶⁴, D. De Pedis^{132a}, A. De Salvo^{132a}, U. De Sanctis¹⁴⁹, A. De Santo¹⁴⁹, J.B. De Vivie De Regie¹¹⁷, W.J. Dearnaley⁷², R. Debbe²⁵, C. Debenedetti¹³⁷, D.V. Dedovich⁶⁵, I. Deigaard¹⁰⁷, J. Del Peso⁸², T. Del Prete^{124a,124b}, D. Delgove¹¹⁷, F. Deliot¹³⁶, C.M. Delitzsch⁴⁹, M. Deliyergiyev⁷⁵, A. Dell'Acqua³⁰, L. Dell'Asta²², M. Dell'Orso^{124a,124b}, M. Della Pietra^{104a,j}, D. della Volpe⁴⁹, M. Delmastro⁵, P.A. Delsart⁵⁵, C. Deluca¹⁰⁷, D.A. DeMarco¹⁵⁸, S. Demers¹⁷⁶, M. Demichev⁶⁵, A. Demilly⁸⁰, S.P. Denisov¹³⁰, D. Derendarz³⁹, J.E. Derkaoui^{135d}, F. Derue⁸⁰, P. Dervan⁷⁴, K. Desch²¹, C. Deterre⁴², P.O. Deviveiros³⁰, A. Dewhurst¹³¹, S. Dhaliwal²³, A. Di Ciaccio^{133a,133b}, L. Di Ciaccio⁵, A. Di Domenico^{132a,132b}, C. Di Donato^{104a,104b}, A. Di Girolamo³⁰, B. Di Girolamo³⁰, A. Di Mattia¹⁵², B. Di Micco^{134a,134b}, R. Di Nardo⁴⁷, A. Di Simone⁴⁸, R. Di Sipio¹⁵⁸, D. Di Valentino²⁹, C. Diaconu⁸⁵, M. Diamond¹⁵⁸, F.A. Dias⁴⁶, M.A. Diaz^{32a}, E.B. Diehl⁸⁹, J. Dietrich¹⁶, S. Diglio⁸⁵, A. Dimitrievska¹³, J. Dingfelder²¹, P. Dita^{26a}, S. Dita^{26a}, F. Dittus³⁰, F. Djama⁸⁵, T. Djobava^{51b}, J.I. Djuvsland^{58a}, M.A.B. do Vale^{24c}, D. Dobos³⁰, M. Dobre^{26a}, C. Doglioni⁸¹, T. Dohmae¹⁵⁵, J. Dolejsi¹²⁹, Z. Dolezal¹²⁹, B.A. Dolgoshein^{98,*}, M. Donadelli^{24d}, S. Donati^{124a,124b}, P. Dondero^{121a,121b}, J. Donini³⁴, J. Dopke¹³¹, A. Doria^{104a}, M.T. Dova⁷¹, A.T. Doyle⁵³, E. Drechsler⁵⁴, M. Dris¹⁰, E. Dubreuil³⁴, E. Duchovni¹⁷², G. Duckeck¹⁰⁰, O.A. Ducu^{26a,85}, D. Duda¹⁰⁷, A. Dudarev³⁰, L. Duflot¹¹⁷, L. Duguid⁷⁷, M. Dührssen³⁰, M. Dunford^{58a}, H. Duran Yildiz^{4a}, M. Düren⁵², A. Durglishvili^{51b}, D. Duschinger⁴⁴, M. Dyndal^{38a}, C. Eckardt⁴², K.M. Ecker¹⁰¹, R.C. Edgar⁸⁹, W. Edson², N.C. Edwards⁴⁶, W. Ehrenfeld²¹, T. Eifert³⁰, G. Eigen¹⁴, K. Einsweiler¹⁵, T. Ekelof¹⁶⁶, M. El Kacimi^{135c}, M. Ellert¹⁶⁶, S. Elles⁵, F. Ellinghaus¹⁷⁵, A.A. Elliot¹⁶⁹, N. Ellis³⁰, J. Elmsheuser¹⁰⁰, M. Elsing³⁰, D. Emelianov¹³¹, Y. Enari¹⁵⁵, O.C. Endner⁸³, M. Endo¹¹⁸, J. Erdmann⁴³, A. Ereditato¹⁷, G. Ernis¹⁷⁵, J. Ernst², M. Ernst²⁵, S. Errede¹⁶⁵, E. Ertel⁸³, M. Escalier¹¹⁷, H. Esch⁴³, C. Escobar¹²⁵, B. Esposito⁴⁷, A.I. Etienvre¹³⁶, E. Etzion¹⁵³, H. Evans⁶¹, A. Ezhilov¹²³, L. Fabbri^{20a,20b}, G. Facini³¹, R.M. Fakhruddinov¹³⁰, S. Falciano^{132a}, R.J. Falla⁷⁸, J. Faltova¹²⁹, Y. Fang^{33a}, M. Fanti^{91a,91b}, A. Farbin⁸, A. Farilla^{134a}, T. Farooque¹², S. Farrell¹⁵, S.M. Farrington¹⁷⁰, P. Farthouat³⁰, F. Fassi^{135e}, P. Fassnacht³⁰, D. Fassouliotis⁹, M. Fauci Giannelli⁷⁷, A. Favareto^{50a,50b}, L. Fayard¹¹⁷, P. Federic^{144a}, O.L. Fedin^{123,m}, W. Fedorko¹⁶⁸, S. Feigl³⁰, L. Feligioni⁸⁵, C. Feng^{33d}, E.J. Feng⁶, H. Feng⁸⁹, A.B. Fenyuk¹³⁰, L. Feremenga⁸, P. Fernandez Martinez¹⁶⁷, S. Fernandez Perez³⁰, J. Ferrando⁵³, A. Ferrari¹⁶⁶, P. Ferrari¹⁰⁷, R. Ferrari^{121a}, D.E. Ferreira de Lima⁵³, A. Ferrer¹⁶⁷, D. Ferrere⁴⁹, C. Ferretti⁸⁹, A. Ferretto Parodi^{50a,50b}, M. Fiascaris³¹, F. Fiedler⁸³, A. Filipčić⁷⁵, M. Filipuzzi⁴², F. Filthaut¹⁰⁶, M. Fincke-Keeler¹⁶⁹, K.D. Finelli¹⁵⁰, M.C.N. Fiolhais^{126a,126c}, L. Fiorini¹⁶⁷, A. Firan⁴⁰, A. Fischer², C. Fischer¹², J. Fischer¹⁷⁵, W.C. Fisher⁹⁰, E.A. Fitzgerald²³, N. Flaschel⁴², I. Fleck¹⁴¹, P. Fleischmann⁸⁹, S. Fleischmann¹⁷⁵, G.T. Fletcher¹³⁹, G. Fletcher⁷⁶, R.R.M. Fletcher¹²², T. Flick¹⁷⁵, A. Floderus⁸¹, L.R. Flores Castillo^{60a}, M.J. Flowerdew¹⁰¹, A. Formica¹³⁶, A. Forti⁸⁴, D. Fournier¹¹⁷, H. Fox⁷², S. Fracchia¹², P. Francavilla⁸⁰, M. Franchini^{20a,20b}, D. Francis³⁰, L. Franconi¹¹⁹, M. Franklin⁵⁷, M. Frate¹⁶³, M. Fraternali^{121a,121b}, D. Freeborn⁷⁸, S.T. French²⁸, F. Friedrich⁴⁴, D. Froidevaux³⁰, J.A. Frost¹²⁰, C. Fukunaga¹⁵⁶, E. Fullana Torregrosa⁸³, B.G. Fulson¹⁴³, T. Fusayasu¹⁰², J. Fuster¹⁶⁷, C. Gabaldon⁵⁵, O. Gabizon¹⁷⁵, A. Gabrielli^{20a,20b}, A. Gabrielli^{132a,132b}, G.P. Gach^{38a}, S. Gadatsch³⁰, S. Gadomski⁴⁹, G. Gagliardi^{50a,50b}, P. Gagnon⁶¹, C. Galea¹⁰⁶, B. Galhardo^{126a,126c}, E.J. Gallas¹²⁰, B.J. Gallop¹³¹, P. Gallus¹²⁸, G. Galster³⁶, K.K. Gan¹¹¹, J. Gao^{33b,85}, Y. Gao⁴⁶, Y.S. Gao^{143,e}, F.M. Garay Walls⁴⁶, F. Garbersson¹⁷⁶, C. García¹⁶⁷, J.E. García Navarro¹⁶⁷, M. Garcia-Sciveres¹⁵, R.W. Gardner³¹, N. Garelli¹⁴³, V. Garonne¹¹⁹, C. Gatti⁴⁷, A. Gaudiello^{50a,50b}, G. Gaudio^{121a}, B. Gaur¹⁴¹, L. Gauthier⁹⁵, P. Gauzzi^{132a,132b}, I.L. Gavrilenko⁹⁶,

C. Gay¹⁶⁸, G. Gaycken²¹, E.N. Gazis¹⁰, P. Ge^{33d}, Z. Gecse¹⁶⁸, C.N.P. Gee¹³¹, Ch. Geich-Gimbel²¹, M.P. Geisler^{58a}, C. Gemme^{50a}, M.H. Genest⁵⁵, S. Gentile^{132a,132b}, M. George⁵⁴, S. George⁷⁷, D. Gerbaudo¹⁶³, A. Gershon¹⁵³, S. Ghasemi¹⁴¹, H. Ghazlane^{135b}, B. Giacobbe^{20a}, S. Giagu^{132a,132b}, V. Giangiobbe¹², P. Giannetti^{124a,124b}, B. Gibbard²⁵, S.M. Gibson⁷⁷, M. Gilchriese¹⁵, T.P.S. Gillam²⁸, D. Gillberg³⁰, G. Gilles³⁴, D.M. Gingrich^{3,d}, N. Giokaris⁹, M.P. Giordani^{164a,164c}, F.M. Giorgi^{20a}, F.M. Giorgi¹⁶, P.F. Giraud¹³⁶, P. Giromini⁴⁷, D. Giugni^{91a}, C. Giuliani⁴⁸, M. Giulini^{58b}, B.K. Gjelsten¹¹⁹, S. Gkaitatzis¹⁵⁴, I. Gkialas¹⁵⁴, E.L. Gkoukousis¹¹⁷, L.K. Gladilin⁹⁹, C. Glasman⁸², J. Glatzer³⁰, P.C.F. Glaysher⁴⁶, A. Glazov⁴², M. Goblirsch-Kolb¹⁰¹, J.R. Goddard⁷⁶, J. Godlewski³⁹, S. Goldfarb⁸⁹, T. Golling⁴⁹, D. Golubkov¹³⁰, A. Gomes^{126a,126b,126d}, R. Gonçalo^{126a}, J. Goncalves Pinto Firmino Da Costa¹³⁶, L. Gonella²¹, S. González de la Hoz¹⁶⁷, G. Gonzalez Parra¹², S. Gonzalez-Sevilla⁴⁹, L. Goossens³⁰, P.A. Gorbounov⁹⁷, H.A. Gordon²⁵, I. Gorelov¹⁰⁵, B. Gorini³⁰, E. Gorini^{73a,73b}, A. Gorišek⁷⁵, E. Gornicki³⁹, A.T. Goshaw⁴⁵, C. Gössling⁴³, M.I. Gostkin⁶⁵, D. Goujdami^{135c}, A.G. Goussiou¹³⁸, N. Govender^{145b}, E. Gozani¹⁵², H.M.X. Grabas¹³⁷, L. Graber⁵⁴, I. Grabowska-Bold^{38a}, P.O.J. Gradin¹⁶⁶, P. Grafström^{20a,20b}, K-J. Grahn⁴², J. Gramling⁴⁹, E. Gramstad¹¹⁹, S. Grancagnolo¹⁶, V. Gratchev¹²³, H.M. Gray³⁰, E. Graziani^{134a}, Z.D. Greenwood^{79,n}, C. Grefe²¹, K. Gregersen⁷⁸, I.M. Gregor⁴², P. Grenier¹⁴³, J. Griffiths⁸, A.A. Grillo¹³⁷, K. Grimm⁷², S. Grinstein^{12,o}, Ph. Gris³⁴, J.-F. Grivaz¹¹⁷, J.P. Grohs⁴⁴, A. Grohsjean⁴², E. Gross¹⁷², J. Grosse-Knetter⁵⁴, G.C. Grossi⁷⁹, Z.J. Groul¹⁴⁹, L. Guan⁸⁹, J. Guenther¹²⁸, F. Guescini⁴⁹, D. Guest¹⁷⁶, O. Gueta¹⁵³, E. Guido^{50a,50b}, T. Guillemain¹¹⁷, S. Guindon², U. Gul⁵³, C. Gumpert⁴⁴, J. Guo^{33e}, Y. Guo^{33b}, S. Gupta¹²⁰, G. Gustavino^{132a,132b}, P. Gutierrez¹¹³, N.G. Gutierrez Ortiz⁷⁸, C. Gutschow⁴⁴, C. Guyot¹³⁶, C. Gwenlan¹²⁰, C.B. Gwilliam⁷⁴, A. Haas¹¹⁰, C. Haber¹⁵, H.K. Hadavand⁸, N. Haddad^{135e}, P. Haefner²¹, S. Hageböck²¹, Z. Hajduk³⁹, H. Hakobyan¹⁷⁷, M. Haleem⁴², J. Haley¹¹⁴, D. Hall¹²⁰, G. Halladjian⁹⁰, G.D. Hallewell⁸⁵, K. Hamacher¹⁷⁵, P. Hamal¹¹⁵, K. Hamano¹⁶⁹, A. Hamilton^{145a}, G.N. Hamity¹³⁹, P.G. Hamnett⁴², L. Han^{33b}, K. Hanagaki^{66,p}, K. Hanawa¹⁵⁵, M. Hance¹⁵, P. Hanke^{58a}, R. Hanna¹³⁶, J.B. Hansen³⁶, J.D. Hansen³⁶, M.C. Hansen²¹, P.H. Hansen³⁶, K. Hara¹⁶⁰, A.S. Hard¹⁷³, T. Harenberg¹⁷⁵, F. Hariri¹¹⁷, S. Harkusha⁹², R.D. Harrington⁴⁶, P.F. Harrison¹⁷⁰, F. Hartjes¹⁰⁷, M. Hasegawa⁶⁷, Y. Hasegawa¹⁴⁰, A. Hasib¹¹³, S. Hassani¹³⁶, S. Haug¹⁷, R. Hauser⁹⁰, L. Hauswald⁴⁴, M. Havranek¹²⁷, C.M. Hawkes¹⁸, R.J. Hawkins³⁰, A.D. Hawkins⁸¹, T. Hayashi¹⁶⁰, D. Hayden⁹⁰, C.P. Hays¹²⁰, J.M. Hays⁷⁶, H.S. Hayward⁷⁴, S.J. Haywood¹³¹, S.J. Head¹⁸, T. Heck⁸³, V. Hedberg⁸¹, L. Heelan⁸, S. Heim¹²², T. Heim¹⁷⁵, B. Heinemann¹⁵, L. Heinrich¹¹⁰, J. Hejbal¹²⁷, L. Helary²², S. Hellman^{146a,146b}, D. Hellmich²¹, C. Helsens¹², J. Henderson¹²⁰, R.C.W. Henderson⁷², Y. Heng¹⁷³, C. Hengler⁴², S. Henkelmann¹⁶⁸, A. Henrichs¹⁷⁶, A.M. Henriques Correia³⁰, S. Henrot-Versille¹¹⁷, G.H. Herbert¹⁶, Y. Hernández Jiménez¹⁶⁷, R. Herrberg-Schubert¹⁶, G. Herten⁴⁸, R. Hertenberger¹⁰⁰, L. Hervas³⁰, G.G. Hesketh⁷⁸, N.P. Hessey¹⁰⁷, J.W. Hetherly⁴⁰, R. Hickling⁷⁶, E. Higón-Rodríguez¹⁶⁷, E. Hill¹⁶⁹, J.C. Hill²⁸, K.H. Hiller⁴², S.J. Hillier¹⁸, I. Hinchliffe¹⁵, E. Hines¹²², R.R. Hinman¹⁵, M. Hirose¹⁵⁷, D. Hirschbuehl¹⁷⁵, J. Hobbs¹⁴⁸, N. Hod¹⁰⁷, M.C. Hodgkinson¹³⁹, P. Hodgson¹³⁹, A. Hoecker³⁰, M.R. Hoferkamp¹⁰⁵, F. Hoenic¹⁰⁰, M. Hohlfeld⁸³, D. Hohn²¹, T.R. Holmes¹⁵, M. Homann⁴³, T.M. Hong¹²⁵, L. Hooft van Huysduynen¹¹⁰, W.H. Hopkins¹¹⁶, Y. Hori¹⁰³, A.J. Horton¹⁴², J.-Y. Hostachy⁵⁵, S. Hou¹⁵¹, A. Hoummada^{135a}, J. Howard¹²⁰, J. Howarth⁴², M. Hrabovsky¹¹⁵, I. Hristova¹⁶, J. Hrivnac¹¹⁷, T. Hryn'ova⁵, A. Hrynevich⁹³, C. Hsu^{145c}, P.J. Hsu^{151,q}, S.-C. Hsu¹³⁸, D. Hu³⁵, Q. Hu^{33b}, X. Hu⁸⁹, Y. Huang⁴², Z. Hubacek¹²⁸, F. Hubaut⁸⁵, F. Huegging²¹, T.B. Huffman¹²⁰, E.W. Hughes³⁵, G. Hughes⁷², M. Huhtinen³⁰, T.A. Hülsing⁸³, N. Huseynov^{65,b}, J. Huston⁹⁰, J. Huth⁵⁷, G. Iacobucci⁴⁹, G. Iakovidis²⁵, I. Ibragimov¹⁴¹, L. Iconomidou-Fayard¹¹⁷, E. Ideal¹⁷⁶, Z. Idrissi^{135e}, P. Iengo³⁰, O. Igonkina¹⁰⁷, T. Iizawa¹⁷¹, Y. Ikegami⁶⁶, K. Ikematsu¹⁴¹, M. Ikeno⁶⁶, Y. Ilchenko^{31,r}, D. Iliadis¹⁵⁴, N. Ilic¹⁴³, T. Ince¹⁰¹, G. Introzzi^{121a,121b}, P. Ioannou⁹, M. Iodice^{134a}, K. Iordanidou³⁵, V. Ippolito⁵⁷, A. Irlles Quiles¹⁶⁷, C. Isaksson¹⁶⁶, M. Ishino⁶⁸, M. Ishitsuka¹⁵⁷, R. Ishmukhametov¹¹¹, C. Issever¹²⁰, S. Istin^{19a}, J.M. Iturbe Ponce⁸⁴, R. Iuppa^{133a,133b},

J. Ivarsson⁸¹, W. Iwanski³⁹, H. Iwasaki⁶⁶, J.M. Izen⁴¹, V. Izzo^{104a}, S. Jabbar³, B. Jackson¹²², M. Jackson⁷⁴, P. Jackson¹, M.R. Jaekel³⁰, V. Jain², K. Jakobs⁴⁸, S. Jakobsen³⁰, T. Jakoubek¹²⁷, J. Jakubek¹²⁸, D.O. Jamin¹¹⁴, D.K. Jana⁷⁹, E. Jansen⁷⁸, R. Jansky⁶², J. Janssen²¹, M. Janus⁵⁴, G. Jarlskog⁸¹, N. Javadov^{65,b}, T. Javůrek⁴⁸, L. Jeanty¹⁵, J. Jejelava^{51a,s}, G.-Y. Jeng¹⁵⁰, D. Jennens⁸⁸, P. Jenni^{48,t}, J. Jentzsch⁴³, C. Jeske¹⁷⁰, S. Jézéquel⁵, H. Ji¹⁷³, J. Jia¹⁴⁸, Y. Jiang^{33b}, S. Jiggins⁷⁸, J. Jimenez Pena¹⁶⁷, S. Jin^{33a}, A. Jinaru^{26a}, O. Jinnouchi¹⁵⁷, M.D. Joergensen³⁶, P. Johansson¹³⁹, K.A. Johns⁷, K. Jon-And^{146a,146b}, G. Jones¹⁷⁰, R.W.L. Jones⁷², T.J. Jones⁷⁴, J. Jongmanns^{58a}, P.M. Jorge^{126a,126b}, K.D. Joshi⁸⁴, J. Jovicevic^{159a}, X. Ju¹⁷³, C.A. Jung⁴³, P. Jussel⁶², A. Juste Rozas^{12,o}, M. Kaci¹⁶⁷, A. Kaczmarek³⁹, M. Kado¹¹⁷, H. Kagan¹¹¹, M. Kagan¹⁴³, S.J. Kahn⁸⁵, E. Kajomovitz⁴⁵, C.W. Kalderon¹²⁰, S. Kama⁴⁰, A. Kamenshchikov¹³⁰, N. Kanaya¹⁵⁵, S. Kaneti²⁸, V.A. Kantserov⁹⁸, J. Kanzaki⁶⁶, B. Kaplan¹¹⁰, L.S. Kaplan¹⁷³, A. Kapliy³¹, D. Kar^{145c}, K. Karakostas¹⁰, A. Karamaoun³, N. Karastathis^{10,107}, M.J. Kareem⁵⁴, E. Karentzos¹⁰, M. Karneveskiy⁸³, S.N. Karpov⁶⁵, Z.M. Karpova⁶⁵, K. Karthik¹¹⁰, V. Kartvelishvili⁷², A.N. Karyukhin¹³⁰, L. Kashif¹⁷³, R.D. Kass¹¹¹, A. Kastanas¹⁴, Y. Kataoka¹⁵⁵, C. Kato¹⁵⁵, A. Katre⁴⁹, J. Katzy⁴², K. Kawagoe⁷⁰, T. Kawamoto¹⁵⁵, G. Kawamura⁵⁴, S. Kazama¹⁵⁵, V.F. Kazanin^{109,c}, R. Keeler¹⁶⁹, R. Kehoe⁴⁰, J.S. Keller⁴², J.J. Kempster⁷⁷, H. Keoshkerian⁸⁴, O. Kepka¹²⁷, B.P. Kerševan⁷⁵, S. Kersten¹⁷⁵, R.A. Keyes⁸⁷, F. Khalil-zada¹¹, H. Khandanyan^{146a,146b}, A. Khanov¹¹⁴, A.G. Kharlamov^{109,c}, T.J. Khoo²⁸, V. Khovanskiy⁹⁷, E. Khramov⁶⁵, J. Khubua^{51b,u}, S. Kido⁶⁷, H.Y. Kim⁸, S.H. Kim¹⁶⁰, Y.K. Kim³¹, N. Kimura¹⁵⁴, O.M. Kind¹⁶, B.T. King⁷⁴, M. King¹⁶⁷, S.B. King¹⁶⁸, J. Kirk¹³¹, A.E. Kiryunin¹⁰¹, T. Kishimoto⁶⁷, D. Kisielewska^{38a}, F. Kiss⁴⁸, K. Kiuchi¹⁶⁰, O. Kiverny¹³⁶, E. Kladiva^{144b}, M.H. Klein³⁵, M. Klein⁷⁴, U. Klein⁷⁴, K. Kleinknecht⁸³, P. Klimek^{146a,146b}, A. Klimentov²⁵, R. Klingenberg⁴³, J.A. Klinger¹³⁹, T. Klioutchnikova³⁰, E.-E. Kluge^{58a}, P. Kluit¹⁰⁷, S. Kluth¹⁰¹, J. Knapik³⁹, E. Kneringer⁶², E.B.F.G. Knoop⁸⁵, A. Knue⁵³, A. Kobayashi¹⁵⁵, D. Kobayashi¹⁵⁷, T. Kobayashi¹⁵⁵, M. Kobel⁴⁴, M. Kocian¹⁴³, P. Kodys¹²⁹, T. Koffas²⁹, E. Koffeman¹⁰⁷, L.A. Kogan¹²⁰, S. Kohlmann¹⁷⁵, Z. Kohout¹²⁸, T. Kohriki⁶⁶, T. Koi¹⁴³, H. Kolanoski¹⁶, I. Koletsou⁵, A.A. Komar^{96,*}, Y. Komori¹⁵⁵, T. Kondo⁶⁶, N. Kondrashova⁴², K. Köneke⁴⁸, A.C. König¹⁰⁶, T. Kono⁶⁶, R. Konoplich^{110,v}, N. Konstantinidis⁷⁸, R. Kopeliansky¹⁵², S. Koperny^{38a}, L. Köpke⁸³, A.K. Kopp⁴⁸, K. Korcyl³⁹, K. Kordas¹⁵⁴, A. Korn⁷⁸, A.A. Korol^{109,c}, I. Korolkov¹², E.V. Korolkova¹³⁹, O. Kortner¹⁰¹, S. Kortner¹⁰¹, T. Kosek¹²⁹, V.V. Kostyukhin²¹, V.M. Kotov⁶⁵, A. Kotwal⁴⁵, A. Kourkouveli-Charalampidi¹⁵⁴, C. Kourkouvelis⁹, V. Kouskoura²⁵, A. Koutsman^{159a}, R. Kowalewski¹⁶⁹, T.Z. Kowalski^{38a}, W. Kozanecki¹³⁶, A.S. Kozhin¹³⁰, V.A. Kramarenko⁹⁹, G. Kramberger⁷⁵, D. Krasnopevtsev⁹⁸, M.W. Krasny⁸⁰, A. Krasznahorkay³⁰, J.K. Kraus²¹, A. Kravchenko²⁵, S. Kreiss¹¹⁰, M. Kretz^{58c}, J. Kretzschmar⁷⁴, K. Kreutzfeldt⁵², P. Krieger¹⁵⁸, K. Krizka³¹, K. Kroeninger⁴³, H. Kroha¹⁰¹, J. Kroll¹²², J. Kroseberg²¹, J. Krstic¹³, U. Kruchonak⁶⁵, H. Krüger²¹, N. Krumnack⁶⁴, A. Kruse¹⁷³, M.C. Kruse⁴⁵, M. Kruskal²², T. Kubota⁸⁸, H. Kucuk⁷⁸, S. Kudah^{4b}, S. Kuehn⁴⁸, A. Kugel^{58c}, F. Kuger¹⁷⁴, A. Kuhl¹³⁷, T. Kuhl⁴², V. Kukhtin⁶⁵, R. Kukla¹³⁶, Y. Kulchitsky⁹², S. Kuleshov^{32b}, M. Kuna^{132a,132b}, T. Kunigo⁶⁸, A. Kupco¹²⁷, H. Kurashige⁶⁷, Y.A. Kurochkin⁹², V. Kus¹²⁷, E.S. Kuwertz¹⁶⁹, M. Kuze¹⁵⁷, J. Kvita¹¹⁵, T. Kwan¹⁶⁹, D. Kyriazopoulos¹³⁹, A. La Rosa¹³⁷, J.L. La Rosa Navarro^{24d}, L. La Rotonda^{37a,37b}, C. Lacasta¹⁶⁷, F. Lacava^{132a,132b}, J. Lacey²⁹, H. Lacker¹⁶, D. Lacour⁸⁰, V.R. Lacuesta¹⁶⁷, E. Ladygin⁶⁵, R. Lafaye⁵, B. Laforge⁸⁰, T. Lagouri¹⁷⁶, S. Lai⁵⁴, L. Lambourne⁷⁸, S. Lammers⁶¹, C.L. Lampen⁷, W. Lampl⁷, E. Lançon¹³⁶, U. Landgraf⁴⁸, M.P.J. Landon⁷⁶, V.S. Lang^{58a}, J.C. Lange¹², A.J. Lankford¹⁶³, F. Lanni²⁵, K. Lantzsche²¹, A. Lanza^{121a}, S. Laplace⁸⁰, C. Lapoire³⁰, J.F. Laporte¹³⁶, T. Lari^{91a}, F. Lasagni Manghi^{20a,20b}, M. Lassnig³⁰, P. Laurelli⁴⁷, W. Lavrijsen¹⁵, A.T. Law¹³⁷, P. Laycock⁷⁴, T. Lazovich⁵⁷, O. Le Dortz⁸⁰, E. Le Guirriec⁸⁵, E. Le Menedeu¹², M. LeBlanc¹⁶⁹, T. LeCompte⁶, F. Ledroit-Guillon⁵⁵, C.A. Lee^{145b}, S.C. Lee¹⁵¹, L. Lee¹, G. Lefebvre⁸⁰, M. Lefebvre¹⁶⁹, F. Legger¹⁰⁰, C. Leggett¹⁵, A. Lehan⁷⁴, G. Lehmann Miotto³⁰, X. Lei⁷, W.A. Leight²⁹, A. Leisos^{154,w}, A.G. Leister¹⁷⁶, M.A.L. Leite^{24d}, R. Leitner¹²⁹, D. Lellouch¹⁷², B. Lemmer⁵⁴, K.J.C. Leney⁷⁸, T. Lenz²¹, B. Lenzi³⁰,

R. Leone⁷, S. Leone^{124a,124b}, C. Leonidopoulos⁴⁶, S. Leontsinis¹⁰, C. Leroy⁹⁵, C.G. Lester²⁸, M. Levchenko¹²³, J. Levêque⁵, D. Levin⁸⁹, L.J. Levinson¹⁷², M. Levy¹⁸, A. Lewis¹²⁰, A.M. Leyko²¹, M. Leyton⁴¹, B. Li^{33b,x}, H. Li¹⁴⁸, H.L. Li³¹, L. Li⁴⁵, L. Li^{33e}, S. Li⁴⁵, X. Li⁸⁴, Y. Li^{33c,y}, Z. Liang¹³⁷, H. Liao³⁴, B. Liberti^{133a}, A. Liblong¹⁵⁸, P. Lichard³⁰, K. Lie¹⁶⁵, J. Liebal²¹, W. Liebig¹⁴, C. Limbach²¹, A. Limosani¹⁵⁰, S.C. Lin^{151,z}, T.H. Lin⁸³, F. Linde¹⁰⁷, B.E. Lindquist¹⁴⁸, J.T. Linnemann⁹⁰, E. Lipeles¹²², A. Lipniacka¹⁴, M. Lisovyi^{58b}, T.M. Liss¹⁶⁵, D. Lissauer²⁵, A. Lister¹⁶⁸, A.M. Litke¹³⁷, B. Liu^{151,aa}, D. Liu¹⁵¹, H. Liu⁸⁹, J. Liu⁸⁵, J.B. Liu^{33b}, K. Liu⁸⁵, L. Liu¹⁶⁵, M. Liu⁴⁵, M. Liu^{33b}, Y. Liu^{33b}, M. Livan^{121a,121b}, A. Lleres⁵⁵, J. Llorente Merino⁸², S.L. Lloyd⁷⁶, F. Lo Sterzo¹⁵¹, E. Lobodzinska⁴², P. Loch⁷, W.S. Lockman¹³⁷, F.K. Loebinger⁸⁴, A.E. Loeschall-Jensen³⁶, A. Loginov¹⁷⁶, T. Lohse¹⁶, K. Lohwasser⁴², M. Lokajicek¹²⁷, B.A. Long²², J.D. Long⁸⁹, R.E. Long⁷², K.A. Looper¹¹¹, L. Lopes^{126a}, D. Lopez Mateos⁵⁷, B. Lopez Paredes¹³⁹, I. Lopez Paz¹², J. Lorenz¹⁰⁰, N. Lorenzo Martinez⁶¹, M. Losada¹⁶², P.J. Lösel¹⁰⁰, X. Lou^{33a}, A. Lounis¹¹⁷, J. Love⁶, P.A. Love⁷², N. Lu⁸⁹, H.J. Lubatti¹³⁸, C. Luci^{132a,132b}, A. Lucotte⁵⁵, F. Luehring⁶¹, W. Lukas⁶², L. Luminari^{132a}, O. Lundberg^{146a,146b}, B. Lund-Jensen¹⁴⁷, D. Lynn²⁵, R. Lysak¹²⁷, E. Lytken⁸¹, H. Ma²⁵, L.L. Ma^{33d}, G. Maccarrone⁴⁷, A. Macchiolo¹⁰¹, C.M. Macdonald¹³⁹, B. Maček⁷⁵, J. Machado Miguens^{122,126b}, D. Macina³⁰, D. Madaffari⁸⁵, R. Madar³⁴, H.J. Maddocks⁷², W.F. Mader⁴⁴, A. Madsen¹⁶⁶, J. Maeda⁶⁷, S. Maeland¹⁴, T. Maeno²⁵, A. Maevskiy⁹⁹, E. Magradze⁵⁴, K. Mahboubi⁴⁸, J. Mahlstedt¹⁰⁷, C. Maiani¹³⁶, C. Maidantchik^{24a}, A.A. Maier¹⁰¹, T. Maier¹⁰⁰, A. Maio^{126a,126b,126d}, S. Majewski¹¹⁶, Y. Makida⁶⁶, N. Makovec¹¹⁷, B. Malaescu⁸⁰, Pa. Malecki³⁹, V.P. Maleev¹²³, F. Malek⁵⁵, U. Mallik⁶³, D. Malon⁶, C. Malone¹⁴³, S. Maltezos¹⁰, V.M. Malyshev¹⁰⁹, S. Malyukov³⁰, J. Mamuzic⁴², G. Mancini⁴⁷, B. Mandelli³⁰, L. Mandelli^{91a}, I. Mandić⁷⁵, R. Mandrysch⁶³, J. Maneira^{126a,126b}, A. Manfredini¹⁰¹, L. Manhaes de Andrade Filho^{24b}, J. Manjarres Ramos^{159b}, A. Mann¹⁰⁰, A. Manousakis-Katsikakis⁹, B. Mansoulie¹³⁶, R. Mantifel⁸⁷, M. Mantoani⁵⁴, L. Mapelli³⁰, L. March^{145c}, G. Marchiori⁸⁰, M. Marcisovsky¹²⁷, C.P. Marino¹⁶⁹, M. Marjanovic¹³, D.E. Marley⁸⁹, F. Marroquim^{24a}, S.P. Marsden⁸⁴, Z. Marshall¹⁵, L.F. Marti¹⁷, S. Marti-Garcia¹⁶⁷, B. Martin⁹⁰, T.A. Martin¹⁷⁰, V.J. Martin⁴⁶, B. Martin dit Latour¹⁴, M. Martinez^{12,o}, S. Martin-Haugh¹³¹, V.S. Martoiu^{26a}, A.C. Martyniuk⁷⁸, M. Marx¹³⁸, F. Marzano^{132a}, A. Marzin³⁰, L. Masetti⁸³, T. Mashimo¹⁵⁵, R. Mashinistov⁹⁶, J. Masik⁸⁴, A.L. Maslennikov^{109,c}, I. Massa^{20a,20b}, L. Massa^{20a,20b}, P. Mastrandrea¹⁴⁸, A. Mastroberardino^{37a,37b}, T. Masubuchi¹⁵⁵, P. Mättig¹⁷⁵, J. Mattmann⁸³, J. Maurer^{26a}, S.J. Maxfield⁷⁴, D.A. Maximov^{109,c}, R. Mazini¹⁵¹, S.M. Mazza^{91a,91b}, L. Mazzaferro^{133a,133b}, G. Mc Goldrick¹⁵⁸, S.P. Mc Kee⁸⁹, A. McCarn⁸⁹, R.L. McCarthy¹⁴⁸, T.G. McCarthy²⁹, N.A. McCubbin¹³¹, K.W. McFarlane^{56,*}, J.A. Mcfayden⁷⁸, G. Mchedlidze⁵⁴, S.J. McMahon¹³¹, R.A. McPherson^{169,k}, M. Medinnis⁴², S. Meehan^{145a}, S. Mehlhase¹⁰⁰, A. Mehta⁷⁴, K. Meier^{58a}, C. Meineck¹⁰⁰, B. Meirose⁴¹, B.R. Mellado Garcia^{145c}, F. Meloni¹⁷, A. Mengarelli^{20a,20b}, S. Menke¹⁰¹, E. Meoni¹⁶¹, K.M. Mercurio⁵⁷, S. Mergelmeyer²¹, P. Mermod⁴⁹, L. Merola^{104a,104b}, C. Meroni^{91a}, F.S. Merritt³¹, A. Messina^{132a,132b}, J. Metcalfe²⁵, A.S. Mete¹⁶³, C. Meyer⁸³, C. Meyer¹²², J-P. Meyer¹³⁶, J. Meyer¹⁰⁷, H. Meyer Zu Theenhausen^{58a}, R.P. Middleton¹³¹, S. Miglioranza^{164a,164c}, L. Mijović²¹, G. Mikenberg¹⁷², M. Mikestikova¹²⁷, M. Mikuž⁷⁵, M. Milesi⁸⁸, A. Milic³⁰, D.W. Miller³¹, C. Mills⁴⁶, A. Milov¹⁷², D.A. Milstead^{146a,146b}, A.A. Minaenko¹³⁰, Y. Minami¹⁵⁵, I.A. Minashvili⁶⁵, A.I. Mincer¹¹⁰, B. Mindur^{38a}, M. Mineev⁶⁵, Y. Ming¹⁷³, L.M. Mir¹², T. Mitani¹⁷¹, J. Mitrevski¹⁰⁰, V.A. Mitsou¹⁶⁷, A. Miucci⁴⁹, P.S. Miyagawa¹³⁹, J.U. Mjörnmark⁸¹, T. Moa^{146a,146b}, K. Mochizuki⁸⁵, S. Mohapatra³⁵, W. Mohr⁴⁸, S. Molander^{146a,146b}, R. Moles-Valls²¹, R. Monden⁶⁸, K. Mönig⁴², C. Monini⁵⁵, J. Monk³⁶, E. Monnier⁸⁵, J. Montejo Berlingen¹², F. Monticelli⁷¹, S. Monzani^{132a,132b}, R.W. Moore³, N. Morange¹¹⁷, D. Moreno¹⁶², M. Moreno Llácer⁵⁴, P. Morettini^{50a}, D. Mori¹⁴², M. Morii⁵⁷, M. Morinaga¹⁵⁵, V. Morisbak¹¹⁹, S. Moritz⁸³, A.K. Morley¹⁵⁰, G. Mornacchi³⁰, J.D. Morris⁷⁶, S.S. Mortensen³⁶, A. Morton⁵³, L. Morvaj¹⁰³, M. Mosidze^{51b}, J. Moss¹⁴³, K. Motohashi¹⁵⁷, R. Mount¹⁴³, E. Mountricha²⁵, S.V. Mouraviev^{96,*}, E.J.W. Moyse⁸⁶, S. Muanza⁸⁵, R.D. Mudd¹⁸,

F. Mueller¹⁰¹, J. Mueller¹²⁵, R.S.P. Mueller¹⁰⁰, T. Mueller²⁸, D. Muenstermann⁴⁹, P. Mullen⁵³,
 G.A. Mullier¹⁷, J.A. Murillo Quijada¹⁸, W.J. Murray^{170,131}, H. Musheghyan⁵⁴, E. Musto¹⁵²,
 A.G. Myagkov^{130,ab}, M. Myska¹²⁸, B.P. Nachman¹⁴³, O. Nackenhorst⁵⁴, J. Nadal⁵⁴, K. Nagai¹²⁰,
 R. Nagai¹⁵⁷, Y. Nagai⁸⁵, K. Nagano⁶⁶, A. Nagarkar¹¹¹, Y. Nagasaka⁵⁹, K. Nagata¹⁶⁰, M. Nagel¹⁰¹,
 E. Nagy⁸⁵, A.M. Nairz³⁰, Y. Nakahama³⁰, K. Nakamura⁶⁶, T. Nakamura¹⁵⁵, I. Nakano¹¹²,
 H. Namasivayam⁴¹, R.F. Naranjo Garcia⁴², R. Narayan³¹, D.I. Narrias Villar^{58a}, T. Naumann⁴²,
 G. Navarro¹⁶², R. Nayyar⁷, H.A. Neal⁸⁹, P.Yu. Nechaeva⁹⁶, T.J. Neep⁸⁴, P.D. Nef¹⁴³, A. Negri^{121a,121b},
 M. Negrini^{20a}, S. Nektarijevic¹⁰⁶, C. Nellist¹¹⁷, A. Nelson¹⁶³, S. Nemecek¹²⁷, P. Nemethy¹¹⁰,
 A.A. Nepomuceno^{24a}, M. Nessi^{30,ac}, M.S. Neubauer¹⁶⁵, M. Neumann¹⁷⁵, R.M. Neves¹¹⁰, P. Nevski²⁵,
 P.R. Newman¹⁸, D.H. Nguyen⁶, R.B. Nickerson¹²⁰, R. Nicolaidou¹³⁶, B. Nicquevert³⁰, J. Nielsen¹³⁷,
 N. Nikiforou³⁵, A. Nikiforov¹⁶, V. Nikolaenko^{130,ab}, I. Nikolic-Audit⁸⁰, K. Nikolopoulos¹⁸,
 J.K. Nilsen¹¹⁹, P. Nilsson²⁵, Y. Ninomiya¹⁵⁵, A. Nisati^{132a}, R. Nisius¹⁰¹, T. Nobe¹⁵⁵, M. Nomachi¹¹⁸,
 I. Nomidis²⁹, T. Nooney⁷⁶, S. Norberg¹¹³, M. Nordberg³⁰, O. Novgorodova⁴⁴, S. Nowak¹⁰¹,
 M. Nozaki⁶⁶, L. Nozka¹¹⁵, K. Ntekas¹⁰, G. Nunes Hanninger⁸⁸, T. Nunnemann¹⁰⁰, E. Nurse⁷⁸, F. Nuti⁸⁸,
 B.J. O'Brien⁴⁶, F. O'Grady⁷, D.C. O'Neil¹⁴², V. O'Shea⁵³, F.G. Oakham^{29,d}, H. Oberlack¹⁰¹,
 T. Obermann²¹, J. Ocariz⁸⁰, A. Ochi⁶⁷, I. Ochoa⁷⁸, J.P. Ochoa-Ricoux^{32a}, S. Oda⁷⁰, S. Odaka⁶⁶,
 H. Ogren⁶¹, A. Oh⁸⁴, S.H. Oh⁴⁵, C.C. Ohm¹⁵, H. Ohman¹⁶⁶, H. Oide³⁰, W. Okamura¹¹⁸, H. Okawa¹⁶⁰,
 Y. Okumura³¹, T. Okuyama⁶⁶, A. Olariu^{26a}, S.A. Olivares Pino⁴⁶, D. Oliveira Damazio²⁵,
 E. Oliver Garcia¹⁶⁷, A. Olszewski³⁹, J. Olszowska³⁹, A. Onofre^{126a,126e}, K. Onogi¹⁰³, P.U.E. Onyisi^{31,r},
 C.J. Oram^{159a}, M.J. Oreglia³¹, Y. Oren¹⁵³, D. Orestano^{134a,134b}, N. Orlando¹⁵⁴, C. Oropeza Barrera⁵³,
 R.S. Orr¹⁵⁸, B. Osculati^{50a,50b}, R. Ospanov⁸⁴, G. Otero y Garzon²⁷, H. Otono⁷⁰, M. Ouchrif^{135d},
 F. Ould-Saada¹¹⁹, A. Ouraou¹³⁶, K.P. Oussoren¹⁰⁷, Q. Ouyang^{33a}, A. Ovcharova¹⁵, M. Owen⁵³,
 R.E. Owen¹⁸, V.E. Ozcan^{19a}, N. Ozturk⁸, K. Pachal¹⁴², A. Pacheco Pages¹², C. Padilla Aranda¹²,
 M. Pagáčová⁴⁸, S. Pagan Griso¹⁵, E. Paganis¹³⁹, F. Paige²⁵, P. Pais⁸⁶, K. Pajchel¹¹⁹, G. Palacino^{159b},
 S. Palestini³⁰, M. Palka^{38b}, D. Pallin³⁴, A. Palma^{126a,126b}, Y.B. Pan¹⁷³, E. Panagiotopoulou¹⁰,
 C.E. Pandini⁸⁰, J.G. Panduro Vazquez⁷⁷, P. Pani^{146a,146b}, S. Panitkin²⁵, D. Pantea^{26a}, L. Paolozzi⁴⁹,
 Th.D. Papadopoulou¹⁰, K. Papageorgiou¹⁵⁴, A. Paramonov⁶, D. Paredes Hernandez¹⁵⁴, M.A. Parker²⁸,
 K.A. Parker¹³⁹, F. Parodi^{50a,50b}, J.A. Parsons³⁵, U. Parzefall⁴⁸, E. Pasqualucci^{132a}, S. Passaggio^{50a},
 F. Pastore^{134a,134b,*}, Fr. Pastore⁷⁷, G. Pásztor²⁹, S. Patariaia¹⁷⁵, N.D. Patel¹⁵⁰, J.R. Pater⁸⁴, T. Pauly³⁰,
 J. Pearce¹⁶⁹, B. Pearson¹¹³, L.E. Pedersen³⁶, M. Pedersen¹¹⁹, S. Pedraza Lopez¹⁶⁷, R. Pedro^{126a,126b},
 S.V. Peleganchuk^{109,c}, D. Pelikan¹⁶⁶, O. Penc¹²⁷, C. Peng^{33a}, H. Peng^{33b}, B. Penning³¹, J. Penwell⁶¹,
 D.V. Perepelitsa²⁵, E. Perez Codina^{159a}, M.T. Pérez García-Estañ¹⁶⁷, L. Perini^{91a,91b}, H. Pernegger³⁰,
 S. Perrella^{104a,104b}, R. Peschke⁴², V.D. Peshekhonov⁶⁵, K. Peters³⁰, R.F.Y. Peters⁸⁴, B.A. Petersen³⁰,
 T.C. Petersen³⁶, E. Petit⁴², A. Petridis¹, C. Petridou¹⁵⁴, P. Petroff¹¹⁷, E. Petrolu^{132a}, F. Petrucci^{134a,134b},
 N.E. Pettersson¹⁵⁷, R. Pezoa^{32b}, P.W. Phillips¹³¹, G. Piacquadio¹⁴³, E. Pianori¹⁷⁰, A. Picazio⁴⁹,
 E. Piccaro⁷⁶, M. Piccinini^{20a,20b}, M.A. Pickering¹²⁰, R. Piegaia²⁷, D.T. Pignotti¹¹¹, J.E. Pilcher³¹,
 A.D. Pilkington⁸⁴, J. Pina^{126a,126b,126d}, M. Pinamonti^{164a,164c,ad}, J.L. Pinfold³, A. Pingel³⁶, S. Pires⁸⁰,
 H. Pirumov⁴², M. Pitt¹⁷², C. Pizio^{91a,91b}, L. Plazak^{144a}, M.-A. Pleier²⁵, V. Pleskot¹²⁹, E. Plotnikova⁶⁵,
 P. Plucinski^{146a,146b}, D. Pluth⁶⁴, R. Poettgen^{146a,146b}, L. Poggioli¹¹⁷, D. Pohl²¹, G. Polesello^{121a},
 A. Poley⁴², A. Policicchio^{37a,37b}, R. Polifka¹⁵⁸, A. Polini^{20a}, C.S. Pollard⁵³, V. Polychronakos²⁵,
 K. Pommès³⁰, L. Pontecorvo^{132a}, B.G. Pope⁹⁰, G.A. Popeneciu^{26b}, D.S. Popovic¹³, A. Poppleton³⁰,
 S. Pospisil¹²⁸, K. Potamianos¹⁵, I.N. Potrap⁶⁵, C.J. Potter¹⁴⁹, C.T. Potter¹¹⁶, G. Poulard³⁰, J. Poveda³⁰,
 V. Pozdnyakov⁶⁵, P. Pralavorio⁸⁵, A. Pranko¹⁵, S. Prasad³⁰, S. Prell⁶⁴, D. Price⁸⁴, L.E. Price⁶,
 M. Primavera^{73a}, S. Prince⁸⁷, M. Proissl⁴⁶, K. Prokofiev^{60c}, F. Prokoshin^{32b}, E. Protopapadaki¹³⁶,
 S. Protopopescu²⁵, J. Proudfoot⁶, M. Przybycien^{38a}, E. Ptacek¹¹⁶, D. Puddu^{134a,134b}, E. Pueschel⁸⁶,
 D. Puldon¹⁴⁸, M. Purohit^{25,ae}, P. Puzo¹¹⁷, J. Qian⁸⁹, G. Qin⁵³, Y. Qin⁸⁴, A. Quadt⁵⁴, D.R. Quarrie¹⁵,
 W.B. Quayle^{164a,164b}, M. Queitsch-Maitland⁸⁴, D. Quilty⁵³, S. Raddum¹¹⁹, V. Radeka²⁵, V. Radescu⁴²,

S.K. Radhakrishnan¹⁴⁸, P. Radloff¹¹⁶, P. Rados⁸⁸, F. Ragusa^{91a,91b}, G. Rahal¹⁷⁸, S. Rajagopalan²⁵,
 M. Rammensee³⁰, C. Rangel-Smith¹⁶⁶, F. Rauscher¹⁰⁰, S. Rave⁸³, T. Ravenscroft⁵³, M. Raymond³⁰,
 A.L. Read¹¹⁹, N.P. Readioff⁷⁴, D.M. Rebutzi^{121a,121b}, A. Redelbach¹⁷⁴, G. Redlinger²⁵, R. Reece¹³⁷,
 K. Reeves⁴¹, L. Rehnisch¹⁶, J. Reichert¹²², H. Reisin²⁷, M. Relich¹⁶³, C. Rembser³⁰, H. Ren^{33a},
 A. Renaud¹¹⁷, M. Rescigno^{132a}, S. Resconi^{91a}, O.L. Rezanova^{109,c}, P. Reznicek¹²⁹, R. Rezvani⁹⁵,
 R. Richter¹⁰¹, S. Richter⁷⁸, E. Richter-Was^{38b}, O. Ricken²¹, M. Ridel⁸⁰, P. Rieck¹⁶, C.J. Riegel¹⁷⁵,
 J. Rieger⁵⁴, O. Rifki¹¹³, M. Rijssenbeek¹⁴⁸, A. Rimoldi^{121a,121b}, L. Rinaldi^{20a}, B. Ristić⁴⁹, E. Ritsch³⁰,
 I. Riu¹², F. Rizatdinova¹¹⁴, E. Rizvi⁷⁶, S.H. Robertson^{87,k}, A. Robichaud-Veronneau⁸⁷, D. Robinson²⁸,
 J.E.M. Robinson⁴², A. Robson⁵³, C. Roda^{124a,124b}, S. Roe³⁰, O. Røhne¹¹⁹, S. Rolli¹⁶¹, A. Romaniouk⁹⁸,
 M. Romano^{20a,20b}, S.M. Romano Saez³⁴, E. Romero Adam¹⁶⁷, N. Rompotis¹³⁸, M. Ronzani⁴⁸,
 L. Roos⁸⁰, E. Ros¹⁶⁷, S. Rosati^{132a}, K. Rosbach⁴⁸, P. Rose¹³⁷, P.L. Rosendahl¹⁴, O. Rosenthal¹⁴¹,
 V. Rossetti^{146a,146b}, E. Rossi^{104a,104b}, L.P. Rossi^{50a}, J.H.N. Rosten²⁸, R. Rosten¹³⁸, M. Rotaru^{26a},
 I. Roth¹⁷², J. Rothberg¹³⁸, D. Rousseau¹¹⁷, C.R. Royon¹³⁶, A. Rozanov⁸⁵, Y. Rozen¹⁵², X. Ruan^{145c},
 F. Rubbo¹⁴³, I. Rubinskiy⁴², V.I. Rud⁹⁹, C. Rudolph⁴⁴, M.S. Rudolph¹⁵⁸, F. Rühr⁴⁸, A. Ruiz-Martinez³⁰,
 Z. Rurikova⁴⁸, N.A. Rusakovich⁶⁵, A. Ruschke¹⁰⁰, H.L. Russell¹³⁸, J.P. Rutherford⁷, N. Ruthmann⁴⁸,
 Y.F. Ryabov¹²³, M. Rybar¹⁶⁵, G. Rybkin¹¹⁷, N.C. Ryder¹²⁰, A.F. Saavedra¹⁵⁰, G. Sabato¹⁰⁷,
 S. Sacerdoti²⁷, A. Saddique³, H.F.-W. Sadrozinski¹³⁷, R. Sadykov⁶⁵, F. Safai Tehrani^{132a},
 M. Sahinsoy^{58a}, M. Saimpert¹³⁶, T. Saito¹⁵⁵, H. Sakamoto¹⁵⁵, Y. Sakurai¹⁷¹, G. Salamanna^{134a,134b},
 A. Salamon^{133a}, J.E. Salazar Loyola^{32b}, M. Saleem¹¹³, D. Salek¹⁰⁷, P.H. Sales De Bruin¹³⁸,
 D. Salihagic¹⁰¹, A. Salnikov¹⁴³, J. Salt¹⁶⁷, D. Salvatore^{37a,37b}, F. Salvatore¹⁴⁹, A. Salvucci^{60a},
 A. Salzburger³⁰, D. Sammel⁴⁸, D. Sampsonidis¹⁵⁴, A. Sanchez^{104a,104b}, J. Sánchez¹⁶⁷,
 V. Sanchez Martinez¹⁶⁷, H. Sandaker¹¹⁹, R.L. Sandbach⁷⁶, H.G. Sander⁸³, M.P. Sanders¹⁰⁰,
 M. Sandhoff¹⁷⁵, C. Sandoval¹⁶², R. Sandstroem¹⁰¹, D.P.C. Sankey¹³¹, M. Sannino^{50a,50b}, A. Sansoni⁴⁷,
 C. Santoni³⁴, R. Santonico^{133a,133b}, H. Santos^{126a}, I. Santoyo Castillo¹⁴⁹, K. Sapp¹²⁵, A. Saponov⁶⁵,
 J.G. Saraiva^{126a,126d}, B. Sarrazin²¹, O. Sasaki⁶⁶, Y. Sasaki¹⁵⁵, K. Sato¹⁶⁰, G. Sauvage^{5,*}, E. Sauvan⁵,
 G. Savage⁷⁷, P. Savard^{158,d}, C. Sawyer¹³¹, L. Sawyer^{79,n}, J. Saxon³¹, C. Sbarra^{20a}, A. Sbrizzi^{20a,20b},
 T. Scanlon⁷⁸, D.A. Scannicchio¹⁶³, M. Scarcella¹⁵⁰, V. Scarfone^{37a,37b}, J. Schaarschmidt¹⁷²,
 P. Schacht¹⁰¹, D. Schaefer³⁰, R. Schaefer⁴², J. Schaeffer⁸³, S. Schaepe²¹, S. Schaetzl^{58b}, U. Schäfer⁸³,
 A.C. Schaffer¹¹⁷, D. Schaile¹⁰⁰, R.D. Schamberger¹⁴⁸, V. Scharf^{58a}, V.A. Schegelsky¹²³, D. Scheirich¹²⁹,
 M. Schernau¹⁶³, C. Schiavi^{50a,50b}, C. Schillo⁴⁸, M. Schioppa^{37a,37b}, S. Schlenker³⁰, K. Schmieden³⁰,
 C. Schmitt⁸³, S. Schmitt^{58b}, S. Schmitt⁴², B. Schneider^{159a}, Y.J. Schnellbach⁷⁴, U. Schnoor⁴⁴,
 L. Schoeffel¹³⁶, A. Schoening^{58b}, B.D. Schoenrock⁹⁰, E. Schopf²¹, A.L.S. Schorlemmer⁵⁴, M. Schott⁸³,
 D. Schouten^{159a}, J. Schovancova⁸, S. Schramm⁴⁹, M. Schreyer¹⁷⁴, C. Schroeder⁸³, N. Schuh⁸³,
 M.J. Schultens²¹, H.-C. Schultz-Coulon^{58a}, H. Schulz¹⁶, M. Schumacher⁴⁸, B.A. Schumm¹³⁷,
 Ph. Schune¹³⁶, C. Schwanenberger⁸⁴, A. Schwartzman¹⁴³, T.A. Schwarz⁸⁹, Ph. Schwegler¹⁰¹,
 H. Schweiger⁸⁴, Ph. Schwemling¹³⁶, R. Schwienhorst⁹⁰, J. Schwindling¹³⁶, T. Schwindt²¹,
 F.G. Sciacca¹⁷, E. Scifo¹¹⁷, G. Sciolla²³, F. Scuri^{124a,124b}, F. Scutti²¹, J. Searcy⁸⁹, G. Sedov⁴²,
 E. Sedykh¹²³, P. Seema²¹, S.C. Seidel¹⁰⁵, A. Seiden¹³⁷, F. Seifert¹²⁸, J.M. Seixas^{24a}, G. Sekhniaidze^{104a},
 K. Sekhon⁸⁹, S.J. Sekula⁴⁰, D.M. Seliverstov^{123,*}, N. Semprini-Cesari^{20a,20b}, C. Serfon³⁰, L. Serin¹¹⁷,
 L. Serkin^{164a,164b}, T. Serre⁸⁵, M. Sessa^{134a,134b}, R. Seuster^{159a}, H. Severini¹¹³, T. Sfiligoj⁷⁵, F. Sforza³⁰,
 A. Sfyrlla³⁰, E. Shabalina⁵⁴, M. Shamim¹¹⁶, L.Y. Shan^{33a}, R. Shang¹⁶⁵, J.T. Shank²², M. Shapiro¹⁵,
 P.B. Shatalov⁹⁷, K. Shaw^{164a,164b}, S.M. Shaw⁸⁴, A. Shcherbakova^{146a,146b}, C.Y. Shehu¹⁴⁹, P. Sherwood⁷⁸,
 L. Shi^{151,af}, S. Shimizu⁶⁷, C.O. Shimmin¹⁶³, M. Shimojima¹⁰², M. Shiyakova⁶⁵, A. Shmeleva⁹⁶,
 D. Shoaleh Saadi⁹⁵, M.J. Shochet³¹, S. Shojaii^{91a,91b}, S. Shrestha¹¹¹, E. Shulga⁹⁸, M.A. Shupe⁷,
 S. Shushkevich⁴², P. Sicho¹²⁷, P.E. Sidebo¹⁴⁷, O. Sidiropoulou¹⁷⁴, D. Sidorov¹¹⁴, A. Sidoti^{20a,20b},
 F. Siegert⁴⁴, Dj. Sijacki¹³, J. Silva^{126a,126d}, Y. Silver¹⁵³, S.B. Silverstein^{146a}, V. Simak¹²⁸, O. Simard⁵,
 Lj. Simic¹³, S. Simion¹¹⁷, E. Simioni⁸³, B. Simmons⁷⁸, D. Simon³⁴, P. Sinervo¹⁵⁸, N.B. Sinev¹¹⁶,

M. Sioli^{20a,20b}, G. Siragusa¹⁷⁴, A.N. Sisakyan^{65,*}, S.Yu. Sivoklokov⁹⁹, J. Sjölin^{146a,146b}, T.B. Sjursen¹⁴,
M.B. Skinner⁷², H.P. Skottowe⁵⁷, P. Skubic¹¹³, M. Slater¹⁸, T. Slavicek¹²⁸, M. Slawinska¹⁰⁷,
K. Sliwa¹⁶¹, V. Smakhtin¹⁷², B.H. Smart⁴⁶, L. Smestad¹⁴, S.Yu. Smirnov⁹⁸, Y. Smirnov⁹⁸,
L.N. Smirnova^{99,ag}, O. Smirnova⁸¹, M.N.K. Smith³⁵, R.W. Smith³⁵, M. Smizanska⁷², K. Smolek¹²⁸,
A.A. Snesarev⁹⁶, G. Snidero⁷⁶, S. Snyder²⁵, R. Sobie^{169,k}, F. Socher⁴⁴, A. Soffer¹⁵³, D.A. Soh^{151,af},
G. Sokhrannyi⁷⁵, C.A. Solans³⁰, M. Solar¹²⁸, J. Solc¹²⁸, E.Yu. Soldatov⁹⁸, U. Soldevila¹⁶⁷,
A.A. Solodkov¹³⁰, A. Soloshenko⁶⁵, O.V. Solovyanov¹³⁰, V. Solovyev¹²³, P. Sommer⁴⁸, H.Y. Song^{33b},
N. Soni¹, A. Sood¹⁵, A. Sopczyk¹²⁸, B. Sopko¹²⁸, V. Sopko¹²⁸, V. Sorin¹², D. Sosa^{58b}, M. Sosebee⁸,
C.L. Sotiropoulou^{124a,124b}, R. Soualah^{164a,164c}, A.M. Soukharev^{109,c}, D. South⁴², B.C. Sowden⁷⁷,
S. Spagnolo^{73a,73b}, M. Spalla^{124a,124b}, M. Spangenberg¹⁷⁰, F. Spanò⁷⁷, W.R. Spearman⁵⁷, D. Sperlich¹⁶,
F. Spettel¹⁰¹, R. Spighi^{20a}, G. Spigo³⁰, L.A. Spiller⁸⁸, M. Spousta¹²⁹, T. Spreitzer¹⁵⁸, R.D. St. Denis^{53,*},
A. Stabile^{91a}, S. Staerz⁴⁴, J. Stahlman¹²², R. Stamen^{58a}, S. Stamm¹⁶, E. Stanecka³⁹, C. Stanescu^{134a},
M. Stanescu-Bellu⁴², M.M. Stanitzki⁴², S. Stappes¹¹⁹, E.A. Starchenko¹³⁰, J. Stark⁵⁵, P. Staroba¹²⁷,
P. Starovoitov^{58a}, R. Staszewski³⁹, P. Steinberg²⁵, B. Stelzer¹⁴², H.J. Stelzer³⁰, O. Stelzer-Chilton^{159a},
H. Stenzel⁵², G.A. Stewart⁵³, J.A. Stillings²¹, M.C. Stockton⁸⁷, M. Stoebe⁸⁷, G. Stoicea^{26a}, P. Stolte⁵⁴,
S. Stonjek¹⁰¹, A.R. Stradling⁸, A. Straessner⁴⁴, M.E. Stramaglia¹⁷, J. Strandberg¹⁴⁷,
S. Strandberg^{146a,146b}, A. Strandlie¹¹⁹, E. Strauss¹⁴³, M. Strauss¹¹³, P. Strizenec^{144b}, R. Ströhmer¹⁷⁴,
D.M. Strom¹¹⁶, R. Stroynowski⁴⁰, A. Strubig¹⁰⁶, S.A. Stucci¹⁷, B. Stugu¹⁴, N.A. Styles⁴², D. Su¹⁴³,
J. Su¹²⁵, R. Subramaniam⁷⁹, A. Succurro¹², Y. Sugaya¹¹⁸, M. Suk¹²⁸, V.V. Sulin⁹⁶, S. Sultansoy^{4c},
T. Sumida⁶⁸, S. Sun⁵⁷, X. Sun^{33a}, J.E. Sundermann⁴⁸, K. Suruliz¹⁴⁹, G. Susinno^{37a,37b}, M.R. Sutton¹⁴⁹,
S. Suzuki⁶⁶, M. Svatos¹²⁷, M. Swiatlowski¹⁴³, I. Sykora^{144a}, T. Sykora¹²⁹, D. Ta⁴⁸, C. Taccini^{134a,134b},
K. Tackmann⁴², J. Taenzer¹⁵⁸, A. Taffard¹⁶³, R. Tafirout^{159a}, N. Taiblum¹⁵³, H. Takai²⁵, R. Takashima⁶⁹,
H. Takeda⁶⁷, T. Takeshita¹⁴⁰, Y. Takubo⁶⁶, M. Talby⁸⁵, A.A. Talyshev^{109,c}, J.Y.C. Tam¹⁷⁴, K.G. Tan⁸⁸,
J. Tanaka¹⁵⁵, R. Tanaka¹¹⁷, S. Tanaka⁶⁶, B.B. Tannenwald¹¹¹, N. Tannoury²¹, S. Tapprogge⁸³,
S. Tarem¹⁵², F. Tarrade²⁹, G.F. Tartarelli^{91a}, P. Tas¹²⁹, M. Tasevsky¹²⁷, T. Tashiro⁶⁸, E. Tassi^{37a,37b},
A. Tavares Delgado^{126a,126b}, Y. Tayalati^{135d}, F.E. Taylor⁹⁴, G.N. Taylor⁸⁸, P.T.E. Taylor⁸⁸, W. Taylor^{159b},
F.A. Teischinger³⁰, M. Teixeira Dias Castanheira⁷⁶, P. Teixeira-Dias⁷⁷, K.K. Temming⁴⁸, D. Temple¹⁴²,
H. Ten Kate³⁰, P.K. Teng¹⁵¹, J.J. Teoh¹¹⁸, F. Tepel¹⁷⁵, S. Terada⁶⁶, K. Terashi¹⁵⁵, J. Terron⁸², S. Terzo¹⁰¹,
M. Testa⁴⁷, R.J. Teuscher^{158,k}, T. Theveneaux-Pelzer³⁴, J.P. Thomas¹⁸, J. Thomas-Wilsker⁷⁷,
E.N. Thompson³⁵, P.D. Thompson¹⁸, R.J. Thompson⁸⁴, A.S. Thompson⁵³, L.A. Thomsen¹⁷⁶,
E. Thomson¹²², M. Thomson²⁸, R.P. Thun^{89,*}, M.J. Tibbetts¹⁵, R.E. Ticse Torres⁸⁵,
V.O. Tikhomirov^{96,ah}, Yu.A. Tikhonov^{109,c}, S. Timoshenko⁹⁸, E. Tiouchichine⁸⁵, P. Tipton¹⁷⁶,
S. Tisserant⁸⁵, K. Todome¹⁵⁷, T. Todorov^{5,*}, S. Todorova-Nova¹²⁹, J. Tojo⁷⁰, S. Tokár^{144a},
K. Tokushuku⁶⁶, K. Tollefson⁹⁰, E. Tolley⁵⁷, L. Tomlinson⁸⁴, M. Tomoto¹⁰³, L. Tompkins^{143,ai},
K. Toms¹⁰⁵, E. Torrence¹¹⁶, H. Torres¹⁴², E. Torró Pastor¹³⁸, J. Toth^{85,aj}, F. Touchard⁸⁵, D.R. Tovey¹³⁹,
T. Trefzger¹⁷⁴, L. Tremblet³⁰, A. Tricoli³⁰, I.M. Trigger^{159a}, S. Trincaz-Duvoid⁸⁰, M.F. Tripiana¹²,
W. Trischuk¹⁵⁸, B. Trocmé⁵⁵, C. Troncon^{91a}, M. Trotter-McDonald¹⁵, M. Trovatelli¹⁶⁹, P. True⁹⁰,
L. Truong^{164a,164c}, M. Trzebinski³⁹, A. Trzupek³⁹, C. Tsarouchas³⁰, J.C-L. Tseng¹²⁰, P.V. Tsiareshka⁹²,
D. Tsionou¹⁵⁴, G. Tsipolitis¹⁰, N. Tsirintanis⁹, S. Tsiskaridze¹², V. Tsiskaridze⁴⁸, E.G. Tskhadadze^{51a},
I.I. Tsukerman⁹⁷, V. Tsulaia¹⁵, S. Tsuno⁶⁶, D. Tsybychev¹⁴⁸, A. Tudorache^{26a}, V. Tudorache^{26a},
A.N. Tuna⁵⁷, S.A. Tuppiti^{20a,20b}, S. Turchikhin^{99,ag}, D. Turecek¹²⁸, R. Turra^{91a,91b}, A.J. Turvey⁴⁰,
P.M. Tuts³⁵, A. Tykhonov⁴⁹, M. Tylmad^{146a,146b}, M. Tyndel¹³¹, I. Ueda¹⁵⁵, R. Ueno²⁹,
M. Ughetto^{146a,146b}, M. Ugland¹⁴, F. Ukegawa¹⁶⁰, G. Unal³⁰, A. Undrus²⁵, G. Unel¹⁶³, F.C. Ungaro⁴⁸,
Y. Unno⁶⁶, C. Unverdorben¹⁰⁰, J. Urban^{144b}, P. Urquijo⁸⁸, P. Urrejola⁸³, G. Usai⁸, A. Usanova⁶²,
L. Vacavant⁸⁵, V. Vacek¹²⁸, B. Vachon⁸⁷, C. Valderanis⁸³, N. Valencic¹⁰⁷, S. Valentineti^{20a,20b},
A. Valero¹⁶⁷, L. Valery¹², S. Valkar¹²⁹, E. Valladolid Gallego¹⁶⁷, S. Vallecorsa⁴⁹, J.A. Valls Ferrer¹⁶⁷,
W. Van Den Wollenberg¹⁰⁷, P.C. Van Der Deijl¹⁰⁷, R. van der Geer¹⁰⁷, H. van der Graaf¹⁰⁷,

N. van Eldik¹⁵², P. van Gemmeren⁶, J. Van Nieuwkoop¹⁴², I. van Vulpen¹⁰⁷, M.C. van Woerden³⁰, M. Vanadia^{132a,132b}, W. Vandelli³⁰, R. Vanguri¹²², A. Vaniachine⁶, F. Vannucci⁸⁰, G. Vardanyan¹⁷⁷, R. Vari^{132a}, E.W. Varnes⁷, T. Varol⁴⁰, D. Varouchas⁸⁰, A. Vartapetian⁸, K.E. Varvell¹⁵⁰, F. Vazeille³⁴, T. Vazquez Schroeder⁸⁷, J. Veatch⁷, L.M. Veloce¹⁵⁸, F. Veloso^{126a,126c}, T. Velz²¹, S. Veneziano^{132a}, A. Ventura^{73a,73b}, D. Ventura⁸⁶, M. Venturi¹⁶⁹, N. Venturi¹⁵⁸, A. Venturini²³, V. Vercesi^{121a}, M. Verducci^{132a,132b}, W. Verkerke¹⁰⁷, J.C. Vermeulen¹⁰⁷, A. Vest⁴⁴, M.C. Vetterli^{142,d}, O. Viazlo⁸¹, I. Vichou¹⁶⁵, T. Vickey¹³⁹, O.E. Vickey Boeriu¹³⁹, G.H.A. Viehhauser¹²⁰, S. Viel¹⁵, R. Vigne⁶², M. Villa^{20a,20b}, M. Villaplana Perez^{91a,91b}, E. Vilucchi⁴⁷, M.G. Vincter²⁹, V.B. Vinogradov⁶⁵, I. Vivarelli¹⁴⁹, F. Vives Vaque³, S. Vlachos¹⁰, D. Vladoiu¹⁰⁰, M. Vlasak¹²⁸, M. Vogel^{32a}, P. Vokac¹²⁸, G. Volpi^{124a,124b}, M. Volpi⁸⁸, H. von der Schmitt¹⁰¹, H. von Radziewski⁴⁸, E. von Toerne²¹, V. Vorobel¹²⁹, K. Vorobev⁹⁸, M. Vos¹⁶⁷, R. Voss³⁰, J.H. Vosseveld⁷⁴, N. Vranjes¹³, M. Vranjes Milosavljevic¹³, V. Vrba¹²⁷, M. Vreeswijk¹⁰⁷, R. Vuillermet³⁰, I. Vukotic³¹, Z. Vykydal¹²⁸, P. Wagner²¹, W. Wagner¹⁷⁵, H. Wahlberg⁷¹, S. Wahrmund⁴⁴, J. Wakabayashi¹⁰³, J. Walder⁷², R. Walker¹⁰⁰, W. Walkowiak¹⁴¹, C. Wang¹⁵¹, F. Wang¹⁷³, H. Wang¹⁵, H. Wang⁴⁰, J. Wang⁴², J. Wang^{33a}, K. Wang⁸⁷, R. Wang⁶, S.M. Wang¹⁵¹, T. Wang²¹, T. Wang³⁵, X. Wang¹⁷⁶, C. Wanotayaroj¹¹⁶, A. Warburton⁸⁷, C.P. Ward²⁸, D.R. Wardrope⁷⁸, A. Washbrook⁴⁶, C. Wasicki⁴², P.M. Watkins¹⁸, A.T. Watson¹⁸, I.J. Watson¹⁵⁰, M.F. Watson¹⁸, G. Watts¹³⁸, S. Watts⁸⁴, B.M. Waugh⁷⁸, S. Webb⁸⁴, M.S. Weber¹⁷, S.W. Weber¹⁷⁴, J.S. Webster³¹, A.R. Weidberg¹²⁰, B. Weinert⁶¹, J. Weingarten⁵⁴, C. Weiser⁴⁸, H. Weits¹⁰⁷, P.S. Wells³⁰, T. Wenaus²⁵, T. Wengler³⁰, S. Wenig³⁰, N. Wormes²¹, M. Werner⁴⁸, P. Werner³⁰, M. Wessels^{58a}, J. Wetter¹⁶¹, K. Whalen¹¹⁶, A.M. Wharton⁷², A. White⁸, M.J. White¹, R. White^{32b}, S. White^{124a,124b}, D. Whiteson¹⁶³, F.J. Wickens¹³¹, W. Wiedenmann¹⁷³, M. Wielers¹³¹, P. Wienemann²¹, C. Wiglesworth³⁶, L.A.M. Wiik-Fuchs²¹, A. Wildauer¹⁰¹, H.G. Wilkens³⁰, H.H. Williams¹²², S. Williams¹⁰⁷, C. Willis⁹⁰, S. Willocq⁸⁶, A. Wilson⁸⁹, J.A. Wilson¹⁸, I. Wingerter-Seez⁵, F. Winklmeier¹¹⁶, B.T. Winter²¹, M. Wittgen¹⁴³, J. Wittkowski¹⁰⁰, S.J. Wollstadt⁸³, M.W. Wolter³⁹, H. Wolters^{126a,126c}, B.K. Wosiek³⁹, J. Wotschack³⁰, M.J. Woudstra⁸⁴, K.W. Wozniak³⁹, M. Wu⁵⁵, M. Wu³¹, S.L. Wu¹⁷³, X. Wu⁴⁹, Y. Wu⁸⁹, T.R. Wyatt⁸⁴, B.M. Wynne⁴⁶, S. Xella³⁶, D. Xu^{33a}, L. Xu²⁵, B. Yabsley¹⁵⁰, S. Yacoub^{145a}, R. Yakabe⁶⁷, M. Yamada⁶⁶, D. Yamaguchi¹⁵⁷, Y. Yamaguchi¹¹⁸, A. Yamamoto⁶⁶, S. Yamamoto¹⁵⁵, T. Yamanaka¹⁵⁵, K. Yamauchi¹⁰³, Y. Yamazaki⁶⁷, Z. Yan²², H. Yang^{33e}, H. Yang¹⁷³, Y. Yang¹⁵¹, W-M. Yao¹⁵, Y. Yasu⁶⁶, E. Yatsenko⁵, K.H. Yau Wong²¹, J. Ye⁴⁰, S. Ye²⁵, I. Yeletsikh⁶⁵, A.L. Yen⁵⁷, E. Yildirim⁴², K. Yorita¹⁷¹, R. Yoshida⁶, K. Yoshihara¹²², C. Young¹⁴³, C.J.S. Young³⁰, S. Youssef²², D.R. Yu¹⁵, J. Yu⁸, J.M. Yu⁸⁹, J. Yu¹¹⁴, L. Yuan⁶⁷, S.P.Y. Yuen²¹, A. Yurkewicz¹⁰⁸, I. Yusuff^{28,ak}, B. Zabinski³⁹, R. Zaidan⁶³, A.M. Zaitsev^{130,ab}, J. Zalieckas¹⁴, A. Zaman¹⁴⁸, S. Zambito⁵⁷, L. Zanello^{132a,132b}, D. Zanzi⁸⁸, C. Zeitnitz¹⁷⁵, M. Zeman¹²⁸, A. Zemla^{38a}, Q. Zeng¹⁴³, K. Zengel²³, O. Zenin¹³⁰, T. Ženiš^{144a}, D. Zerwas¹¹⁷, D. Zhang⁸⁹, F. Zhang¹⁷³, H. Zhang^{33c}, J. Zhang⁶, L. Zhang⁴⁸, R. Zhang^{33b}, X. Zhang^{33d}, Z. Zhang¹¹⁷, X. Zhao⁴⁰, Y. Zhao^{33d,117}, Z. Zhao^{33b}, A. Zhemchugov⁶⁵, J. Zhong¹²⁰, B. Zhou⁸⁹, C. Zhou⁴⁵, L. Zhou³⁵, L. Zhou⁴⁰, M. Zhou¹⁴⁸, N. Zhou^{33f}, C.G. Zhu^{33d}, H. Zhu^{33a}, J. Zhu⁸⁹, Y. Zhu^{33b}, X. Zhuang^{33a}, K. Zhukov⁹⁶, A. Zibell¹⁷⁴, D. Zieminska⁶¹, N.I. Zimine⁶⁵, C. Zimmermann⁸³, S. Zimmermann⁴⁸, Z. Zinonos⁵⁴, M. Zinser⁸³, M. Ziolkowski¹⁴¹, L. Živković¹³, G. Zobernig¹⁷³, A. Zoccoli^{20a,20b}, M. zur Nedden¹⁶, G. Zurzolo^{104a,104b}, L. Zwalinski³⁰.

¹ Department of Physics, University of Adelaide, Adelaide, Australia

² Physics Department, SUNY Albany, Albany NY, United States of America

³ Department of Physics, University of Alberta, Edmonton AB, Canada

⁴ (a) Department of Physics, Ankara University, Ankara; (b) Istanbul Aydin University, Istanbul; (c)

Division of Physics, TOBB University of Economics and Technology, Ankara, Turkey

⁵ LAPP, CNRS/IN2P3 and Université Savoie Mont Blanc, Annecy-le-Vieux, France

- ⁶ High Energy Physics Division, Argonne National Laboratory, Argonne IL, United States of America
- ⁷ Department of Physics, University of Arizona, Tucson AZ, United States of America
- ⁸ Department of Physics, The University of Texas at Arlington, Arlington TX, United States of America
- ⁹ Physics Department, University of Athens, Athens, Greece
- ¹⁰ Physics Department, National Technical University of Athens, Zografou, Greece
- ¹¹ Institute of Physics, Azerbaijan Academy of Sciences, Baku, Azerbaijan
- ¹² Institut de Física d'Altes Energies and Departament de Física de la Universitat Autònoma de Barcelona, Barcelona, Spain
- ¹³ Institute of Physics, University of Belgrade, Belgrade, Serbia
- ¹⁴ Department for Physics and Technology, University of Bergen, Bergen, Norway
- ¹⁵ Physics Division, Lawrence Berkeley National Laboratory and University of California, Berkeley CA, United States of America
- ¹⁶ Department of Physics, Humboldt University, Berlin, Germany
- ¹⁷ Albert Einstein Center for Fundamental Physics and Laboratory for High Energy Physics, University of Bern, Bern, Switzerland
- ¹⁸ School of Physics and Astronomy, University of Birmingham, Birmingham, United Kingdom
- ¹⁹ ^(a) Department of Physics, Bogazici University, Istanbul; ^(b) Department of Physics Engineering, Gaziantep University, Gaziantep; ^(c) Department of Physics, Dogus University, Istanbul, Turkey
- ²⁰ ^(a) INFN Sezione di Bologna; ^(b) Dipartimento di Fisica e Astronomia, Università di Bologna, Bologna, Italy
- ²¹ Physikalisches Institut, University of Bonn, Bonn, Germany
- ²² Department of Physics, Boston University, Boston MA, United States of America
- ²³ Department of Physics, Brandeis University, Waltham MA, United States of America
- ²⁴ ^(a) Universidade Federal do Rio De Janeiro COPPE/EE/IF, Rio de Janeiro; ^(b) Electrical Circuits Department, Federal University of Juiz de Fora (UFJF), Juiz de Fora; ^(c) Federal University of Sao Joao del Rei (UFSJ), Sao Joao del Rei; ^(d) Instituto de Física, Universidade de Sao Paulo, Sao Paulo, Brazil
- ²⁵ Physics Department, Brookhaven National Laboratory, Upton NY, United States of America
- ²⁶ ^(a) National Institute of Physics and Nuclear Engineering, Bucharest; ^(b) National Institute for Research and Development of Isotopic and Molecular Technologies, Physics Department, Cluj Napoca; ^(c) University Politehnica Bucharest, Bucharest; ^(d) West University in Timisoara, Timisoara, Romania
- ²⁷ Departamento de Física, Universidad de Buenos Aires, Buenos Aires, Argentina
- ²⁸ Cavendish Laboratory, University of Cambridge, Cambridge, United Kingdom
- ²⁹ Department of Physics, Carleton University, Ottawa ON, Canada
- ³⁰ CERN, Geneva, Switzerland
- ³¹ Enrico Fermi Institute, University of Chicago, Chicago IL, United States of America
- ³² ^(a) Departamento de Física, Pontificia Universidad Católica de Chile, Santiago; ^(b) Departamento de Física, Universidad Técnica Federico Santa María, Valparaíso, Chile
- ³³ ^(a) Institute of High Energy Physics, Chinese Academy of Sciences, Beijing; ^(b) Department of Modern Physics, University of Science and Technology of China, Anhui; ^(c) Department of Physics, Nanjing University, Jiangsu; ^(d) School of Physics, Shandong University, Shandong; ^(e) Department of Physics and Astronomy, Shanghai Key Laboratory for Particle Physics and Cosmology, Shanghai Jiao Tong University, Shanghai; ^(f) Physics Department, Tsinghua University, Beijing 100084, China
- ³⁴ Laboratoire de Physique Corpusculaire, Clermont Université and Université Blaise Pascal and CNRS/IN2P3, Clermont-Ferrand, France
- ³⁵ Nevis Laboratory, Columbia University, Irvington NY, United States of America
- ³⁶ Niels Bohr Institute, University of Copenhagen, Kobenhavn, Denmark
- ³⁷ ^(a) INFN Gruppo Collegato di Cosenza, Laboratori Nazionali di Frascati; ^(b) Dipartimento di Fisica,

Università della Calabria, Rende, Italy

³⁸ ^(a) AGH University of Science and Technology, Faculty of Physics and Applied Computer Science, Krakow; ^(b) Marian Smoluchowski Institute of Physics, Jagiellonian University, Krakow, Poland

³⁹ Institute of Nuclear Physics Polish Academy of Sciences, Krakow, Poland

⁴⁰ Physics Department, Southern Methodist University, Dallas TX, United States of America

⁴¹ Physics Department, University of Texas at Dallas, Richardson TX, United States of America

⁴² DESY, Hamburg and Zeuthen, Germany

⁴³ Institut für Experimentelle Physik IV, Technische Universität Dortmund, Dortmund, Germany

⁴⁴ Institut für Kern- und Teilchenphysik, Technische Universität Dresden, Dresden, Germany

⁴⁵ Department of Physics, Duke University, Durham NC, United States of America

⁴⁶ SUPA - School of Physics and Astronomy, University of Edinburgh, Edinburgh, United Kingdom

⁴⁷ INFN Laboratori Nazionali di Frascati, Frascati, Italy

⁴⁸ Fakultät für Mathematik und Physik, Albert-Ludwigs-Universität, Freiburg, Germany

⁴⁹ Section de Physique, Université de Genève, Geneva, Switzerland

⁵⁰ ^(a) INFN Sezione di Genova; ^(b) Dipartimento di Fisica, Università di Genova, Genova, Italy

⁵¹ ^(a) E. Andronikashvili Institute of Physics, Iv. Javakishvili Tbilisi State University, Tbilisi; ^(b) High Energy Physics Institute, Tbilisi State University, Tbilisi, Georgia

⁵² II Physikalisches Institut, Justus-Liebig-Universität Giessen, Giessen, Germany

⁵³ SUPA - School of Physics and Astronomy, University of Glasgow, Glasgow, United Kingdom

⁵⁴ II Physikalisches Institut, Georg-August-Universität, Göttingen, Germany

⁵⁵ Laboratoire de Physique Subatomique et de Cosmologie, Université Grenoble-Alpes, CNRS/IN2P3, Grenoble, France

⁵⁶ Department of Physics, Hampton University, Hampton VA, United States of America

⁵⁷ Laboratory for Particle Physics and Cosmology, Harvard University, Cambridge MA, United States of America

⁵⁸ ^(a) Kirchoff-Institut für Physik, Ruprecht-Karls-Universität Heidelberg, Heidelberg; ^(b)

Physikalisches Institut, Ruprecht-Karls-Universität Heidelberg, Heidelberg; ^(c) ZITI Institut für technische Informatik, Ruprecht-Karls-Universität Heidelberg, Mannheim, Germany

⁵⁹ Faculty of Applied Information Science, Hiroshima Institute of Technology, Hiroshima, Japan

⁶⁰ ^(a) Department of Physics, The Chinese University of Hong Kong, Shatin, N.T., Hong Kong; ^(b)

Department of Physics, The University of Hong Kong, Hong Kong; ^(c) Department of Physics, The Hong Kong University of Science and Technology, Clear Water Bay, Kowloon, Hong Kong, China

⁶¹ Department of Physics, Indiana University, Bloomington IN, United States of America

⁶² Institut für Astro- und Teilchenphysik, Leopold-Franzens-Universität, Innsbruck, Austria

⁶³ University of Iowa, Iowa City IA, United States of America

⁶⁴ Department of Physics and Astronomy, Iowa State University, Ames IA, United States of America

⁶⁵ Joint Institute for Nuclear Research, JINR Dubna, Dubna, Russia

⁶⁶ KEK, High Energy Accelerator Research Organization, Tsukuba, Japan

⁶⁷ Graduate School of Science, Kobe University, Kobe, Japan

⁶⁸ Faculty of Science, Kyoto University, Kyoto, Japan

⁶⁹ Kyoto University of Education, Kyoto, Japan

⁷⁰ Department of Physics, Kyushu University, Fukuoka, Japan

⁷¹ Instituto de Física La Plata, Universidad Nacional de La Plata and CONICET, La Plata, Argentina

⁷² Physics Department, Lancaster University, Lancaster, United Kingdom

⁷³ ^(a) INFN Sezione di Lecce; ^(b) Dipartimento di Matematica e Fisica, Università del Salento, Lecce, Italy

⁷⁴ Oliver Lodge Laboratory, University of Liverpool, Liverpool, United Kingdom

- ⁷⁵ Department of Physics, Jožef Stefan Institute and University of Ljubljana, Ljubljana, Slovenia
- ⁷⁶ School of Physics and Astronomy, Queen Mary University of London, London, United Kingdom
- ⁷⁷ Department of Physics, Royal Holloway University of London, Surrey, United Kingdom
- ⁷⁸ Department of Physics and Astronomy, University College London, London, United Kingdom
- ⁷⁹ Louisiana Tech University, Ruston LA, United States of America
- ⁸⁰ Laboratoire de Physique Nucléaire et de Hautes Energies, UPMC and Université Paris-Diderot and CNRS/IN2P3, Paris, France
- ⁸¹ Fysiska institutionen, Lunds universitet, Lund, Sweden
- ⁸² Departamento de Física Teórica C-15, Universidad Autónoma de Madrid, Madrid, Spain
- ⁸³ Institut für Physik, Universität Mainz, Mainz, Germany
- ⁸⁴ School of Physics and Astronomy, University of Manchester, Manchester, United Kingdom
- ⁸⁵ CPPM, Aix-Marseille Université and CNRS/IN2P3, Marseille, France
- ⁸⁶ Department of Physics, University of Massachusetts, Amherst MA, United States of America
- ⁸⁷ Department of Physics, McGill University, Montreal QC, Canada
- ⁸⁸ School of Physics, University of Melbourne, Victoria, Australia
- ⁸⁹ Department of Physics, The University of Michigan, Ann Arbor MI, United States of America
- ⁹⁰ Department of Physics and Astronomy, Michigan State University, East Lansing MI, United States of America
- ⁹¹ ^(a) INFN Sezione di Milano; ^(b) Dipartimento di Fisica, Università di Milano, Milano, Italy
- ⁹² B.I. Stepanov Institute of Physics, National Academy of Sciences of Belarus, Minsk, Republic of Belarus
- ⁹³ National Scientific and Educational Centre for Particle and High Energy Physics, Minsk, Republic of Belarus
- ⁹⁴ Department of Physics, Massachusetts Institute of Technology, Cambridge MA, United States of America
- ⁹⁵ Group of Particle Physics, University of Montreal, Montreal QC, Canada
- ⁹⁶ P.N. Lebedev Institute of Physics, Academy of Sciences, Moscow, Russia
- ⁹⁷ Institute for Theoretical and Experimental Physics (ITEP), Moscow, Russia
- ⁹⁸ National Research Nuclear University MEPhI, Moscow, Russia
- ⁹⁹ D.V. Skobeltsyn Institute of Nuclear Physics, M.V. Lomonosov Moscow State University, Moscow, Russia
- ¹⁰⁰ Fakultät für Physik, Ludwig-Maximilians-Universität München, München, Germany
- ¹⁰¹ Max-Planck-Institut für Physik (Werner-Heisenberg-Institut), München, Germany
- ¹⁰² Nagasaki Institute of Applied Science, Nagasaki, Japan
- ¹⁰³ Graduate School of Science and Kobayashi-Maskawa Institute, Nagoya University, Nagoya, Japan
- ¹⁰⁴ ^(a) INFN Sezione di Napoli; ^(b) Dipartimento di Fisica, Università di Napoli, Napoli, Italy
- ¹⁰⁵ Department of Physics and Astronomy, University of New Mexico, Albuquerque NM, United States of America
- ¹⁰⁶ Institute for Mathematics, Astrophysics and Particle Physics, Radboud University Nijmegen/Nikhef, Nijmegen, Netherlands
- ¹⁰⁷ Nikhef National Institute for Subatomic Physics and University of Amsterdam, Amsterdam, Netherlands
- ¹⁰⁸ Department of Physics, Northern Illinois University, DeKalb IL, United States of America
- ¹⁰⁹ Budker Institute of Nuclear Physics, SB RAS, Novosibirsk, Russia
- ¹¹⁰ Department of Physics, New York University, New York NY, United States of America
- ¹¹¹ Ohio State University, Columbus OH, United States of America
- ¹¹² Faculty of Science, Okayama University, Okayama, Japan

- 113 Homer L. Dodge Department of Physics and Astronomy, University of Oklahoma, Norman OK, United States of America
- 114 Department of Physics, Oklahoma State University, Stillwater OK, United States of America
- 115 Palacký University, RCPTM, Olomouc, Czech Republic
- 116 Center for High Energy Physics, University of Oregon, Eugene OR, United States of America
- 117 LAL, Université Paris-Sud and CNRS/IN2P3, Orsay, France
- 118 Graduate School of Science, Osaka University, Osaka, Japan
- 119 Department of Physics, University of Oslo, Oslo, Norway
- 120 Department of Physics, Oxford University, Oxford, United Kingdom
- 121 ^(a) INFN Sezione di Pavia; ^(b) Dipartimento di Fisica, Università di Pavia, Pavia, Italy
- 122 Department of Physics, University of Pennsylvania, Philadelphia PA, United States of America
- 123 National Research Centre "Kurchatov Institute" B.P.Konstantinov Petersburg Nuclear Physics Institute, St. Petersburg, Russia
- 124 ^(a) INFN Sezione di Pisa; ^(b) Dipartimento di Fisica E. Fermi, Università di Pisa, Pisa, Italy
- 125 Department of Physics and Astronomy, University of Pittsburgh, Pittsburgh PA, United States of America
- 126 ^(a) Laboratório de Instrumentação e Física Experimental de Partículas - LIP, Lisboa; ^(b) Faculdade de Ciências, Universidade de Lisboa, Lisboa; ^(c) Department of Physics, University of Coimbra, Coimbra; ^(d) Centro de Física Nuclear da Universidade de Lisboa, Lisboa; ^(e) Departamento de Física, Universidade do Minho, Braga; ^(f) Departamento de Física Teórica y del Cosmos and CAFPE, Universidad de Granada, Granada (Spain); ^(g) Dep Física and CEFITEC of Faculdade de Ciências e Tecnologia, Universidade Nova de Lisboa, Caparica, Portugal
- 127 Institute of Physics, Academy of Sciences of the Czech Republic, Praha, Czech Republic
- 128 Czech Technical University in Prague, Praha, Czech Republic
- 129 Faculty of Mathematics and Physics, Charles University in Prague, Praha, Czech Republic
- 130 State Research Center Institute for High Energy Physics, Protvino, Russia
- 131 Particle Physics Department, Rutherford Appleton Laboratory, Didcot, United Kingdom
- 132 ^(a) INFN Sezione di Roma; ^(b) Dipartimento di Fisica, Sapienza Università di Roma, Roma, Italy
- 133 ^(a) INFN Sezione di Roma Tor Vergata; ^(b) Dipartimento di Fisica, Università di Roma Tor Vergata, Roma, Italy
- 134 ^(a) INFN Sezione di Roma Tre; ^(b) Dipartimento di Matematica e Fisica, Università Roma Tre, Roma, Italy
- 135 ^(a) Faculté des Sciences Ain Chock, Réseau Universitaire de Physique des Hautes Energies - Université Hassan II, Casablanca; ^(b) Centre National de l'Energie des Sciences Techniques Nucleaires, Rabat; ^(c) Faculté des Sciences Semlalia, Université Cadi Ayyad, LPHEA-Marrakech; ^(d) Faculté des Sciences, Université Mohamed Premier and LPTPM, Oujda; ^(e) Faculté des sciences, Université Mohammed V, Rabat, Morocco
- 136 DSM/IRFU (Institut de Recherches sur les Lois Fondamentales de l'Univers), CEA Saclay (Commissariat à l'Energie Atomique et aux Energies Alternatives), Gif-sur-Yvette, France
- 137 Santa Cruz Institute for Particle Physics, University of California Santa Cruz, Santa Cruz CA, United States of America
- 138 Department of Physics, University of Washington, Seattle WA, United States of America
- 139 Department of Physics and Astronomy, University of Sheffield, Sheffield, United Kingdom
- 140 Department of Physics, Shinshu University, Nagano, Japan
- 141 Fachbereich Physik, Universität Siegen, Siegen, Germany
- 142 Department of Physics, Simon Fraser University, Burnaby BC, Canada
- 143 SLAC National Accelerator Laboratory, Stanford CA, United States of America

- ¹⁴⁴ (a) Faculty of Mathematics, Physics & Informatics, Comenius University, Bratislava; (b) Department of Subnuclear Physics, Institute of Experimental Physics of the Slovak Academy of Sciences, Kosice, Slovak Republic
- ¹⁴⁵ (a) Department of Physics, University of Cape Town, Cape Town; (b) Department of Physics, University of Johannesburg, Johannesburg; (c) School of Physics, University of the Witwatersrand, Johannesburg, South Africa
- ¹⁴⁶ (a) Department of Physics, Stockholm University; (b) The Oskar Klein Centre, Stockholm, Sweden
- ¹⁴⁷ Physics Department, Royal Institute of Technology, Stockholm, Sweden
- ¹⁴⁸ Departments of Physics & Astronomy and Chemistry, Stony Brook University, Stony Brook NY, United States of America
- ¹⁴⁹ Department of Physics and Astronomy, University of Sussex, Brighton, United Kingdom
- ¹⁵⁰ School of Physics, University of Sydney, Sydney, Australia
- ¹⁵¹ Institute of Physics, Academia Sinica, Taipei, Taiwan
- ¹⁵² Department of Physics, Technion: Israel Institute of Technology, Haifa, Israel
- ¹⁵³ Raymond and Beverly Sackler School of Physics and Astronomy, Tel Aviv University, Tel Aviv, Israel
- ¹⁵⁴ Department of Physics, Aristotle University of Thessaloniki, Thessaloniki, Greece
- ¹⁵⁵ International Center for Elementary Particle Physics and Department of Physics, The University of Tokyo, Tokyo, Japan
- ¹⁵⁶ Graduate School of Science and Technology, Tokyo Metropolitan University, Tokyo, Japan
- ¹⁵⁷ Department of Physics, Tokyo Institute of Technology, Tokyo, Japan
- ¹⁵⁸ Department of Physics, University of Toronto, Toronto ON, Canada
- ¹⁵⁹ (a) TRIUMF, Vancouver BC; (b) Department of Physics and Astronomy, York University, Toronto ON, Canada
- ¹⁶⁰ Faculty of Pure and Applied Sciences, University of Tsukuba, Tsukuba, Japan
- ¹⁶¹ Department of Physics and Astronomy, Tufts University, Medford MA, United States of America
- ¹⁶² Centro de Investigaciones, Universidad Antonio Narino, Bogota, Colombia
- ¹⁶³ Department of Physics and Astronomy, University of California Irvine, Irvine CA, United States of America
- ¹⁶⁴ (a) INFN Gruppo Collegato di Udine, Sezione di Trieste, Udine; (b) ICTP, Trieste; (c) Dipartimento di Chimica, Fisica e Ambiente, Università di Udine, Udine, Italy
- ¹⁶⁵ Department of Physics, University of Illinois, Urbana IL, United States of America
- ¹⁶⁶ Department of Physics and Astronomy, University of Uppsala, Uppsala, Sweden
- ¹⁶⁷ Instituto de Física Corpuscular (IFIC) and Departamento de Física Atómica, Molecular y Nuclear and Departamento de Ingeniería Electrónica and Instituto de Microelectrónica de Barcelona (IMB-CNM), University of Valencia and CSIC, Valencia, Spain
- ¹⁶⁸ Department of Physics, University of British Columbia, Vancouver BC, Canada
- ¹⁶⁹ Department of Physics and Astronomy, University of Victoria, Victoria BC, Canada
- ¹⁷⁰ Department of Physics, University of Warwick, Coventry, United Kingdom
- ¹⁷¹ Waseda University, Tokyo, Japan
- ¹⁷² Department of Particle Physics, The Weizmann Institute of Science, Rehovot, Israel
- ¹⁷³ Department of Physics, University of Wisconsin, Madison WI, United States of America
- ¹⁷⁴ Fakultät für Physik und Astronomie, Julius-Maximilians-Universität, Würzburg, Germany
- ¹⁷⁵ Fachbereich C Physik, Bergische Universität Wuppertal, Wuppertal, Germany
- ¹⁷⁶ Department of Physics, Yale University, New Haven CT, United States of America
- ¹⁷⁷ Yerevan Physics Institute, Yerevan, Armenia
- ¹⁷⁸ Centre de Calcul de l'Institut National de Physique Nucléaire et de Physique des Particules (IN2P3),

Villeurbanne, France

^a Also at Department of Physics, King's College London, London, United Kingdom

^b Also at Institute of Physics, Azerbaijan Academy of Sciences, Baku, Azerbaijan

^c Also at Novosibirsk State University, Novosibirsk, Russia

^d Also at TRIUMF, Vancouver BC, Canada

^e Also at Department of Physics, California State University, Fresno CA, United States of America

^f Also at Department of Physics, University of Fribourg, Fribourg, Switzerland

^g Also at Departamento de Fisica e Astronomia, Faculdade de Ciencias, Universidade do Porto, Portugal

^h Also at Tomsk State University, Tomsk, Russia

ⁱ Also at CPPM, Aix-Marseille Université and CNRS/IN2P3, Marseille, France

^j Also at Università di Napoli Parthenope, Napoli, Italy

^k Also at Institute of Particle Physics (IPP), Canada

^l Also at Particle Physics Department, Rutherford Appleton Laboratory, Didcot, United Kingdom

^m Also at Department of Physics, St. Petersburg State Polytechnical University, St. Petersburg, Russia

ⁿ Also at Louisiana Tech University, Ruston LA, United States of America

^o Also at Institutio Catalana de Recerca i Estudis Avancats, ICREA, Barcelona, Spain

^p Also at Graduate School of Science, Osaka University, Osaka, Japan

^q Also at Department of Physics, National Tsing Hua University, Taiwan

^r Also at Department of Physics, The University of Texas at Austin, Austin TX, United States of America

^s Also at Institute of Theoretical Physics, Ilia State University, Tbilisi, Georgia

^t Also at CERN, Geneva, Switzerland

^u Also at Georgian Technical University (GTU), Tbilisi, Georgia

^v Also at Manhattan College, New York NY, United States of America

^w Also at Hellenic Open University, Patras, Greece

^x Also at Institute of Physics, Academia Sinica, Taipei, Taiwan

^y Also at LAL, Université Paris-Sud and CNRS/IN2P3, Orsay, France

^z Also at Academia Sinica Grid Computing, Institute of Physics, Academia Sinica, Taipei, Taiwan

^{aa} Also at School of Physics, Shandong University, Shandong, China

^{ab} Also at Moscow Institute of Physics and Technology State University, Dolgoprudny, Russia

^{ac} Also at Section de Physique, Université de Genève, Geneva, Switzerland

^{ad} Also at International School for Advanced Studies (SISSA), Trieste, Italy

^{ae} Also at Department of Physics and Astronomy, University of South Carolina, Columbia SC, United States of America

^{af} Also at School of Physics and Engineering, Sun Yat-sen University, Guangzhou, China

^{ag} Also at Faculty of Physics, M.V.Lomonosov Moscow State University, Moscow, Russia

^{ah} Also at National Research Nuclear University MEPhI, Moscow, Russia

^{ai} Also at Department of Physics, Stanford University, Stanford CA, United States of America

^{aj} Also at Institute for Particle and Nuclear Physics, Wigner Research Centre for Physics, Budapest, Hungary

^{ak} Also at University of Malaya, Department of Physics, Kuala Lumpur, Malaysia

* Deceased